Genetic basis and evolutionary context for structural color shift in the Buckeye butterfly

By

Rachel Christine Thayer

A dissertation submitted in partial satisfaction of the

requirements for the degree of

Doctor of Philosophy

in

Integrative Biology

in the

Graduate Division

of the

University of California, Berkeley

Committee in charge:

Professor Nipam H. Patel, Co-Chair
Professor Michael W. Nachman, Co-Chair
Professor Craig T. Miller

Summer 2020

Genetic basis and evolutionary context for structural color shift in the Buckeye butterfly

By

Rachel Christine Thayer

Abstract

Genetic basis and evolutionary context for structural color shift in the Buckeye butterfly

by

Rachel Christine Thayer

Doctor of Philosophy in Integrative Biology

University of California, Berkeley

Professors Nipam H. Patel & Michael W. Nachman, Co-Chairs

In butterfly scales, nanostructures that scatter light create structural color, often with visually delightful effects like iridescence. Structural colors used for signaling, thermal regulation, or camouflage provide excellent case studies in the ecological multifunctionality of color. Developmentally, intricate nanostructures must be precisely sculpted, as a few nanometers' difference in one dimension would change the hue. In physics, the gyroid, an infinitely connected periodic surface once thought to be a purely theoretical shape, was found reflecting green light in butterfly wings, and naturally occurring photonic structures are a rich source of inspiration for optical engineering. Despite interdisciplinary appeal, the biological processes that produce structural color remain mysterious. Here, I take a telescopic approach to investigate the biology of butterfly structural color, beginning with macroevolutionary trends, proceeding to genus- and species-level variation, and concluding with genetic analysis. In chapter one, I aggregate reflectance and morphological data for all 350 described butterfly structural colors to interrogate the color gamut and phylogenetic distribution of structural color. In the process, I comprehensively review what is known about how structurally colored scales develop and evolve. In chapter two, I show that selective breeding shifted wing color from brown to blue in buckeye butterflies (*Junonia coenia*) via a 74% increase in the thickness of each scale lamina. By comparing ten related species in the genus *Junonia*, I find that evolutionarily tuning lamina thickness has generated a wide range of structural colors, from gold to magenta and green. A similar thickness increase explains the appearance of blue scales in buckeyes with mutations in the *optix* wing patterning gene. In chapter three, I use a large cross-breeding experiment between blue and brown buckeyes and quantitative trait locus mapping to identify genetic loci that control the evolved blue structural color. Hue is controlled by a different set of genes than the arrangement of blue scales over the wing surface, and *optix* is the first specific gene found to regulate the morphology of a photonic structure.

Table of Contents

Acknowledgements

I am grateful to many people for their support during my Ph.D. program, beginning with Clint Whipple, Jack Sites, Madelaine Bartlett, Michael Veeman, Wendy Reeves, and Keith Crandall for mentoring that got me into graduate school. Nipam and Michael admitted me to Berkeley and arranged the opportunity to do lab rotations my first year. The National Science Foundation and the Berkeley Graduate Division awarded me fellowships that enabled me to pull together some financial contributions to my family, including paying my mom's tuition after my dad's disability. Without the financial predictability and higher stipend offered by these fellowships, I probably would have felt that entering a Ph.D. program was too ostentatious and fiscally irresponsible, despite my long-held goal to become a zoologist. Ryan Null taught me that there is such a thing as structural color. Edith Smith created and shared the super blue butterflies that inspired and enabled my entire dissertation. I thank my lab mates, floor mates, and the Berkeley IB and MCB communities for the milestones, camaraderie, training, and stimulating discussions: Erin, Angela, Ryan, Arnaud, Chris, Jaap, Kyle, Aaron, Dennis, Jenny, Sophia, Megan, Katie, Katya, Noëlle, Ke, Taichi, Sarah, Mallory, Sylvia, Erin, David, Kennedy, Libby, Felipe, Priscilla, Jess, Jessen, Jacques, Armando, Andrew, James, Sophie, Marta, Mike, Tyler, Austin, and Steven. Talented undergraduate research assistants asked great questions, made creative contributions, and cared for the butterflies: Yuriko, Madelyn, Ravi, Joey, Holly, Annie, Megan, and Emma. I thank each member of my various academic committees for mentoring, votes of confidence, and scientific critiques: Michael Nachman, Craig Miller, Chelsea Specht, Rosemary Gillespie, Caroline Williams, and most of all Nipam Patel. Lydia Smith, Frances Allen, and Pete Oboyski were friendly gatekeepers who connected me with critical research infrastructure and training. Many professional organizations, conferences, retreats, and bootcamps provided valuable opportunities, material support, new ideas, and my first trips outside the US. I appreciate all the professionals behind internet aliases who have answered my questions about coding, installations, replacing hard drives, setting up mySQL databases, and other daunting tasks. Researchers, collaborators, mentors, and butterfly hobbyists from around the world have shared specimens or good information. UAW 2865 worked to protect livable working conditions and supported my March for Science organizing. I'm obliged to supportive housemates, particularly Erika Anderson who was my housemate of longest tenure, a great friend and fellow biologist, and whose edits rescued my first paper draft. My mom encouraged my earliest biologist tendencies with animal books, zoo trips, and an emphasis on education. My siblings and extended family have shared butterfly-themed questions and paraphernalia, contributions to optically modeling reflectance spectra (Sam), and fun outreach collaborations (Beth).

The final stretch of this endeavor was especially turbulent: the Patel lab moved to Woods Hole in late 2018 while I stayed in Berkeley; a pipetting-related wrist injury prevented me from lab work for months; incessant federal dysfunction and betrayals made me constantly most concerned about topics other than butterflies; and as a grand finale, the pandemic preempted research activities and intensified existing stresses for my final six months. In honor of the struggle, I'm especially grateful to everyone involved in helping me drag myself past the finish line: Nipam for reliable financial support and flexible employment appointments; Michael Nachman and his lab for adopting me into lab meetings and events; Dennis Sun and Aaron Pomerantz for holding down "Patel Lab West" with me; Jess Lyon and Dan Rokhsar for lending me a private cubicle of lab space to finish phenotyping after limited campus reopening; Paula Hollowell and Zach Hallberg for giving me somewhere to live when I was abruptly unable to move to Woods Hole during the last pandemic summer; Stewie the dog for graciously accepting many pets and less than optional cuddles; excellent physical therapists and counseling at the Tang Center; and the continued support of friends and colleagues.

Lastly, thank you to my thousands of butterflies, my ultimate teachers. I loved the sound of dozens of you as caterpillars all simultaneously chomping a batch of leaves, loved watching you get fat rolls, loved your little suctioning pseudo feet and blue-black spikes, loved seeing you scrolling your new tongues to zip the two halves together while you flexed your soggy wet wings, loved the first mellow day of adulthood when I could carry you around, loved your new butterfly smell, and loved opening cups of new adults—like unwrapping presents—to see what colors you'd debut. I loved watching you discover your first drink and bob your antennas and slack your wings in a visual encapsulation of "ahhh!" that could be a Gatorade commercial, delighted to learn how pugnacious you are, and loved watching you busily drum surfaces to find leaves and lay little pearly green eggs. I must admire the butterfly matriarch and possible fertility goddess who laid well over 500 F2 eggs. I'll adapt Barbara McClintock's sentiment:

"I start with the (hatchling), and I don't want to leave it. I don't feel I really know the story if I don't watch the (animal) all the way along. So I know every (butterfly) in the (colony). I know them intimately, and I find it a real pleasure to know them."

Thanks for the unfiltered lessons on life and for giving me your lives. This dissertation is an effort to memorialize and share them.

Chapter 1

A meta-analysis of structural color in butterflies

Introduction

Butterflies are among the most beloved and charismatic animals, largely owing to the beautiful displays on the adults' wings. Wing colors and patterns are diverse and multifunctional, playing roles in camouflage (Suzuki, Tomita, & Sezutsu, 2014; Wilts, Pirih, Arikawa, & Stavenga, 2013), thermal regulation (Biró et al., 2003; Kingsolver & Wiernasz, 1991; Watt, 1968), aposematism (Müller, 1879; van Zandt Brower, 1958), and sexual signalling (Kronforst et al., 2006; Medina, Vega-Trejo, Wallenius, Symonds, & Stuart-Fox, 2020; White, Zeil, & Kemp, 2015).

Many hues in the explosive lepidopteran palette are produced by structural color. In contrast to pigments like melanin, which are small molecules that selectively absorb certain wavelengths to produce subtractive color, structural colors make interference colors in the same way that a soap bubble produces a rainbow sheen. Structural color occurs when light is scattered by nanoscale, precisely shaped, solid structures made of a high-refractive index material, causing constructive and destructive interference effects. Only structural colors can produce certain optical effects like iridescence, in which the reflected light shifts wavelength, flashes, dims, or disappears, depending upon the angle of view. Some photonic structures also interact selectively with polarized light (Saba, Wilts, Hielscher, & Schröder-Turk, 2014; Zhang, K. et al., 2014) or display dynamic colors that change in response to humidity levels (Wilts, Mothander, & Kelber, 2019). Butterflies have an abundance of intricate, highly refractive structures, suitable for structural color, on their wings.

Butterfly wings are tightly tiled with a mosaic of overlapping scales, each an independent epithelial structure around 300 μm long that protrudes from a socket on the wing membrane (Fig. 1A). Scales are inanimate structures made of the polysaccharide chitin, each produced by one cell in the developing pupal wing (Stossberg, 1938). They are evolutionarily derived from sensory bristles like those on fly wings (Galant, Skeath, Paddock, Lewis, & Carroll, 1998). A typical scale is shaped like a flat tile, with a set of conserved subelements that are all made of chitin (defined by Ghiradella, 1984, Fig. 1 B,C). The bottom (adwing) surface of a basic scale is a flat sheet called the lamina which extends the scale's full dimensions and supports the other components (purple, Fig. 1 B,C). On the upper (abwing) surface of the scale, rows of

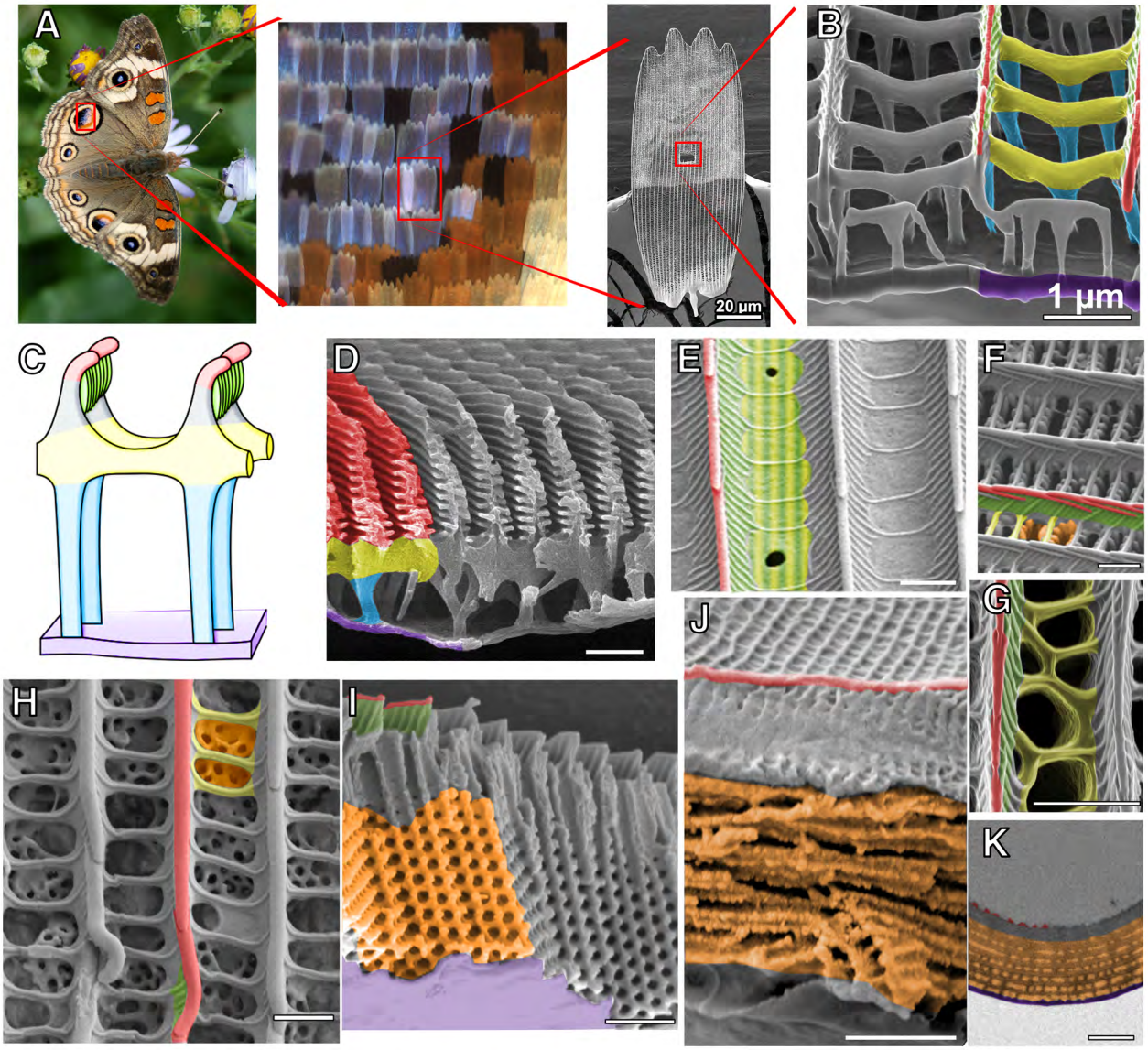

Figure 1: Examples of derived morphologies that cause structural colors in butterfly scales. *(A)* Zooming in on a cross-sectioned scale from a *Junonia coenia* wing. *(B) J. coenia* scale which conforms to the scale Bauplan, with overlaid colors for the general components of a scale (red = ridges, green = microribs, yellow = crossribs, blue = trabeculae, violet = lamina, orange = novel structures, and the lumen is the open space in the center of the scale). This scale has a single layer lamina, which can cause thin film structural color. *(C)* Cartoon with the minimal scale elements color coded. *(D)* Cross-sectioned blue *Morpho cypris* scale with modified ridge lamellae. *(E)* Silver *Agraulis vanillae* scale with filled windows, top view. Filled windows likely require modifications to both micro- and crossribs; for simplicity, I characterized them as modified crossribs throughout this paper. *(F)* White *Colias eurytheme* scale with pigment granules, top view. *(G)* Reticulate crossribs in a *Parides sesostris* scale, top view. *(H)* Perforated multilayer in the lumen of an *Arcas imperialis* scale, top view. *(I)* Green *Teinopalpus imperialis* scale with a 3D crystal structure in the lumen, cross-sectional view. *(J, K)* Cross-sectional SEM and TEM of a green *Papilio palinurus* scale with smooth multilayers in the lumen. *(D, E, J, K)* Image credit Ryan Null. *(F, G, H)* Image credit Woods Hole Embryology class of 2017.

parallel ridges extend from the distal to proximal tip of the scale (red, Fig. 1 B,C). These ridges have smaller subunits which are called ridge lamellae or scutes. Crossribs are oriented perpendicularly to the ridges in the same plane, and connect pairs of ridges to form a grid (yellow, Fig. 1 B,C). On their lateral sides, ridges bear microribs (also called flutes, green, Fig. 1 B,C) that stretch from the ridge's apex to the height at which crossribs join. The entire network of ridges and crossribs is held above the lamina by trabeculae (blue, Fig. 1 B,C). The open space in the scale's interior, around the trabeculae, is the lumen. There may be pigments (e.g. melanin, ommochromes, or papiliochromes) suffused through any part of the scale (Stavenga, Doekele G., Leertouwer, & Wilts, 2014a; Wilts, Matsushita, Arikawa, & Stavenga, 2015). Because chitin has one of the highest refractive indices for any biotic material, around 1.5 (Leertouwer, Wilts, & Stavenga, 2011), and because scales have many intricate parts on the order of hundreds of nanometers in size, scales are an excellent raw material for structural color.

The fine structures and associated optical properties of structurally colored butterfly scales have been progressively elucidated over the last century. By the early 1900s, various researchers recognized that the iridescent colors of *Morpho*, *Papilio, Hypolimnas* and other butterflies were not pigmentary, but rather involved interference effects (Michelson, 1911; Onslow, 1923; Rayleigh, 1919). Mason cleverly used combinations of light microscopy, chemical treatments, and spectral observations under a battery of illumination conditions to correctly deduce the refractive index of chitin and several key aspects of *Urania* and *Morpho* scale morphology (Mason, 1927). But light microscopy cannot resolve features smaller than a few hundred nanometers, including most photonic structures, so diagrams of the nanostructures that underlie structural colors remained coarse. The advent of electron microscopy in the 1930s and '40s provided a crucial new tool, and the first electron micrographs of butterfly nanostructures were taken of *Morpho cypris* (Anderson & Richards Jr, 1942). EM technology gradually improved and slowly more butterfly scale micrographs were published (Huxley, 1975; Lippert & Gentil, 1959; Morris, 1975; Schmidt & Paulus, 1970). Ghiradella was the first prolific source for micrographs of photonic nanostructures. Her work in the 1970s-90s catalogued nanostructures from many taxa (Ghiradella, 2010), interrogated the processes of scale development (Ghiradella, 1974; Ghiradella, 1989), and described both the scale bauplan and the classes of morphological departures from it that produce structural color (Ghiradella, 1985; Ghiradella, 1998).

Ghiradella's micrographs, together with subsequent studies and reviews (Biró & Vigneron, 2011; Ingram & Parker, 2008; Mouchet & Vukusic, 2018; Srinivasarao, 1999; Zhang, D. et al., 2015), showed that any part of a scale may become a photonic nanostructure with the right evolved modifications and certain morphologies with

vivid optical properties arise recurrently. In many species, elongated ridge lamellae overlap each other to form multilayers (Fig. 1D). This characteristic morphology has been called "ridge iridescence" or "fir-tree structures," while scales that bear such ridge structures are often termed "*Morpho*-type" scales. For a similar effect, other scales have tilted ridge lamellae or microribs, such that the microribs overlap to form a multilayer (e.g. *Eryphanis aesacus*, *Caligo martia,* Wickham, Large, Poladian, & Jermiin, 2006). Microribs may also be extended and/or fused with the crossribs to fill the windows, forming a solid upper surface (Fig. 1E). Crossribs can also be reticulated (Fig. 1G) or form a reflective 2D lattice (Trzeciak, Wilts, Stavenga, & Vukusic, 2012). In Pierid butterflies, pterin pigments are clustered into granules that are suspended in the lumen of the scale (Fig. 1F) where the granules cause incoherent scattering (Stavenga, D. G., Stowe, Siebke, Zeil, & Arikawa, 2004). A standard lamina can act as a simple thin film reflector (Fig. 1B Stavenga et al., 2014; Thayer, Allen, & Patel, 2020). Three general categories of novel structures may develop inside the scale lumen. Multiple smooth, continuous layers in the lumen form a multilayer in *Papilio* and other butterflies (Fig. 1 J-K, Vukusic, Sambles, & Lawrence, 2000). Scales with lumen multilayers are often called "*Urania*-type" after the first-reported lumen multilayers in Sunset Moth scales (since reclassified as *Chrysiridia,* Lippert & Gentil, 1959; Yoshioka & Kinoshita, 2007). Perforated multilayers, also called "pepper-pot" structures, are common in Lycaenid butterflies (Fig. 1H). Lastly, the lumens of yet other scales are full of highly derived 3D crystal lattices, including inverse opals and gyroids (Fig. 1I).

Since the 1970s, an accelerating number of studies have characterized photonic structures with increasing sophistication from a growing number of butterfly species. The literature is now sufficiently deep to justify a meta-analysis. Here, I systematically analyze the reflectance spectra and morphology of all reported butterfly photonic structures. I use these aggregated data to address a deeper set of questions about structural color, including how structural color is phylogenetically distributed, which kinds of photonic structures are most and least common, which parts of a scale can evolve the most versatile and heterogeneous photonic structures, and how much of color space each type of structure accesses. Next, I review what is known about the biological processes that generate structural colors, including developmental events, genetic regulation, and macro and microevolution. Throughout, I highlight outstanding questions and understudied taxa as suggestions for future research.

Methods

I used several intersecting approaches to search for articles, book chapters, and theses that characterize photonic properties of butterfly scale structures. First, I used Google

Scholar searches with combinations of these keywords: structural color, butterfly, Lepidoptera, iridescence, scale, and Ghiradella. Searches on each subset of those terms brought up tens of thousands of hits, most of which were not pertinent, so I used search results as a starting point but did not evaluate every result. Rather, I used high-quality results to find cited and citing references and noted every species which was mentioned in connection with structural color, iridescence, or derived scale morphology. Finally, I used a database search on each species name that had been mentioned in any prior included reference. When a search on species name returned many results, I searched again with the name in combination with my key words. If the search on species name returned no relevant results, I tried searches with only the genus name and also checked for alternate nomenclature. I continued snowballing references and running database searches on species until I could no longer find any new species mentioned in connection with structural color. Criteria for inclusion were that the reference must include either (1) reflectance or color measurements or (2) electron microscope images of photonic structures in a butterfly. I also included studies which provided additional characterizations (e.g. absorption measurements, mathematical modeling, scatterometry) for structures that had been included on the basis of (1) or (2). I excluded transparent butterflies because although they have nanostructures with significant optical properties (Pinna et al., 2020), transparency, by definition, is the absence of color. I also excluded the few studies on structural colors in butterfly pupae (e.g. Neville, 1977; Steinbrecht, Mohren, Pulker, & Schneider, 1985).

This literature review strategy yielded 151 included references, which described 361 scale types from 356 species. Note that a species could have different structural colors on different body parts; for example, blue dorsal wings with ventral green (e.g. *Cyanophrys remus* and *Albulina metallica*, Biró et al., 2007). Data on both color and morphology were available for 282 photonic structures. Eleven cases out of the 361 did not evidently have a photonic structure. Usually these negative results were reported as a comparison to specimens that were structurally colored (e.g. *Troides aeacus* versus *Troides magellanus*, Dechkrong et al., 2011; Lawrence, Vukusic, & Sambles, 2002) or because the scale morphology was unusual, but with no reported consequences for structural coloration (e.g. *Caligo ilioneus*, Ghiradella, 2010).

To compare color between structures, I noted the peak reflected wavelength for each structural color. Due to iridescence, quantification of structural color is extremely sensitive to the measurement protocol, specifically illumination angle, detection angle, light source, specular or diffuse reference sample, and spot size (Meadows, Morehouse, Rutowski, Douglas, & McGraw, 2011). No aspect of spectroscopy methodology was consistent across all the included studies, and indeed, there is no single best choice that applies to every structure and research question. For example, an ecologically-minded

researcher may opt to measure color from an intact wing under diffuse lighting that resembles natural conditions. By contrast, a researcher interested in biomimetic engineering is more likely to assess an isolated structure using whichever methods best expose its most distinctive properties. By necessity, I defer to the authors' judgment and use the available spectra, so it should be kept in mind that my summaries use imperfect comparisons and therefore only show broad trends. When multiple spectra were available, I used the following rules. When reflectance was reported from more than one angle, I used the peak wavelength at the maximally reflective angle. If reflectance was reported for more than one specimen, I used the average. When reflectance was measured both from an isolated scale and the intact wing, I prioritized the single scale reflectance, so as to eliminate reflectance from neighboring scales of other types (e.g. ground scales). Some structures produced two reflectance peaks, as in multiple *Chrysozephyrus* species with both a UV and a green peak (Imafuku, Hirose, & Takeuchi, 2002). In such cases I used the brighter peak in my graphical summaries, but listed both in the spreadsheet. Authors did not usually name the maximally reflected wavelength, so I estimated the peak wavelengths by eye from the graphs, which limited accuracy to a 5-10 nm window around the true peak. Note that many reflectance spectra are also influenced by co-occurring pigments. When no reflectance spectra were available but a color image or a qualitative descriptor (e.g. "blue", "UV") was given, I noted the qualitative color.

To compare scale morphological modifications, I noted which part (Fig. 1A) of each scale formed the photonic structure. I categorized structures in the scale lumen as a smooth multilayer, a perforated multilayer, or a crystal (examples in Fig. 1 F-I). Generally I used the author's conclusion. If the author's description was brief but a micrograph was provided, I assigned the structure to the same category as the well-studied examples that it most resembled. In a few cases when an author's explanation seemed unlikely, I noted the explanation in the spreadsheet but did not include that example in my analysis (for example, structural color attributed to a multilayer in a scale element that is morphologically typical, without a multilayer, in the micrograph provided). Filled-in windows likely involve modifications of both the crossribs and microribs in most cases. To simplify the analysis, I designated filled windows only as modified crossribs unless the author explicitly called them extended microribs (e.g. *Battus philenor*, Ghiradella, 1985).

Results

Scale morphology

The literature review identified 299 photonic nanostructures whose location in the scale anatomy could be determined. Nearly all of these structures were documented by at least one micrograph; exceptions were species in larger studies that were simply described as having the same scale anatomy as a relative for which data was shown (Giraldo, Yoshioka, Liu, & Stavenga, 2016; Wilts et al., 2015). The large majority of these structures were recognizable as belonging to the same category as one of the examples presented in Fig. 1, at least in general terms (allowing for variation in the number of layers in a multilayer, the angular orientation of the layers, the filling fraction of crystals and perforated multilayers, etc.).

There were multiple examples of photonic structures in each scale part (Fig. 2). Perforated multilayers were the most common structure, with 77 examples. Ridge structures were nearly as common, with 69 occurrences, all multilayers. Microrib photonic structures were the least common (19 examples) and the most likely to co-occur with another photonic structure elsewhere in the scale. Microrib structures were also morphologically heterogeneous. Most of the microrib structures were multilayers, many reminiscent of ridge multilayers, however the angle of the multilayer relative to the scale lamina was more variable. In *Troides magellanus* and *Rapala manea*, microrib multilayers were oriented nearly vertically, which produces only grazing-angle reflectance (Lawrence et al., 2002; Tilley, Eliot, & Yoshimoto, 2002). *Trogonoptera brookiana* had a unique microrib multilayer in which the microribs were large and extended nearly continuously over the full scale (Wilts, Giraldo, & Stavenga, 2016). Three microrib structures in *Battus* species were partly filled windows that formed a thin film (Ghiradella, 1985). Crossrib structures were also very heterogeneous. There were 31 crossrib modifications of which 20 were filled windows and four, all *Papilio* species, were 2D crystals (Trzeciak, Wilts, Stavenga, & Vukusic, 2012). *Euptychia tricolor* and *Lamprolenis nitida* had flattened, tiled crossribs, suggested to form a multilayer (Ingram & Parker, 2008). It was disputed whether *Papilio zalmoxis*' proposed crossrib structures played a role in producing color, or whether the color was really pigmentary (Huxley, 1976; Kinoshita, Yoshioka, & Miyazaki, 2008; Prum, Quinn, & Torres, 2006). There were 40 lumen multilayers, including 6-10 *Papilio* species with the entire multilayer surface deformed into an array of regular concavities, which create color mixing (Vukusic et al., 2000). This last count is approximate because several micrographs looked potentially curved, but there was no statement on whether the curvature affects color. Three Pierid species with scattering pigment granules were reported (these are "other" structures in Fig. 2). Lastly, there were 33 lamina thin films

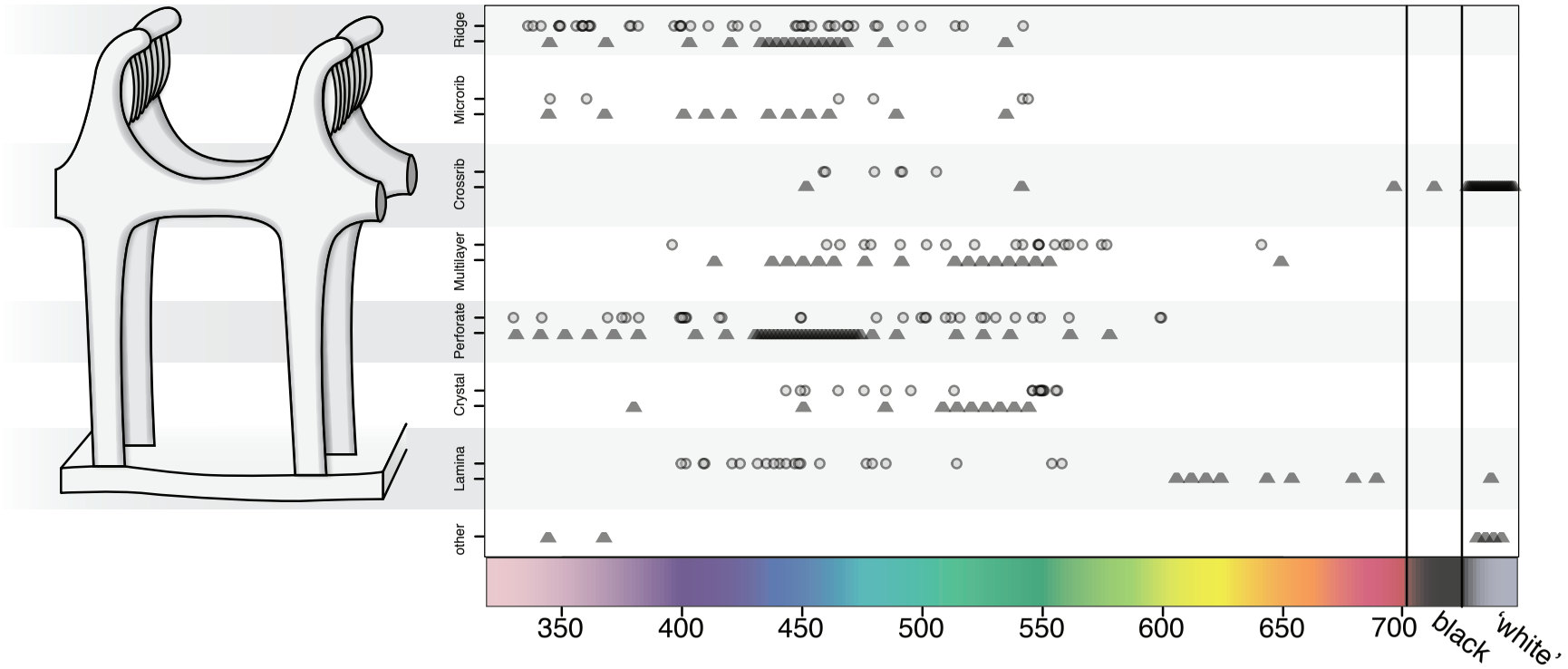

Figure 2: Peak structural color wavelengths, shown clustered by type of scale modification. Each point represents one characterized photonic structure. When quantitative reflectance spectra were reported, the peak wavelength is plotted as a circle. When the authors qualitatively described the color (e.g. “blue,” “UV”) or showed a color photo, the color is plotted as a triangle. Broadband reflectance spectra, such as white, silver, golden, or copper colors, do not have one peak reflectance wavelength and are also plotted as triangles.

and 29 3D crystals (including an *Urbanus proteus* bristle structure that the author describes as a lattice, although the micrograph looks less ordered than other reported crystals (Ghiradella, 1984)).

A subset of the scales were more distinctive, having multiple photonic structures, loss of scale parts, or other peculiarities. Two species' scales had lost the micro- and crossribs. They were reported to have UV reflectance; the mechanism was unclear (*Archon apollinus* and *Parnassius hardwickei*, Ingram & Parker, 2008). Even more severely reduced scales had only "paper maché" vertical structures (*Elbella polyzonella*, Ghiradella, 2010). A few studied scales contained multiple photonic structures. For example, *Chliaria othona* had both a perforated multilayer and a microrib multilayer (Tilley et al., 2002). *Heliconius sara* and *Morpho deidamia* had both a lamina thin film and a ridge multilayer (Giraldo et al., 2016; Wilts, Vey, Briscoe, & Stavenga, 2017). *Lamprolenis nitida*, *Caligo memnon*, and *Caligo beltrao* have microrib multilayers that slant in opposing directions to the ridge multilayers (*Caligo*, Ghiradella, 1991; Ghiradella, 1994) or crossrib multilayers (*L. nitida*, Ingram & Parker, 2008) in the same scale. In certain scales, the anatomy of each part was typical, but the scale's orientation changed the optical effects. *Carystoides escalantei*'s scales have typical anatomy but stand vertically, perpendicular to the wing membrane, with both the micro- and crossribs suggested to cause incoherent scattering (Ge et al., 2017). In *Pierella luna*, the distal tip of each scale curled over, making the crossribs form a vertical grating (Vigneron et al., 2010). Many of these peculiar scales have only been described with a single micrograph and are excellent candidates for further investigation.

Wavelength

To define the color gamut that butterfly photonic structures produce, I recorded the color of each specimen, using quantitatively measured peak reflectance wavelength values when possible (Fig. 2, circles) and a qualitative descriptor of color for broadband reflectors and when no spectra were available (Fig. 2, triangles). Long wavelength structural colors were extremely rare. While it is often informally repeated that, as a general rule, blue and green colors in animals are structural colors, I was surprised by how sharply divided the color space was. Only three structural colors had a defined spectral peak with maximum reflectance at or above 600 nm. Of these, the longest wavelength specimen was *Ornithoptera croesus lydius*, reported to reflect at 640 or 670 nm by different studies (Kazama et al., 2017; Zhang et al., 2014). The next longest wavelength structural colors were the perforated multilayers of *Chrysozephyrus brillantinus* and *Jalmenus evagoras*, which both had reflectance peaks around 600 nm (Wilts, Leertouwer, & Stavenga, 2009). *J. evagoras* has a relatively broad reflectance peak, and by eye looks a weakly saturated green color; *C. brillantus* looks yellow-green. Additionally, one multilayer structure was qualitatively described as 'bronze,'

(*Heliophorus brahma,* Ingram & Parker, 2008) and eight thin films were broadly reflective in long wavelengths, resulting in golden and copper colors (Stavenga et al., 2014a; Stavenga, Leertouwer, & Wilts, 2014b; Thayer et al., 2020). All colors between 350-550 nm occurred many times. Broadband reflectance colors, including white, silver, and pearlescent, were common as well. There were several reports of structurally-enhanced black, although all such examples were also melanic (Davis, Nijhout, & Johnsen, 2020; Sackey, Berthier, Maaza, Beuvier, & Gibaud, 2018).

The color red deserves special consideration. It is striking that although red is a common wing color, only three structures among 361 could be described as reddish. Two were lamina thin films, with modest reflectance in both far red and violet that combined to a dim magenta (Thayer et al., 2020). *Lamprolenis nitida* males reflect brightly at 700-800 nm, but only under controlled lighting conditions: the wing must be both illuminated and viewed from a grazing angle in the anteroposterior direction (Ingram, Lousse, Parker, & Vigneron, 2008). Yet there are examples of structural red from other Lepidoptera. Sunset moths have red scales with multilayers that reflect 700-800 nm (Yoshioka & Kinoshita, 2006), and under high humidity, the green forester moth's multilayer structures reflectance approaches 700 nm (Wilts, Mothander, & Kelber, 2019). Taken together, there is evidence that structural red is possible in lepidopteran scales, but there are no compelling examples of a butterfly with a red wing that is predominantly structurally colored.

Intersection of morphology and wavelength

I next investigated how scale morphology informs or constrains the color gamut (Fig. 2). The most accessible section of the color spectrum was 450-550 nm, as these wavelengths were generated by structures in every part of the scale. Lamina thin films and perforated multilayers produced the broadest swaths of the color spectrum, making them the most versatile structures in terms of wavelength. No ridge, microrib, or lumen crystal structures reflected long wavelength colors. 3D crystals may be restricted to 440-560 nm: there is one report of a violet crystal lattice in an unspecified *Hypochrysops* species (Morris, 1975) but no quantitative color measurement. This structure is known only from one older, low-resolution micrograph, so it is hard to be sure whether this sample is in fact a crystal rather than a perforated multilayer, as in *Hypochrysops delicia* and *H. polycletus* (Ingram & Parker, 2008; Wilts et al., 2009). Follow-up on this outlier, or identification of other 3D lumen crystals that reflect outside blue and green, would be interesting. If indeed there are no violet crystals, then only ridge, microrib, and perforated multilayers optimally reflect UV.

Phylogenetic distribution of structural color

To investigate which taxa have the most photonic structures, I compared the number of species with the number of described structural colors in each subfamily (Fig. 3). I found that reports of photonic structures are very unevenly distributed. Morphini and Papilioninae have the most described structural colors, although these groups include many fewer species than, for example, Hesperiinae, Pyriginae, Riodininae, or the rest of Satyrinae. Possibly, taxa with disproportionately more described photonic structures (i.e., taxa with a much longer blue bar, Fig. 3) really do have more structural coloration. However, there are certainly many uncharacterized iridescent blues and greens among the speciose taxa with few reported structures (i.e. subfamilies with a much longer red bar, Fig. 3). For example, blue wing displays show interesting patterns of convergence in Hesperiidae (Li et al., 2019). Given that scale anatomy has been investigated in few of the roughly 18,000 butterfly species, it is more likely that the current distribution only highlights which taxa have been understudied to date. An attention bias in favor of groups like Morphos, Lycaeninae, and Papilionids may be explained by the fact that the first elaborate structures were discovered in species from these clades, generating sustained interest in their relatives. Yet now, more research on structural color in the understudied groups is needed to flesh out evolutionary patterns of convergence, homology, and constraint in photonic nanostructures. Less-studied groups, including small subfamilies, may actually present the best opportunities to find novel structures, because more independent evolutionary history presents more opportunity for divergence.

Although the phylogenetic distribution of structural color is certainly still coming into focus, overlaying morphology and color on the phylogeny reveals some interesting trends (Fig. 4). Ridge multilayers and broadband reflecting scales with filled windows have evolved convergently many times. By contrast, perforated multilayers are taxonomically constrained. Although they are the most commonly reported type of structure, they occur almost exclusively in Lycaenidae, with one exception in Satyrinae (*Euptychia cephus*, Ingram & Parker, 2008). Dimpled lumen multilayers and crossrib-derived 2D crystals occur only in Papilioninae. Butterflies in the subfamily Nymphalinae use structural colors to produce a broader color range than any other subfamily, even though only three types of structures occur in this group, namely ridge multilayers, lumen multilayers, and lamina thin films. Riodinid butterflies also produce an impressive range of colors, given that they use only ridge multilayers, and that only a few species have been studied. Blue wavelengths occur in more subfamilies than the rest of the rainbow, although all hues from UV to green occur in most subfamilies that have more than a handful of described structures. Papilioninae is the only subfamily for which photonic structures have been reported in every scale part, and Satyrinae has the next most morphological diversity. It is intriguing that most of the peculiar scales

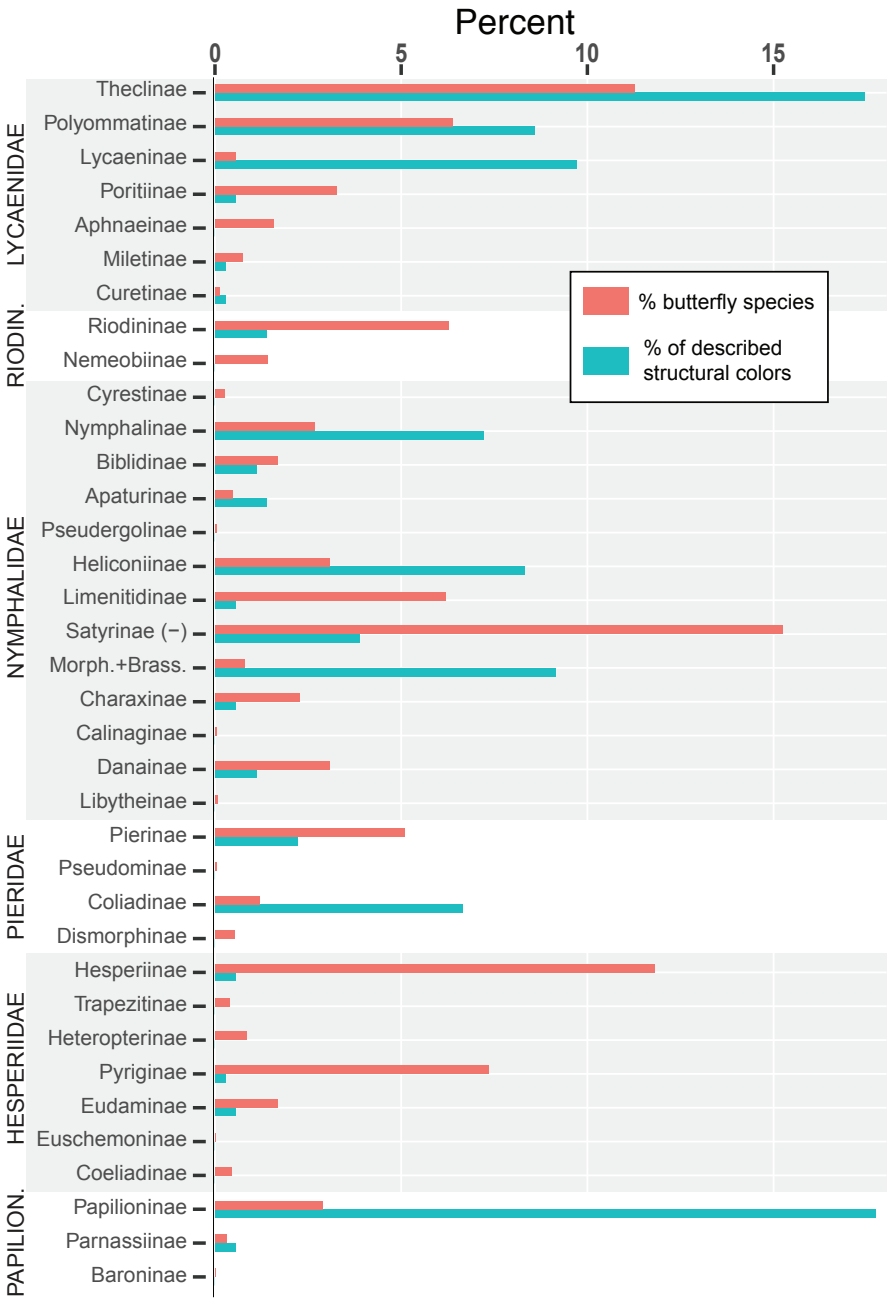

Figure 3: Reports of photonic structures are unevenly distributed among butterfly subfamilies. The vertical axis lists groups of butterflies by family and subfamily. Morphini and Brassolini (Peña et al., 2006) are displayed separately from the rest of Satyrinae because the photonics of scale structures in this clade have been intensively studied. Red bars show the percent of described butterfly species that belong to each subfamily. Species counts are approximations only, based on (Boyle et al., 2015; Mielke, 2005; Shields, 1989) and Wahlberg & Peña's nymphalidae.net database, which compiles findings from dozens of papers (e.g. Heikkilä, Kaila, Mutanen, Pena, & Wahlberg, 2012; Peña et al., 2006). Blue bars show the percent of all described structural colors that occur in each subfamily. Subfamilies with a much larger proportion of described species than of described structural colors have likely been understudied to date, and are among the best candidates for future photonics investigations.

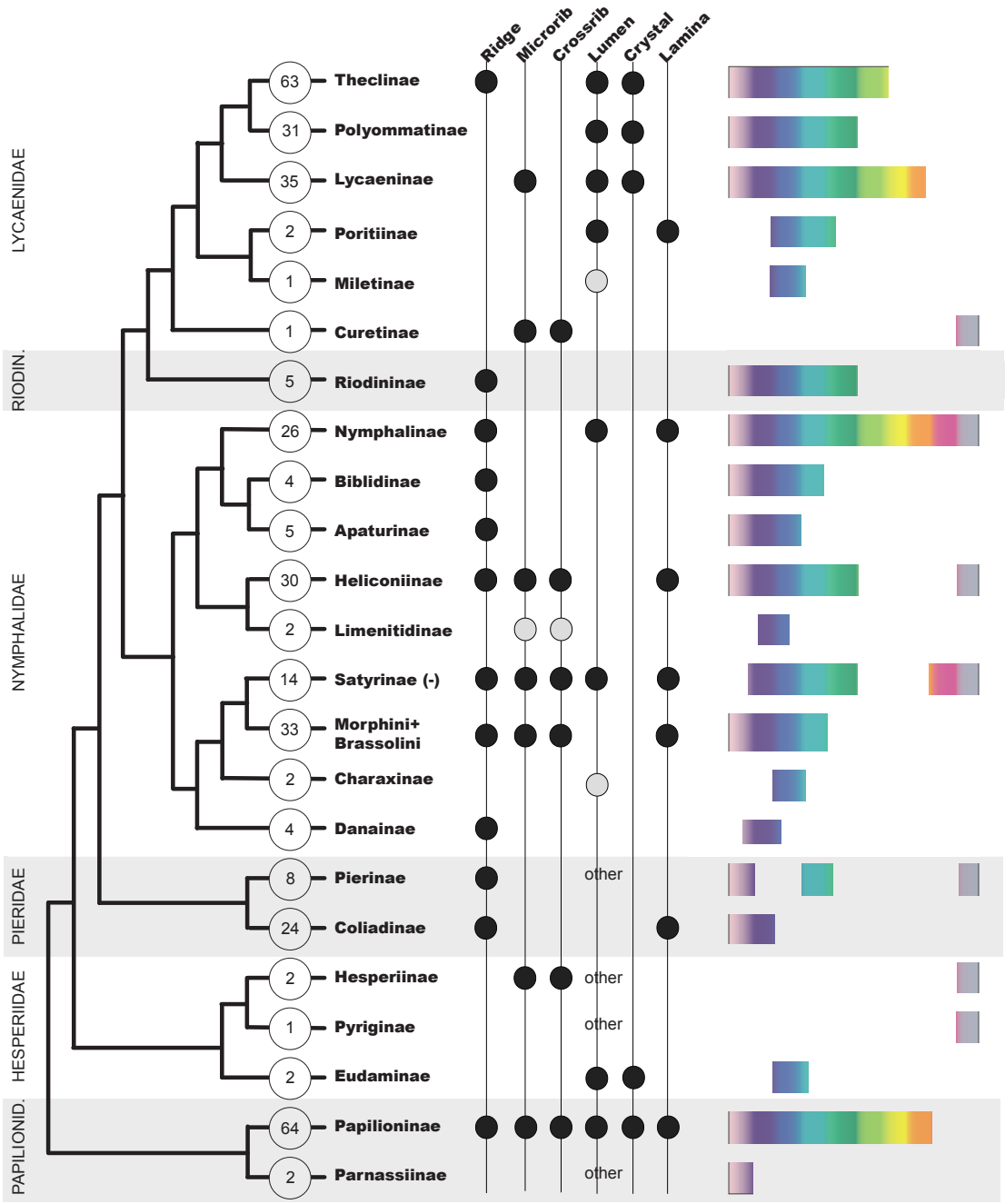

Figure 4: Distribution of photonic scale modifications and color by subfamily. At left is a butterfly cladogram based on Espeland 2018, with a tip for each subfamily that has at least one reported photonic structure. Morphini and Brassolini are displayed separately from the rest of Satyrinae because scale structures in this clade have been intensively studied. Bubbles at the cladogram tips contain the number of described photonic structures per subfamily. The middle section shows which parts of the scale form the photonic structures ('Lumen' includes both smooth and perforated multilayers). Black circles show reported structures. A grey circle means there is only suggestive evidence that the structure occurs (for example, the structure in passing in a larger work without data, or the specimen's identity was imprecise). "Other" can mean scattering by pigment granules (Pierinae); vertical scales (Hesperiinae, Ge 2017), or reduced scales (Parnassiinae, Ingram 2008) with crinkled, "paper maché" structures (Pyrginae, Ghiradella 2010). Right column shows which colors are produced structurally in each subfamily. From left to right: UV, the visible spectrum from violet to red, and broadband reflection (e.g. white, silver).

("other" in Fig. 4 and described in the Morphology section) are found in subfamilies that have been studied very little. This pattern further suggests that such taxa well deserve more research.

Biological processes that generate structural color

Developmental genetics

Relatively little is known about how photonic structures in butterfly scales develop, but some details are available. Normal scale development begins with the specification of scale cells by Delta-Notch signalling and *As-c* expression, a homologous process to the specification of sensory bristles in *Drosophila* (Galant et al., 1998; Reed, 2004). As development proceeds, the scale cell grows apically outward from the wing membrane (Stossberg, 1938), and actin rods, which are regularly arranged intercalating the future positions of ridges, appear to assist with apical extension (Dinwiddie et al., 2014). Once the scale cell has reached full length, it flattens, which may be mediated by microtubules (Overton, 1966). Finer structural elaboration occurs, then chitin is deposited. The actin filaments subsequently break down, and pigments are deposited late, shortly before the adult's emergence from the pupa (Iwata, Ohno, & Otaki, 2014; Koch et al., 1998). TEM micrographs of developing ridge multilayer (*Colias eurytheme*, Ghiradella, 1974) and gyroid (*Callophrys rubi*, Ghiradella, 1989) scales provide some insight on how the photonic structures are formed. The gyroid scales have expansive and convoluted endoplasmic reticulum membranes, which appear to be important for organizing the crystal domains. Moreover, because pockets of crystals are biggest at the distal tip of mature scales, both (Ghiradella, 1989) and (Wilts et al., 2017) have suggested that crystals begin developing earlier at the distal tip.

Relatedly, the molecular and genetic regulation of photonic structures is largely mysterious. Structural colors must be patterned on at least two levels: first, it must be determined which scale cells will go on to differentiate into structurally colored scales--this sets up the distribution of photonic structures across the mature wing surface. Second, individual photonic structures must be patterned and built, each within a single cell. Even small deviations in a structure's dimensions can shift wavelength dramatically, so patterning at the second level must be precise and repeatable. In both cases, the genes that regulate patterning are almost entirely unknown. The first study on the genetics of butterfly structural colors tracked inheritance patterns in experimentally crossbred *Colias* butterflies and concluded that the presence of UV-reflective ridge multilayers was controlled by a single sex-linked gene (Gerould, 1943; Silberglied & Taylor, 1973). More recently, it was found that the color and spacing of ridge multilayers in *Heliconius erato* are also sex-linked, but controlled by multiple genes

(Brien et al., 2019). A pair of recent papers used CRISPR/Cas9 genetically engineered *Junonia* butterflies to show that the gene *optix* determines a switch between whether scales will produce thick, blue lamina thin films or thinner golden ones (Thayer et al., 2020; Zhang, L., Mazo-Vargas, & Reed, 2017). *Optix*, a gene previously known for its role patterning pigmentation in butterflies (Reed et al., 2011), is the first specific gene known to regulate structural colors. These initial findings open the door wider to address the many remaining questions, especially what class of genes work on the second level of patterning. Are nanostructures molded directly, such as via cytoskeleton and membrane folding dynamics, or do structures self-assemble under the indirect influence of genes that regulate pressure and osmolarity in the cell? It is also unknown the extent to which the same genes may pattern both the distribution of structurally colored scales across the wing and the dimensions of the structures themselves. While we have only small hints about the genetic regulation of lamina thin films and ridge multilayers, nothing is yet known about the genetic basis of the other kinds of nanostructures.

Evolution

This review is the first attempt to look holistically at the phylogenetic distribution of structures across all butterfly families. Although the picture is certainly still incomplete, as previously discussed, we can make several observations. To briefly repeat, all hues between UV and green are common across families, although blue is the most common. Long wavelength structural colors are exceptionally rare. In terms of morphology, ridge multilayers and filled windows have evolved convergently many times, while perforated multilayers, 2D crossrib crystals, and lumen multilayers that also have a tertiary dimpled structure are phylogenetically limited. Photonic structures derived from micro- and crossribs are the most morphologically heterogeneous. Some previous studies also speak to macroevolutionary dynamics of butterfly structural colors. Because the undifferentiated scale bauplan has a lower lamina that is morphologically suitable to be a thin film reflector, and because lamina thin films have been reported in disparate butterflies and moths, (Thayer et al., 2020) argued that lamina thin films were likely present in the common ancestors of Lepidoptera, and are likely much more common than has yet been reported. (Wilts, IJbema, & Stavenga, 2014) hypothesized that perhaps lumen crystals evolve from ancestors with a lumen multilayer and discussed this interesting idea in the context of a parsimony-based phylogeny for the genus *Parides*, but the parsimony tree did not agree with the best available molecular phylogeny. A larger, phylogenetically robust study on character state changes in photonic structures could be interesting. Taken together, we have only an immature understanding of broad macroevolutionary patterns.

Fortunately, variation among smaller sets of closely related species is rather better studied. A number of studies have systematically examined structures in a set of closely related species, such as for the following genera: *Morpho*, *Argynnis*, *Cyanophrys*, *Ornithoptera*, *Junonia*, *Polyommatus*, *Parides*, and *Heliconius* (Bálint, Moser, Kertesz, Biró, & Parker, 2009; Bálint, Kertész, Piszter, Vértesy, & Biró, 2012; Giraldo et al., 2016; Kazama et al., 2017; Parnell et al., 2018; Simonsen, 2007; Thayer et al., 2020; Wilts et al., 2014). Genera-focused studies mainly find that essentially similar structures exist in many related species, which is useful for unraveling how small modulations in the structure, e.g. ridge density, number of layers, tapering, or thickness each affect the structure's optical properties. In addition to being evolutionarily interesting, these are among the best case studies on how each parameter of a photonic structure affects hue, brightness, and angle-dependence.

Most species' structures have been characterized from only a single individual, and often from only one scale. This is problematic from a sample size and replication perspective, but it also points to an opportunity for better evolutionary research. Variation within and between populations is the substrate on which evolutionary selection acts, but it has been examined very little. The best population-level work to date, by Bálint and Biró, carefully outlines individual and population variation in *Polyommatus* butterflies. Spectra of *P. icarus* butterflies are stable between seasons and over 100 years within Hungary, but vary biogeographically across Eurasia (Kertész, Piszter, Bálint, & Biró, 2019). Although *P. icarus* has cold-stress induced plastic responses, including melanization and disordered scales, photonic structure reflectance was not plastic in males (Kertész, Piszter, Horváth, Bálint, & Biró, 2017). By contrast, cold stress induced ectopic blue scales in females. In *P. dorylas*, photonic structures are invariant between bivoltine lowland and univoltine upland populations (Bálint et al., 2019). Given that *Heliconius* species and color races are interfertile, descriptions of their structures are helpful here as well (Parnell et al., 2018). Lastly, two studies documented rapid evolutionary responses to artificial selection on structural color in *Bicyclus anynana* and *Junonia coenia* (Thayer et al., 2020; Wasik et al., 2014). In both studies, thin film laminae increased thickness, producing violet and blue reflectance. These rapid evolved responses point to selectable standing variation in the studied populations before artificial selection, a useful contrast to the largely invariant structures in *P. icarus* populations. More studies of how structures vary between individuals and populations will be crucial, because variation at this level is the most useful tool to unravel genetic control of variation, such as with association mapping, breeding experiments, or comparative transcriptomics.

Discussion

In this review, I have examined how photonic structure morphology interacts with wavelength across butterfly taxa. It should be kept in mind that photonic structures have more properties than just the maximally-reflected wavelength, including spectral purity, brightness, angle-dependence, polarization, and how specular or diffuse the reflections are. All of these properties differ among the structures I have reviewed, and certainly not all "blue" structures that have peak reflectance at 400 nm are functionally equivalent. By considering structures' full optical properties, more differences between classes emerge, and these likely help explain evolutionary patterns. For example, although I have shown that lamina thin films are among the most versatile structure types in terms of wavelength, thin films never reflect more than 20% of incoming light, making them much dimmer than multilayers and 3D crystals. Ridge multilayers are highly iridescent, while gyroids with chirped domains in each scale are not; this may make the former better for flashy sexual signaling and the latter more optimal for camouflage against a green leaf. With spectra that were not acquired or processed uniformly, it was not possible to compare all these properties, but a future study that uses full spectral data and interprets it in butterfly vision color space would be enlightening.

Structural colors frequently co-occur with pigments on the same wing or in the same scale, and interactions between them are consequential. By absorbing off-color light that would otherwise be backscattered, a layer of melanin under or behind a structural color makes the structural color more saturated (Giraldo et al., 2016; Siddique, Vignolini, Bartels, Wacker, & Hölscher, 2016). The Queen Purple Tip butterfly, *Colitis regina*, has scales with both a red pigment and a blue structural color, and these colors spectrally mix to generate an overall purple color (Giraldo, Yoshioka, & Stavenga, 2008). UV structural colors can also be combined with longer wavelength pigmentary colors, as in *Colotis danae* (Wijnen, Leertouwer, & Stavenga, 2007). In addition to spectral mixing when they co-occur, pigments can also directly alter reflectance and structural coloration by changing the shape and refractive index of the scale. For example, chitin suffused with melanin has a higher refractive index than pure chitin (Noyes, Vukusic, & Hooper, 2007; Stavenga, Leertouwer, Hariyama, De Raedt, & Wilts, 2012). Structurally-enhanced "ultra black" scales are all melanic, but according to modeling work (Davis et al., 2020), it is actually melanin's effect on the refractive index, rather than its absorption properties, that is required to suppress reflection in such scales. In pierids with pigments clustered in granules, the granules also cause incoherent scattering (Morehouse, Vukusic, & Rutowski, 2007).

Blue and green structural colors are common, while long wavelengths are extremely rare. Interestingly, the pigment color gamut is arguably the opposite. Blue pigments are rare (but see *Graphium sarpedon*, Stavenga, Giraldo, & Leertouwer, 2010) and yellow, red, and brown pigments are common, along with melanin. Why is color space so crisply divided between pigments and structural colors? Is either blue pigment or red structural color fundamentally hard to biosynthesize or evolve? Are there fundamental physical constraints on one that make the other functionally better? Alternatively, the answer may lie in the coevolutionary history of pigments and structural colors. It would be helpful to know the relative ages of each family of pigments, compared to the earliest appearances of different types of photonic structures. For example, if pigments are older, do photonic structures mainly arise in short wavelengths to fill the gap in color space? The answers to many exciting questions await in the next century of research on butterfly structural color.

Chapter 2

Structural color in *Junonia* butterflies evolves by tuning scale lamina thickness

This chapter has been published in Thayer, R. C., Allen, F. I., & Patel, N. H. (2020). *Elife 9*, e52187.

Introduction

Structural colors are both visually delightful and abundant in nature. Organisms deploy structural colors to display hues for which they lack pigments (frequently blues and greens), to create specific optical effects such as iridescence or light polarization, and to mediate ecological interactions, including intraspecific signaling and camouflage. Unlike pigmentary color, which is caused by molecules that selectively absorb certain wavelengths of light, structural colors result from the constructive and destructive interference of light as it interacts with nanoscale, precisely-shaped physical structures that are made of a high refractive index material (e.g. keratin, chitin, or cellulose).

Despite the clear importance of structural color for living systems, the biological production of structural colors has long eluded characterization (Cuthill et al., 2017). Many experimental techniques depend on harnessing variation to dissect biological processes, but photonic structures are so small that quantitatively measuring variation in their dimensions is technically demanding, especially for high-throughput sampling, detecting subtle variation that may segregate within populations, or analyzing over developmental time *in vivo*. The color itself is easier to quantify, but has limited utility as a proxy for nanostructural dimensions, since structural colors and pigments often co-occur and covary. While recent studies (Brien et al., 2019; Matsuoka & Monteiro, 2018; Parnell et al., 2018) have made early headway toward describing genetic regulation of structural colors, much work remains to decipher the evolutionary, developmental, and genetic bases of structural coloration, and lab-tractable systems with intraspecific variation in structural coloration are needed. We present a promising system, the butterfly genus *Junonia,* with extensive variation in a simple structural color, and show how structural simplicity is a tactical advantage when seeking to unravel mechanisms for the biological production of nanostructures.

In butterflies, photonic nanostructures occur within the architecture of scales. Scales are the fundamental coloration unit on butterfly wings and have a Bauplan consisting of a grid of ridges and ribs, supported by a lower lamina that is a simple plane (Fig. 1A). Scales are composed of chitin and may also have embedded pigments. Intricate architecture and a high refractive index make scales a pliable substrate for photonic innovations, and indeed scales have been evolutionarily elaborated in many ways for impressive optical effects (Ghiradella, 1985). Even the simplest butterfly scales can produce structural color, via the lower lamina acting as a thin film reflector. Thin films are the simplest photonic structure and consist of a layer of high refractive index material, on the order of hundreds of nanometers thick, surrounded by a material with a contrasting refractive index, i.e. air (Fig. 1B). Light is reflected from each surface of the film, and these two reflections interfere with each other. If the two reflections remain in phase, which depends on the extra distance traveled through the film and the wavelength, then they interfere constructively to produce observable color (Mason, 1927; Yeh, Yariv, & Cho, 1978). Conversely, wavelengths (colors) that undergo destructive interference have decreased brightness.

While it is known that the thickness of the lower lamina is one parameter that controls structural color wavelength (Stavenga, Leertouwer, & Wilts, 2014a) and that thickness can respond to artificial selection in the laboratory (Wasik et al., 2014), it is not known how general this mechanism is in natural evolution. It is also unknown how lamina structural colors are genetically regulated and whether any recognized butterfly wing patterning genes regulate lamina thickness. Here, we use mutants with deletion of the *optix* wing patterning gene, artificial selection on wing color, and genus-wide wing color variation to test the role of lamina thickness in generating butterfly color. We show that butterflies in the genus *Junonia* thoroughly exploit the relationship between film thickness and color, using the thin films necessarily present in their scales to produce a broad spectrum of hues by tuning lamina thickness. These lamina colors work in tandem with pigments to define the wing pattern elements that distinguish populations, sexes, and species, indicating that the ability to vary lamina thickness has been an important microevolutionary and macroevolutionary tool in this group, and likely in butterflies more broadly.

Results

Artificial selection for blue wing color increases lamina thickness

Here we describe a novel instance of rapid, artificially selected color shift from brown to blue wing color in *J. coenia* buckeye butterflies (Fig. 1D-E) and identify the structural changes that enabled the color shift. Edith Smith, a private butterfly breeder, began

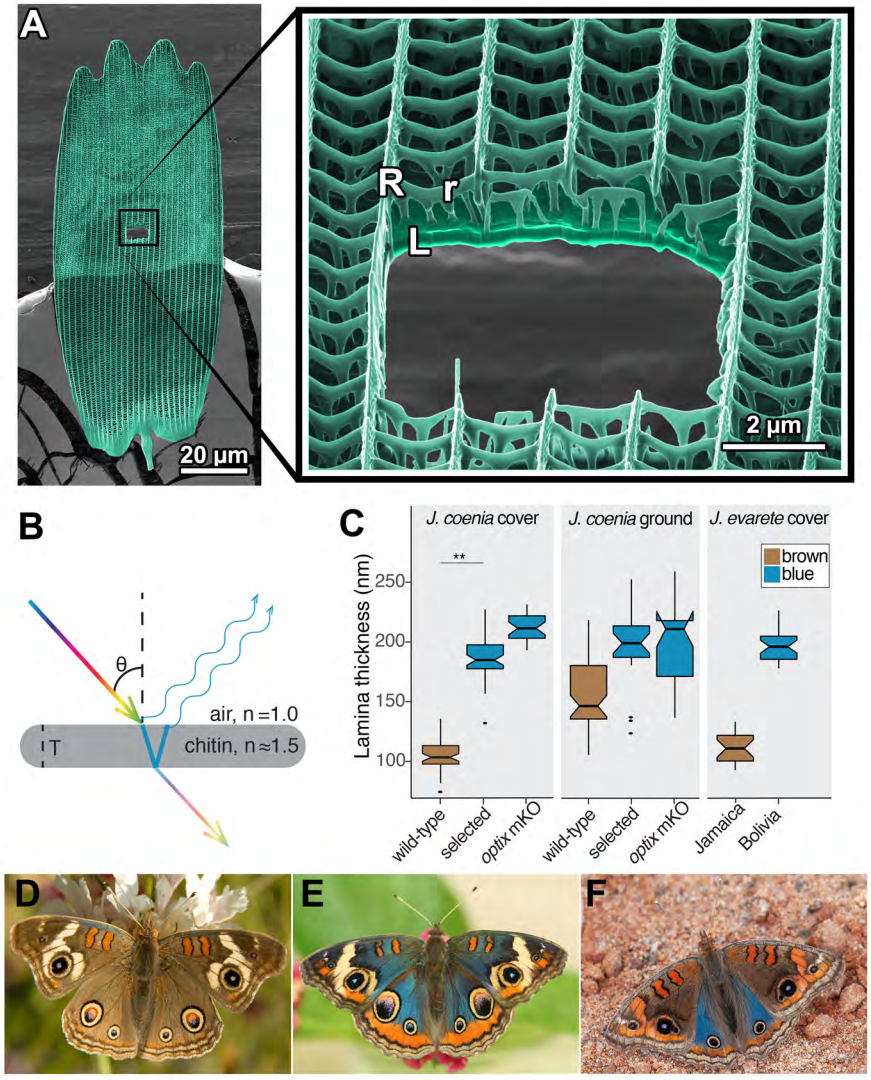

Figure 1: The lamina of a typical butterfly scale functions as a thin film reflector. (A) Colorized helium ion micrograph of a nymphaline scale, with a window milled using a gallium focused ion beam. Inset at higher magnification, with labels for general architectural components of a scale (R = ridges, r = cross-ribs, L = lamina). (B) Diagram of reflection and refraction in a chitin thin film. White light enters, reflections are produced at each surface of the film, and reflections of select wavelengths remain in phase as a function of film thickness (T). (C) Experimental disruptions of wing color are associated with altered lamina thickness. In *J. coenia*, artificial selection for blue color increased lamina thickness in both cover and ground scales. In optix mosaic knockout mutants, certain wing regions have similar thickness increases. This trend recapitulates natural variation in *J. evarete*, where blue butterflies have thick laminae relative to brown individuals. Bars show mean thickness, with error bars of one standard deviation. Minimum N= 20 measures drawn from different lateral and distal positions within 3 scales (see Methods). (*** = $p < 1x10\text{-}7$) (D) Wild-type *J. coenia*. (E) Blue artificially selected *J. coenia*. Image by Edith Smith. (F) *J. evarete*.

selectively mating buckeyes with a few blue scales on the costal margin of the dorsal forewing (E. Smith, personal communication, Sep. 2014). After five months of selective breeding, blue spread to the dorsal hindwing of some individuals. By eight months, there was a noticeable increase in blue surface area, and within roughly 12 months (on the order of 12 generations), most butterflies in the breeding colony were visibly blue over the majority of their dorsal wing surface. On the forewing, areas proximal to M1 were visibly blue, except the discal bars (Figure 1—figure supplement 1). On the hindwing, blue shift did not include the distal-most wing pattern elements, i.e. EI-EIII and eyespots. At its strongest, the phenotype may include blue scales cupping the posterior forewing eyespot and/or a blue sheen in all distal elements of the forewing. Smith maintained the blue colony for several years, introgressing a few progeny from crosses to wild-caught buckeyes about once per year to maintain genetic diversity. Over time, she noted the emergence of a variety of short-wavelength colors, ranging from purple to green. Two years after focused selection, she estimated that the population was 85% blue, 8% green, 2% purple, and 5% brown. Like many familiar examples of human selection (e.g. domesticated animals, crop plants), outcomes are informative even without complete experimental documentation of the selective process (Akey et al., 2010; Wright et al., 2005). These selected blue buckeyes provide a previously unexploited opportunity to study structural color. They demonstrate rapid and extensive evolutionary color change, and are a stark contrast to wild-type brown populations with which they are still interfertile. Conveniently, the artificially selected taxon, *J. coenia*, is a recognized model species for butterfly developmental genetics (Carroll et al., 1994; Nijhout, 1980a). The selected blue individuals resemble naturally evolved color variants in the sister species, *J. evarete* (Fig. 1F), and offer a useful comparison to a previously reported artificial selection experiment in butterflies (Wasik et al., 2014).

To pinpoint the cause of blueness in artificially selected butterfly scales, we characterized cover scales from the dorsal hindwing (Fig. 2A-D). Butterfly wings have two classes of scales arranged in alternating rows that form two layers: superficial cover scales and underlying ground scales. Cover and ground scales frequently have contrasting size, shape, and color, and their juxtaposition can be important for wing color (Stavenga et al., 2014a). When isolated and laid in the abwing orientation they occupy on the wing, cover scales were blue (Fig. 2B). However, when flipped over and viewed in adwing orientation, which exposes only the lower lamina, scales appeared more brightly blue and iridescence was more apparent (Fig. 2B′, 2D). We tested whether the blue was structural rather than pigment-based by immersing the full scale in oil with a refractive index matched to that of chitin (Fig. 2B′′′). Index-matching eliminates the possibility of reflection and structural color, leaving only pigment-based coloration. We measured the scale's absorption spectrum under these conditions (Fig. 3A), which

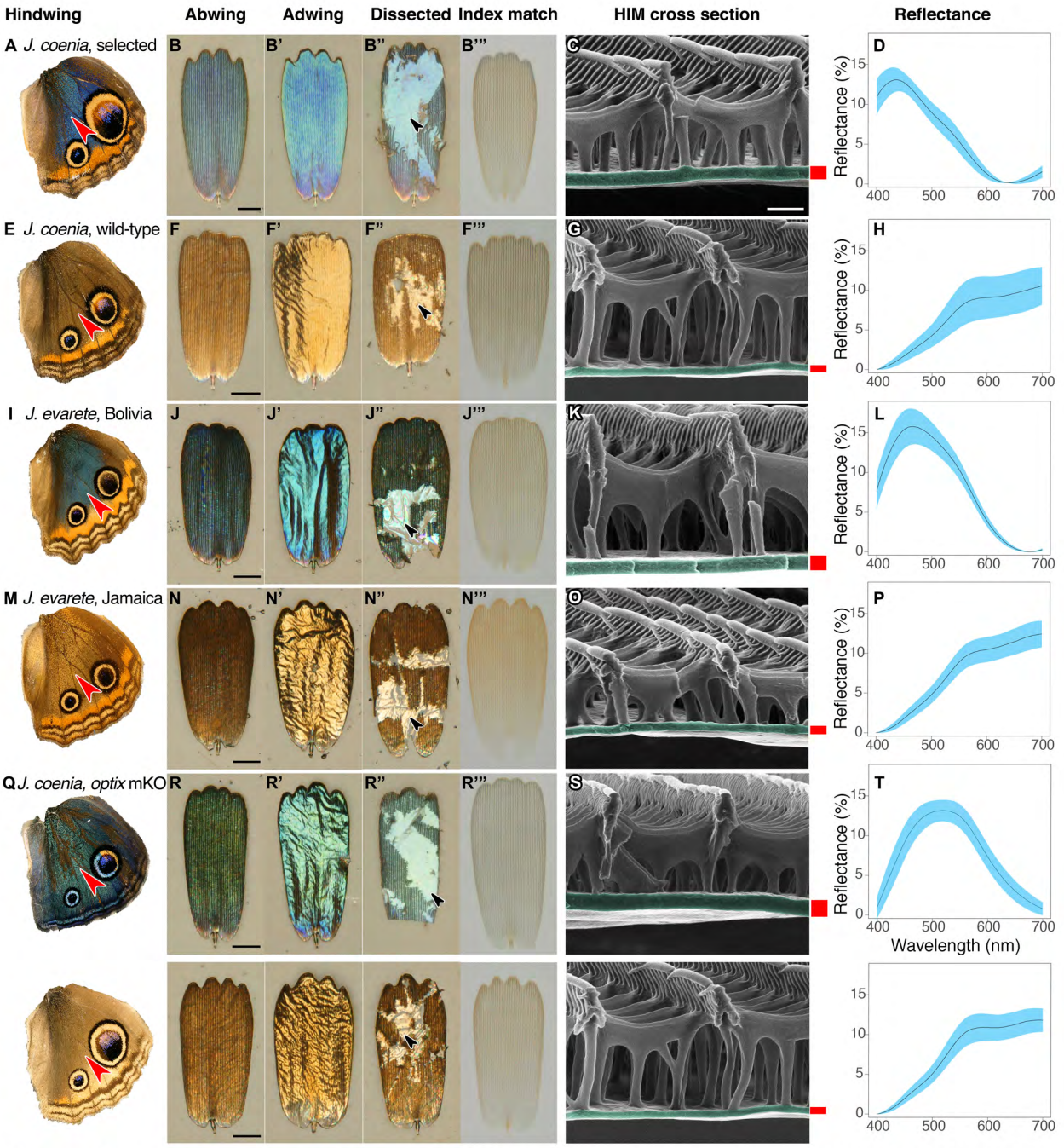

Figure 2: Structure and color of *Junonia* cover scales. (A-D) Artificially selected blue *J. coenia*. (E-H) Wild-type *J. coenia*. (I-L) *J. evarete*, blue male from Bolivia. (M–P) *J. evarete*, brown male from Jamaica. (Q-T) *optix* mosaic knockout mutant (mKO) in *J. coenia*. (A,E,I,M,Q) Dorsal hindwing, red arrowhead indicates the characterized scale's location. (B,F,J,N,R) Scale in the orientation it would occupy on the wing, showing the abwing surface of the cover scale. Black scale bars are 25 µm. (B',F',J',N',R') Adwing surface of cover scale, showing the underside of the lamina. (B",F",J",N",R") Dissected scale with arrow showing regions where all ridges and ribs are removed to expose the bare lamina. The lamina is sufficient to create iridescent blue and gold structural colors. (B"',F"',J",N"',R"') Scale immersed in fluid with a refractive index matched to chitin, thus eliminating reflection to show only pigmentary color. Blue and brown scales have comparable amounts of a brown pigment. (C,G,K,O,S) Helium ion micrograph of cross-sectioned scale. Each lamina is colorized, with approximate thickness indicated by an adjacent red bar (precise measurements were taken at sites chosen as in Methods). White scale bar is 500 nm and applies to all HIM images. (D,H,L,P,T) Reflection spectra for the adwing surface of disarticulated scales. Solid line is the mean spectrum, and blue envelope is one standard deviation; minimum N=3 scales per graph.

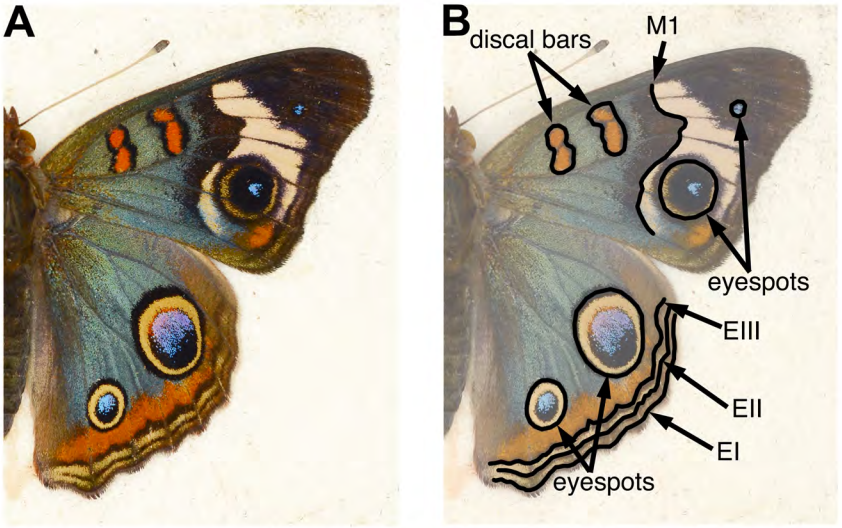

Figure 1—figure supplement 1: (A) The artificially selected blue phenotype in *J. coenia* includes much of the dorsal wing surfaces. (B) Pattern elements of the nymphalid ground plan (Nijhout, 1991), which delineate the boundaries of blue regions, are labeled: discal bars, distal band of central symmetry system (M1), eyespots, parafocal element (EIII), and marginal and submarginal bands (EI, EII).

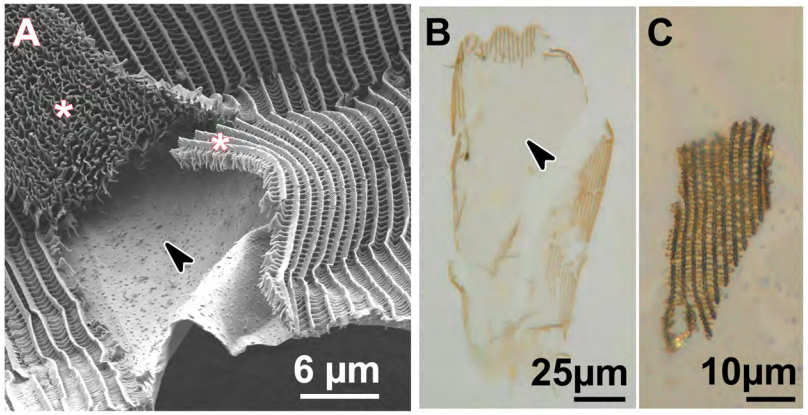

Figure 2—figure supplement 1 : Detailed characterization of dissected scales. (A) HIM image of a partially dissected scale. The arrow shows the exposed lamina and asterisks show detached swaths of all other scale components, i.e. ridges and cross-ribs. (B) Dissected cover scale from artificially selected *J. coenia* immersed in index-matched oil. Pigments are not primarily localized within the exposed lamina, shown by the arrowhead. (C) A swath of ridges and ribs removed intact from the scale in panel B. This piece of lamina-less scale is not blue.

revealed that blue scales did have some pigment, presumably a brown ommochrome (Nijhout & Koch, 1991), but this pigment cannot account for blueness. The pigment was located in the scale ridges (Fig. 2—supplement 1B). Lepidopteran structural colors may occur in the lamina, lumen, ridges, or cross-ribs. To isolate which of these features had the nanostructure responsible for blue structural color, we dissected the scales (Fig. 2B″, Fig. 2—figure supplement 1A). After removing all other scale components, we found that the bare lower lamina was sufficient for blue structural color. We also examined regions with all scale components except the lamina and found that these pieces of lamina-less scale were not blue (Fig. 2—figure supplement 1C). We thus focused on investigating nanostructure in the lamina. To discern between a single or multilayer lamina and take precise measurements, we cross-sectioned the lamina and viewed it with Helium Ion Microscopy (HIM) (Fig. 2C). HIM imaging indicated the lower lamina was a simple monolayer of chitin with a thickness of 187 ± 13 nm (SD, Fig. 1C), which is a reasonable thickness to reflect blue as a dielectric thin film (Stavenga et al., 2014a).

We next investigated whether ground scales also contributed to blueness after artificial selection. The ground scales generally had similar architecture to the cover scales, but with less uniform lamina color: ground scales exhibited a color gradient from the stalk outward (Fig. 4A-B′). Correspondingly, ground scales had a similar mean thickness but more variability than cover scales (190 ± 29 nm). Ground scales were much more heavily pigmented than cover scales (Fig. 3B, Fig. 4B″), such that the abwing surface was black (Fig. 4B). The extra pigmentation in ground scales enhances spectral purity by absorbing light transmitted through the cover scales, thus reducing backscatter and making the observed blue color more saturated (similar to Siddique, Vignolini, Bartels, Wacker, & Hölscher, 2016). We conclude that cover scale laminae are the major source of blueness in artificially selected buckeye butterfly scales, while melanic ground scales secondarily enhance spectral purity.

For comparison, we tested the source of color in wild-type brown scales and found that they also had structural color (Fig. 2E-H). Brown cover scales had the same general architecture and no significant difference in the amount of brown pigment compared to blue cover scales (Fig. 3A, Mann-Whitney *U*, Figure 3—table 1). The salient difference was lamina thickness: brown scales were markedly thinner, measuring only 109 ± 12 nm (Analysis of Variance (ANOVA), $p < 2x10^{-16}$, Fig. 1C, Fig. 2G). A 109 nm chitin thin film reflects a desaturated golden color due to reflectance of many long wavelengths. This golden structural color was confirmed by the adwing scale color, the color of the bare lamina in dissected scales, and the adwing reflectance spectra of brown scales (Fig. 2F′-F″, H). Therefore, though brown coloration is often attributed to pigmentation, wild-type brown cover scales also had a structural color, one simply tuned to enhance different wavelengths.

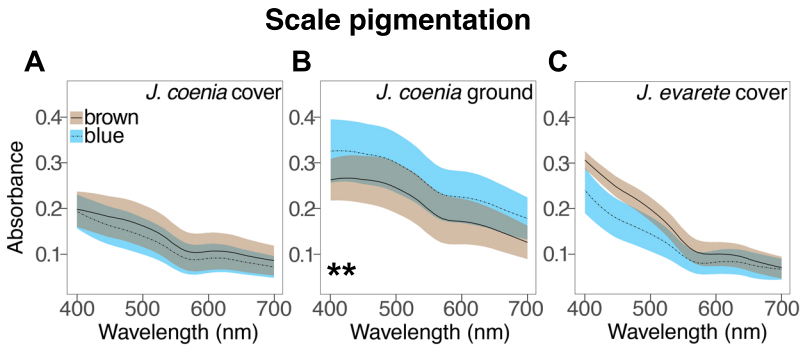

Figure 3: Absorbance spectra show the effect of artificial selection on scale pigmentation. (A) Absorbance measures in *J. coenia* wild-type (brown), and artificially selected (blue) cover scales show that both have comparable pigmentation (Mann-Whitney *U*, Figure 3—table 1). (B) Absorbance of selected *J. coenia* ground scales is increased relative to brown wild-type scales. (C) Absorbance does not differ between blue and brown *J. evarete* cover scales, and is similar to pigmentation in *J. coenia* cover scales. Plots show mean spectra with envelope of one standard deviation, minimum N=6 scales per sample.

***J. coenia:* wild-type vs artificially selected**

nm	WT cover mean	WT cover SD	AS cover mean	AS cover SD	*F*	*p*	
400	0.199	0.039	0.194	0.037	0.06	0.8111	
500	0.162	0.046	0.140	0.040	1.02	0.3223	
600	0.106	0.041	0.091	0.032	0.48	0.4950	
700	0.086	0.033	0.072	0.024	1.04	0.3170	
nm	**WT ground mean**	**WT ground SD**	**AS ground mean**	**AS ground SD**	***F***	***p***	
400	0.263	0.045	0.326	0.070	8.01	0.0085	**
500	0.245	0.055	0.300	0.065	5.66	0.0245	*
600	0.172	0.050	0.225	0.057	7.15	0.0124	*
700	0.126	0.037	0.178	0.046	11.39	0.0022	**

J. evarete

nm	brown mean	brown SD	blue mean	blue SD
400	0.307	0.020	0.240	0.050
500	0.199	0.026	0.145	0.038
600	0.100	0.026	0.083	0.026
700	0.071	0.024	0.067	0.023

Figure 3—table 1: Comparison of absorbance values for individual scales immersed in refractive index matched oil. Absorbances were compared using the Mann-Whitney *U* rank sum test, due to unequal variances between many of the comparisons. Mean absorbances are reported with standard deviation (SD), U, and exact p-value for selected wavelengths. Minimum N=6 scales per specimen/treatment, with 2 technical replicates of each scale. (* $p < 0.05$; ** $p < .01$) WT = wild-type. AS = artificial selection.

Artificial selection also altered the absorption and lamina thickness of the ground scales relative to wild type (Fig. 4A-D). The wild-type (brown) ground scales were thinner than the blue ground scales (151 ± 30 nm, ANOVA, $p = 2x10^{-6}$, Fig. 1C). However, the mean difference was less extreme than in cover scales: blue cover scales were on average 78 nm thicker than wild-type, while blue ground scales were on average 39 nm thicker. Selected ground scales were substantially more absorbing than wild-type ground scales (Fig. 3B, Mann-Whitney *U*, Figure 3—table 1), which is consistent with increased pigmentation that decreases backscatter in blue wing regions.

We conclude that the artificially selected buckeye butterflies rapidly evolved blue wing color via a 71% mean increase in lamina thickness in cover scales and a similar but less pronounced effect in ground scales. The effect was further amplified by increased pigmentation in ground scales, but without removing brown pigment from cover scales. Our results show that structural color can evolve quickly by modifying one dimension of an existing structure, and the process is facilitated by the initial presence of previously unrecognized structural color in wild-type brown *J. coenia*.

Since the artificially selected *J. coenia* wing pattern resembles natural iridescent variants in the sister species, *J. evarete* (Fig. 1F), we obtained hindwings of brown and blue *J. evarete* individuals from different geographic locations and tested whether blue cover scales in this species were also associated with increased lamina thickness (Fig. 2I-P). We found that the same mechanism explained color differences between geographic color variants: blue scales had 78% thicker scale laminae (blue 199 ± 14 nm; brown 112 ± 13 nm; ANOVA, $p < 2x10^{-16}$, Fig. 1C) and no appreciable difference in pigmentation, compared to brown individuals (Fig. 3C, Mann-Whitney *U,* Figure 3—table 1). Furthermore, in blue *J. evarete*, the ground scales were darkly pigmented. Thus, the artificially selected blue buckeyes recapitulate natural variation at the level of scale coloration between sister species.

Color phenotypes in optix mutants include altered lamina thickness

Recently, Zhang *et al*. used CRISPR/Cas9 to generate mosaic knockout mutants of *optix* (Zhang, Mazo-Vargas, & Reed, 2017), a gene previously associated with pigment variation in butterfly wings (Reed et al., 2011). Surprisingly, in addition to pigmentation phenotypes, *optix* mutants in *J. coenia* gained blue iridescence in wing scales. We tested phenotypically mutant blue scales from mosaic butterflies to determine what structural or pigmentary changes created the color change (Fig. 2Q-T). Where blue scales occured in the background region of the dorsal wing, blueness was due to similar factors as identified in artificially selected buckeye scales. Lamina thickness of blue cover scales was substantially increased compared to wild-type brown scales (212 ±11 nm, ANOVA,

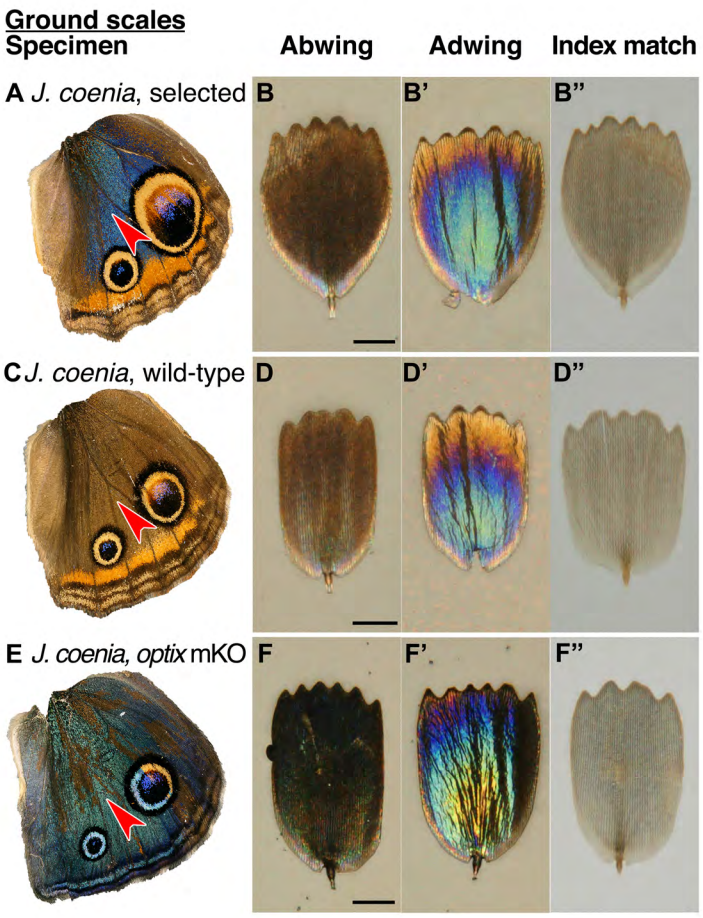

Figure 4: Structure and color of *J. coenia* ground scales. (A,C,E) Wings with red arrowhead indicating the region from which scales were sampled. (B,D,F) Scale in abwing orientation, i.e. ridges facing up. (B',D',F') Scale in adwing orientation, i.e. lamina facing up. (B",D",F") Scale immersed in fluid with a refractive index matched to chitin, thus eliminating reflection to show only pigmentary color. (A-B") *J. coenia* artificially selected ground scales. (C-D") *J. coenia* wild-type ground scales. (E-F") *optix* mKO mutant ground scales. Scale bars are 25 μm.

$p < 2x10^{-16}$, Fig. 1C). The concentration of brown pigment in the cover scales was significantly reduced relative to wild-type scales within the same mosaic wing (Fig. 5A, Mann-Whitney *U*, Figure 5—table 1) but comparable to pigmentation in artificially selected butterfly scales (Fig. 3A, Figure 5—table 1). Ground scales (Fig. 4E-F″) were likewise similar to selected blue ground scales, having thick and variable laminae (199 ±31 nm, ANOVA, $p=5x10^{-5}$ versus wild-type. p=0.36 versus selected, Fig. 1C) and significantly increased pigmentation (Fig. 5B, Mann-Whitney *U*, Figure 5—table 1). Overall, blue scale identity in *optix* mutants was caused by similar mechanisms as artificially selected blue.

optix mutant phenotypes also affected structural colors and pigments differently across wing pattern elements. As originally postulated (Zhang et al., 2017), excess melanin was produced in some ventral wing regions (Fig. 6A-D, Fig. 5C). We also observed regions where both pigment and structure were dramatically changed. For example, discal bars on the dorsal forewing, which are normally orange, gained blue scales through both converting lamina structural color to blue and replacing orange with brown pigment (Fig. 6E-H, Fig. 5D). The kinds of pigmentation effects were diverse: *optix* mutation increased the quantity (Fig. 5B, C), decreased the quantity (Fig. 5A), or switched the identity (Fig. 5D) of the pigment in different scales (Mann-Whitney *U*, Figure 5—table 1). Because the butterflies were mosaic mutants, some of this phenotypic variability could be due to genotypic differences between clones (i.e. mono- versus biallelic gene deletion, as well as the exact size of the deletion) (Zhang et al., 2017). However, much of the variation in outcome could also be observed within single clones that spanned multiple wing pattern elements (defined by the Nymphalid ground plan, Nijhout 1991), Fig. 1—figure supplement 1), suggesting that the patterning roles of *optix* are quite context specific.

In summary, *optix* knockout can have varied effects in a single scale by altering pigmentation, nanostructures, or both. These findings are consistent with *optix*'s described role as a developmental patterning gene that determines gross switches between discrete scale fates, and which, directly or indirectly, can regulate diverse downstream factors (Martin et al., 2014). Since appropriate coloration critically depends on the proper combination of pigment and structural colors in both cover and ground scales (e.g. Wilts, Pirih, & Stavenga, 2011; Wilts, Vey, Briscoe, & Stavenga, 2017), it is of particular interest that *optix* can regulate all of these components simultaneously. *optix* mosaic knockout mutants demonstrate that lamina thickness can be experimentally perturbed and highlight a multifunctional candidate genetic pathway for coordinated color evolution.

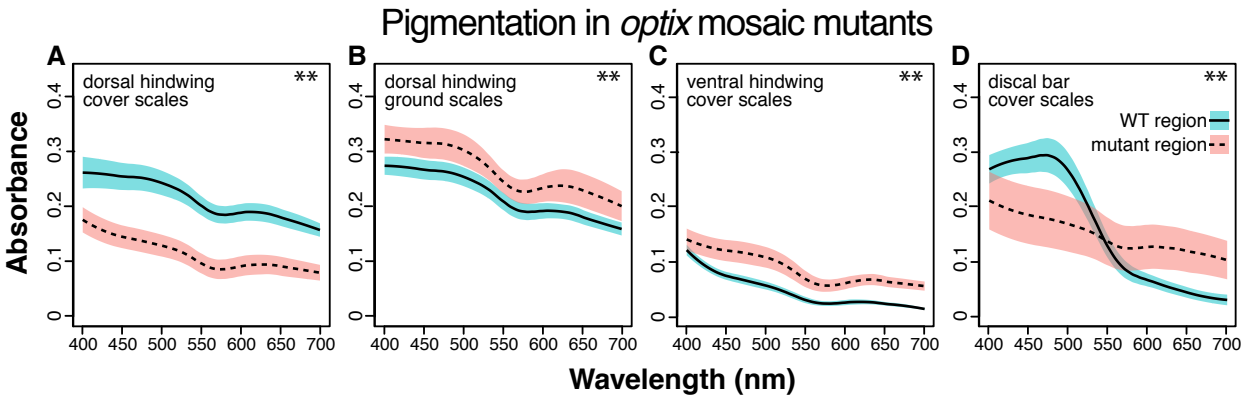

Figure 5: Absorbance spectra show the effect of *optix* knockout on scale pigmentation across wing pattern elements. All comparisons are between wild-type and mutant regions in the same mosaic wing. (A) *optix* mutation decreases absorption in cover scales from the main background region of the dorsal hindwing (Fig. 2Q). (B) Absorbance of ground scales from the dorsal hindwing (Fig. 4E) is increased in mutant scales. (C) Absorbance increases with *optix* mutation in ventral hindwing cover scales (Fig. 6A,C). (D) In the dorsal discal bars, (Fig. 6E,G) *optix* regulates a switch between orange and brown pigment. Plots show mean spectra with envelope of one standard deviation, N=6 scales per sample. Differences for all comparisons are statistically significant (Mann-Whitney *U*, Figure 5—table 1).

optix mutants - regions of same mosaic wing

dorsal hindwing cover scales

nm	WT mean	WT SD	mut mean	mut SD	*U*	*p*	
400	0.262	0.029	0.175	0.023	36	0.0022	**
500	0.243	0.022	0.128	0.020	36	0.0022	**
600	0.188	0.016	0.091	0.018	36	0.0022	**
700	0.157	0.012	0.079	0.014	36	0.0022	**

dorsal hindwing ground scales

nm	WT mean	WT SD	mut mean	mut SD	*U*	*p*	
400	0.274	0.016	0.322	0.026	1	0.0043	**
500	0.253	0.017	0.302	0.029	2	0.0087	**
600	0.191	0.014	0.233	0.025	3	0.0152	*
700	0.158	0.012	0.200	0.027	2	0.0087	**

ventral hindwing cover scales

nm	WT mean	WT SD	mut mean	mut SD	*U*	*p*	
400	0.122	0.010	0.142	0.020	7	0.0931	
500	0.058	0.007	0.109	0.019	0	0.0022	**
600	0.027	0.005	0.062	0.011	0	0.0022	**
700	0.016	0.002	0.057	0.008	0	0.0022	**

dorsal forewing discal bar cover scales

nm	WT mean	WT SD	mut mean	mut SD	*U*	*p*	
400	0.269	0.026	0.212	0.053	34	0.0087	**
500	0.266	0.032	0.169	0.050	36	0.0022	**
600	0.067	0.012	0.128	0.040	6	0.0649	
700	0.031	0.010	0.104	0.035	3	0.0152	*

Figure 5—table 1: Comparison of absorbance values for individual scales immersed in refractive index matched oil. Absorbances were compared using the Mann-Whitney *U* rank sum test, due to unequal variances between many of the comparisons. Mean absorbances are reported with standard deviation (SD), U, and exact p-value for selected wavelengths. Minimum N=6 scales per specimen/treatment, with 2 technical replicates of each scale. (* $p < 0.05$; ** $p < .01$) WT = wild-type. mut=mutant region of mosaic *optix* knockout butterfly.

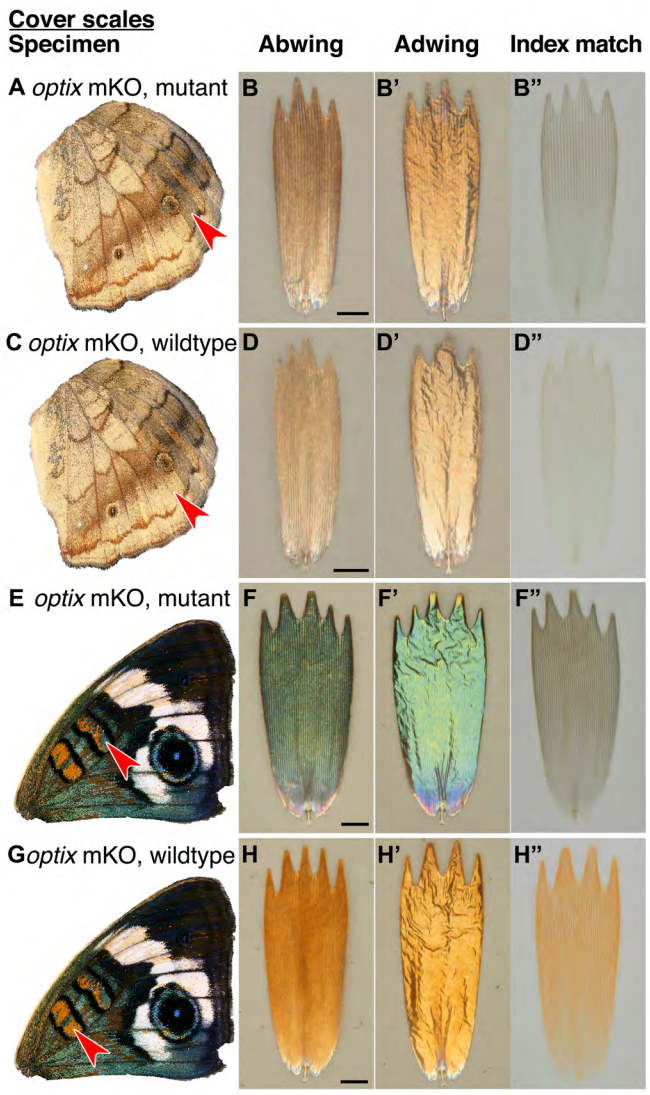

Figure 6: Effects of *optix* mutation on structure and color of *J. coenia* cover scales vary by wing region. (A,C,E,G) Wings with red arrowhead indicating the region from which scales were sampled. (B,D,F,H) Scale in abwing orientation. (B',D',F',H') Scale in adwing orientation. (B",D",F",H") Scale immersed in fluid with a refractive index matched to chitin to show only pigmentary color. (A-B") Mutant cover scales from an *optix* mKO ventral hindwing have increased melanin. (C-D") Wild-type cover scales from an *optix* mKO ventral hindwing. (E-F") Mutant cover scales from an *optix* mKO forewing discal bar have lost orange pigment, gained brown pigment, and increased lamina thickness, resulting in a shift to blue. (G-H") Wild-type cover scales from the *optix* mKO forewing discal bar have both orange pigment and an orange lamina structural color. Scale bars are 25 μm.

Lamina thickness consistently predicts structural color wavelength

Relatives of *J. coenia* exhibit extensive color and pattern diversity, and blue structural colors in particular show patterns of variation that hint at ecological relevance (e.g. sexual dichromatism, seasonal polyphenism) (Fig. 7A). To assess the importance of lamina thickness variation in macroevolutionary color diversity, we sampled cover scales from nine species in the genus *Junonia* and a tenth species, *Precis octavia*, which belongs to the tribe Junoniini and exhibits seasonally polyphenic wing coloration. We prioritized large pattern elements that distinguish color forms within species. We compared scales using optical imaging, immersion index-matching, spectrophotometry, and Helium Ion Microscopy. All scales sampled had typical Nymphalid scale structure with a single plane of chitin forming the lower lamina.

We tested whether the relationship between lamina thickness and color that we observed in experimental contexts applies more broadly. We sought to address two questions: First, does lamina thickness reliably predict lamina color, as measured from the adwing surface? While it is known that the thickness of a dielectric film controls the film's reflectance, other variables such as refractive index, surface roughness, and pigmentation within the film also factor into reflectance, and these could plausibly vary among taxa. Second, how variable is lamina thickness? What range of thicknesses occur, and is there evidence for either quantized or continuous thickness variation? To address these questions, we measured reflectance spectra from the adwing surface of disarticulated cover scales from the 23 wing regions indicated in Fig. 7A. We then cross-sectioned scales, imaged with HIM, and measured thickness.

We found that lamina thickness varied continuously between 90-260 nm, indicating that all thicknesses over a more than 2.5-fold range are accessible (Fig. 8A). To better visualize the relationship between thickness and lamina color, we clustered similar samples into five color groups (Methods). Lamina colors in these groups could be described as gold, indigo, blue, and green, with a fifth variable group that included magenta, copper, and reddish colored scales (labeled as "red" in Fig. 8). Thickness differed significantly between all color group pairwise comparisons (Fig. 8A, ANOVA: $p < 2x10^{-16}$, with *post hoc* Tukey's Honestly Significant Difference test: $p < 2x10^{-6}$ for all pairwise comparisons). The color groups were also associated with different reflectance profiles (Fig. 8B). In some cases, we obtained variable measures within individual specimens, which reflects biological color variation between adjacent scales, as well as varying color within individual scale laminae along their proximal-distal and lateral axes. A particularly striking example of the latter came from *J. atlites*. While the wing appeared light grey, at higher magnification individual scales could be seen to be

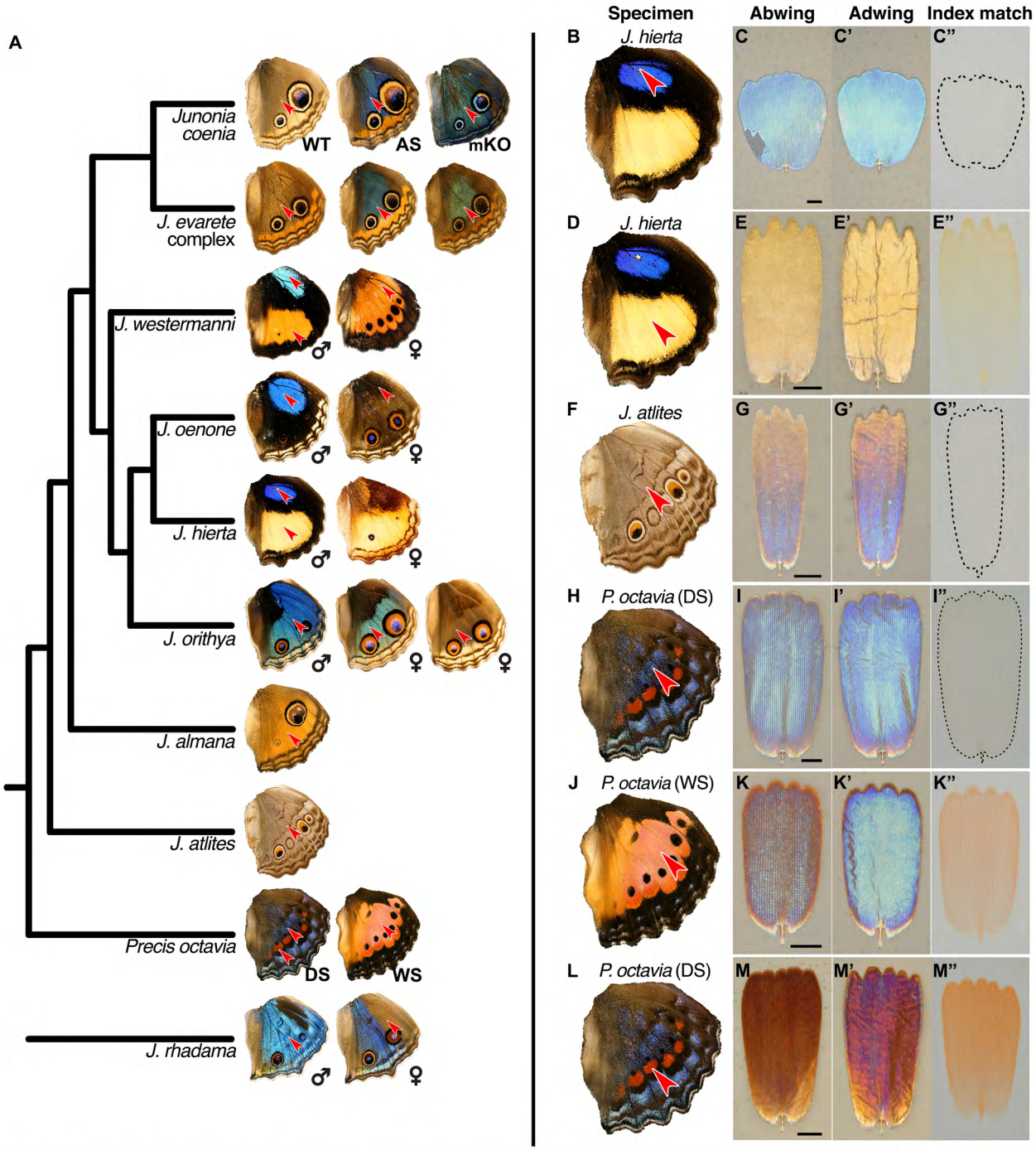

Figure 7: Lamina structural colors are an important component of wing color in *Junonia*. (A) *Junonia* phylogeny based on Kodandaramaiah 2009. WT = wild-type. AS = artificial selection. mKO = *optix* mutant. DS = winter/dry season form. WS = summer/wet season form. *J. evarete* variants are from different places. (B,D,F,H,J,L) Dorsal hindwing; arrow shows the characterized scales' location. (C,E,G,I,K,M) Abwing surface of cover scale. (C',E',G',I',K',M') Adwing surface of cover scale, showing lamina color. (C",E",G",I",K",M") Scale immersed in refractive index-matched fluid to show only pigmentary color. (B-C") *J. hierta* basal aura scales are unpigmented with blue lamina structural color. (D-E") *J. hierta* has coordinated yellow pigment with a structurally yellow lamina. (F-G") Light grey of *J. atlites* is exclusively structural, due to additive color mixing of the multicolored lamina. (H-I") Blue scales of dry season *P. octavia*. (J-K") WS *P. octavia* has discordant red pigment in the ridges and cross-ribs and a blue lamina color that can be seen through the windows between ridges. (L-M") The red band in DS *P. octavia* is more saturated than (J) due to more red pigment and a structurally reddish lamina.

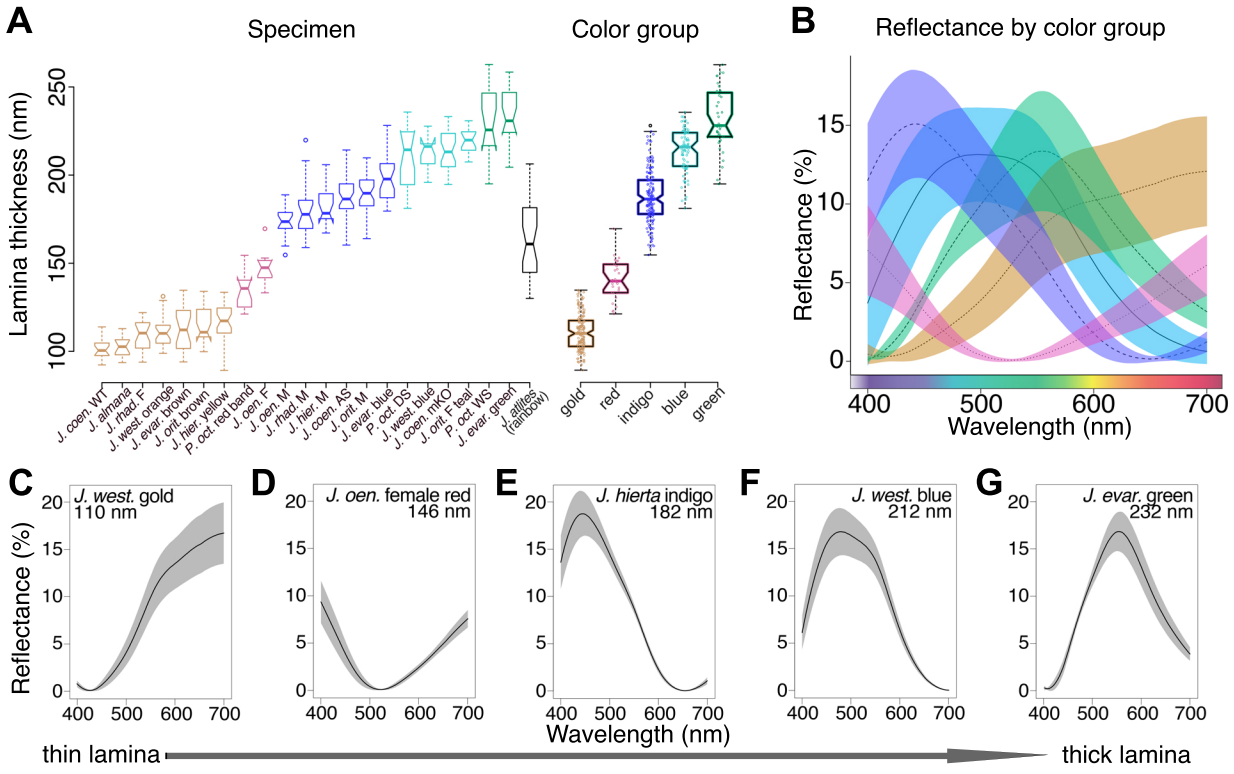

Figure 8: Lamina thickness predicts lamina color across the *Junonia* phylogeny. (A) Thickness measures for the regions indicated in Fig. 7A vary continuously over a 170 nm range (minimum N=3 scales and 12 measures per specimen). To visualize the relationship between thickness and color, we clustered similar specimens into five color groups described as gold, red, indigo, blue, and green. Thickness is significantly different between groups (ANOVA and Tukey's HSD, $p < 2x10\text{-}6$). *J. atlites*, which has rainbow color gradients in each individual scale, has especially variable thickness, with measures overlapping the ranges of all color groups. Boxplots show median and inner quartiles, whiskers extend to 1.5 times the interquartile range, outliers are shown as points, and notches show 95% confidence interval of the median. (B) Color groups are associated with different reflectance profiles. Lines are mean spectra and envelopes show one standard deviation. Minimum N=3 scales per specimen from panel A; clusters follow panel A. (C-G) Adwing reflectance spectra for representative individual specimens with increasing lamina thicknesses. The color sequence follows Newton's series. Solid line is the mean spectrum and the envelope is one standard deviation; N=3 scales and 6 spectra per graph.

multicolored (Fig. 7G'), and thickness measures from *J. atlites* overlapped the ranges of all color groups (Fig. 8A, see further analysis below).

Lamina thickness had a consistent relationship with adwing scale reflectance for the taxa and color range we sampled. The order of color shift as lamina thickness increased followed Newton's series, which is the characteristic color sequence for thin films (Mason, 1927; Shevtsova, Hansson, Janzen, & Kjærandsen, 2011). This sequence can be understood in terms of an oscillating thin film reflectance function, which shifts toward longer wavelengths as film thickness increases (Fig. 8C-G). The thinnest films appeared gold due to reflectance of all the longer wavelengths (Fig. 8C). In mid-thickness laminae, a mix of two oscillations determined color: reflectance of the first oscillation was shifted toward far red wavelengths, while a second reflectance peak rose in the ultraviolet (Fig. 8D). Visible reflectance of thicker laminae was dominated by the peak of the second oscillation as it moved from indigo to green (Fig. 8E-G). That the trend between thickness and reflectance holds broadly suggests that color changes in *Junonia* butterfly scales have recurrently evolved via lamina thickness adjustments. Moreover, the consistency of the relationship between thickness and reflectance is useful. For example, structural variation could be rapidly surveyed by extracting fitted thickness estimates from reflectance measurements, a much less laborious process than sectioning for electron microscopy.

Lamina structural color influences wing color throughout the genus Junonia

We next tested whether the extensive variation in lamina structural color among *Junonia* butterflies, explained by lamina thickness, also drives variation in overall wing color. An alternative hypothesis would be that composite wing color is usually dominated by pigmentation, particularly by pigments distributed on the outward-facing abwing surfaces of cover scales, above the lamina thin film. We measured pigmentation in cover scales from the same regions (Fig. 7A) to test the relative importance of pigments and lamina structural colors for wing color. (Structural colors and pigments are listed per each specimen in Supplementary File 1 and representative examples are shown in Fig. 7B-M".)

Pigmentation was highly variable among *Junonia* species (Fig. 7B-M", Fig. 9, Supplementary File 1). This included marked differences in pigmentation between regions of a single wing (e.g. yellow and blue regions in *J. hierta*, Fig. 7B-E", 9A) and also variation between color forms and species throughout the genus (e.g. between sexes in *J. orithya*, Fig. 9C, and seasonal forms in *P. octavia* Fig. 7H-M", 9B). Absorbance spectra varied in both shape and magnitude. Variation in magnitude, such as between the red band and the wet season morph of *P. octavia* (Fig. 9B), represents differences in pigment abundance. We also observed distinct absorbance spectral shapes, which can

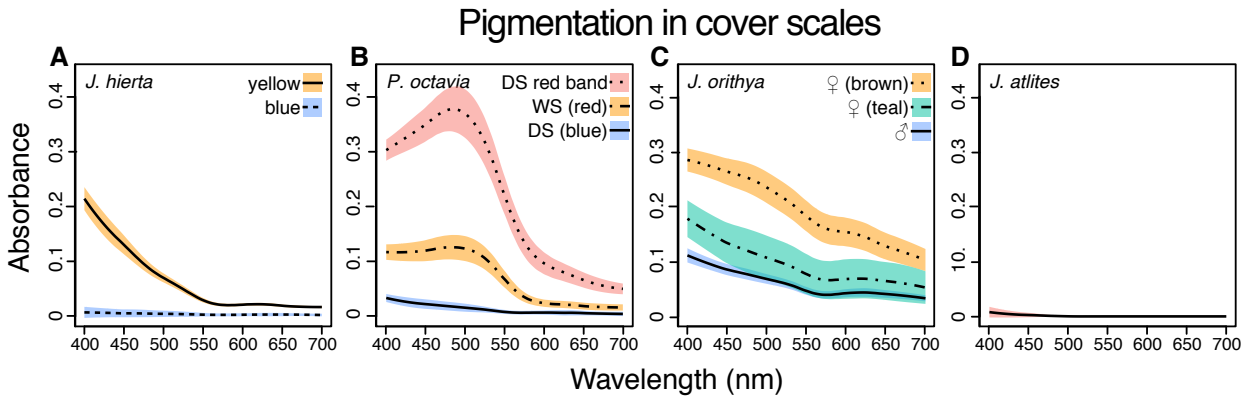

Figure 9: Absorbance spectra show variable pigment concentrations and identities among representative *Junonia* butterflies. Spectra were taken from cover scales from the regions shown in Fig. 7A. (A) *J. hierta* pigmentation varies by wing region (Fig. 7B-E"). (B) Extent of red pigmentation is the most important driver of color difference between seasonal morphs of *P. octavia* (Fig. 7H-M"). (C) Pigment absorbance differs by sex in *J. orithya*. (D) *J. atlites* scales lack pigmentation (Fig. 7F-G"). Plots show mean spectra with envelope of one standard deviation, minimum N=6 scales per sample.

indicate the identity of the pigment (for example, contrast the spectral shape of the yellow pigment in *J. hierta*, Fig. 9A, versus red pigment in *P. octavia*, Fig. 9B, versus brown pigment in *J. orithya*, Fig. 9C).

Notwithstanding the clear importance of pigmentation among *Junonia* butterflies, pigment variation was insufficient to explain the breadth of wing color diversity, and lamina structural colors made up the shortfall. The importance of lamina structural color was most obvious in scales that entirely lacked pigments. For example, the blue basal aura regions of male *J. westermanni*, *J. hierta*, and *J. oenone* wings had unpigmented cover scales with structurally blue laminae (Fig. 7B-C", Fig. 9A). Most of the pigmentless scales we sampled were blue, with the notable exception of *J. atlites* scales (Fig. 7F-G", Fig. 9D). These scales had rainbow gradient laminae, which presumably create the overall light grey by additive color mixing (Vukusic, Peter, Kelly, & Hooper, 2009). *J. atlites* demonstrates that lamina structural color can fundamentally drive wing color even in neutrally colored wing regions that are not obviously iridescent, and also that thickness can be patterned at fine spatial resolution within a single lamina.

In most wing regions, color was determined by the interaction of both lamina structure and pigments. For example, in the cover scales of *J. hierta* (Fig. 7D-E", Fig. 9A), the yellow lamina structural color and yellow pigment were mutually reinforcing, with the lamina sensibly reflecting wavelengths that the pigment does not absorb. Other examples help delineate how much pigment is required to overpower the lamina color. In blue *J. evarete*, pigments in the cover scale ridges absorbed approximately 0.2 AU (Absorbance Units, i.e. 37% of light not transmitted, Fig. 3C) of the blue wavelengths that the lamina reflected most brightly (Fig. 2L). With this ratio, wing hue was still driven by the lamina structural color. The cover scales of *J. orithya* were similar (Fig. 9C), having a neutral dark pigment (i.e. a pigment that absorbs all visible wavelengths) in the scale ridges. Perhaps dark pigment in the ridges functions like a Venetian blind to limit iridescence, so that at high viewing angles, where iridescence would be most pronounced, light from the lamina is quenched.

Because of their range of pigment concentrations, *P. octavia* specimens were also useful to test the tradeoff between pigment abundance and lamina color influence. When viewed at high resolution, scales from the wet season morph of *P. octavia* contained red pigment in the ridges and ribs (max absorbance 0.12 ± 0.02, Fig. 7K,K', Fig. 9B), while reflected light from the blue lamina spilled through the windows between ridges. Viewed macroscopically, this combination made a lightly saturated red. To display a richly saturated red, much more pigment was required, as seen in the red band of the dry season morph (max absorbance 0.38 ± 0.04, Fig. 9B, Fig. 7 L-M"). These reddest scales also had thinner, structurally magenta and copper colored laminae that may

further reinforce redness (Fig. 8A, Fig. 7M'). The concentration of red pigment was the most important driver of the color difference between *P. octavia* seasonal morphs. The blue and red morphs had only a subtle difference in lamina thickness (Fig. 8A), and the laminae of both were blue (Fig. 7 I', K'), but the blue morph lacked any red pigment (Fig. 9B).

Overall, *Junonia* wing color was determined by complex mix-and-matching of different lamina thicknesses and pigments. A thin film lower lamina was present in all scales, but its influence on wing color was adjusted by the amount and placement of pigment, especially in the upper surface of the scale. Pigments can mask lamina structural color at high enough density, depending on the placement and color of the pigment as well as the color of the lamina. In our tests, when pigmentation absorbed ≤ 0.2 AU of the relevant wavelengths, it did not cancel out lamina structural color.

Comparison to thin film equation

We compared our empirical data to Fresnel's classical thin film equations, which model the reflectance of an idealized dielectric thin film (Fresnel, 1834; Yeh et al., 1978). This model has previously been used to estimate the thickness of butterfly scale laminae based on their adwing reflectance spectra (Stavenga et al., 2014a; Wilts et al., 2017). For each sample, we modeled the expected reflectance using our thickness measurements, and then compared to the measured reflectance spectra. We used 1.56 for the refractive index of chitin (Vukusic, Sambles, Lawrence, & Wootton, 1999) and a maximal angle of illumination of 30° following (Stavenga, 2014) (because spectra were measured through an objective lens with a numerical aperture of 0.5). To account for measurement error, we modeled films over all thicknesses within one standard deviation of the measured mean per sample (red envelopes, Fig. 8—figure supplement 1A). We also modeled films with Gaussian thickness distributions for each sample, following (Siddique et al., 2016). This model is analogous to a single uneven film with mean thickness and surface roughness defined by the measured thickness and sample standard deviation (solid red lines, Fig. 8—figure supplement 1A).

We found that qualitatively the model describes the main behaviors of our data: reflectance oscillates with a given frequency and brightness, and the function shifts toward longer wavelengths as thickness increases. Quantitatively, mean maxima and minima in the reflectance function were offset laterally for every specimen, by about 40-80 nm, with the modeled curves blue-shifted relative to the observed. A similar blue shift has been reported in butterfly scale laminae before (Wasik et al., 2014). The comparison improves if we assume a higher refractive index or thickness. However, to align modeled and measured spectra would require either an impossibly high refractive index (around 1.75) or increased thickness outside the error range of our measures (20-

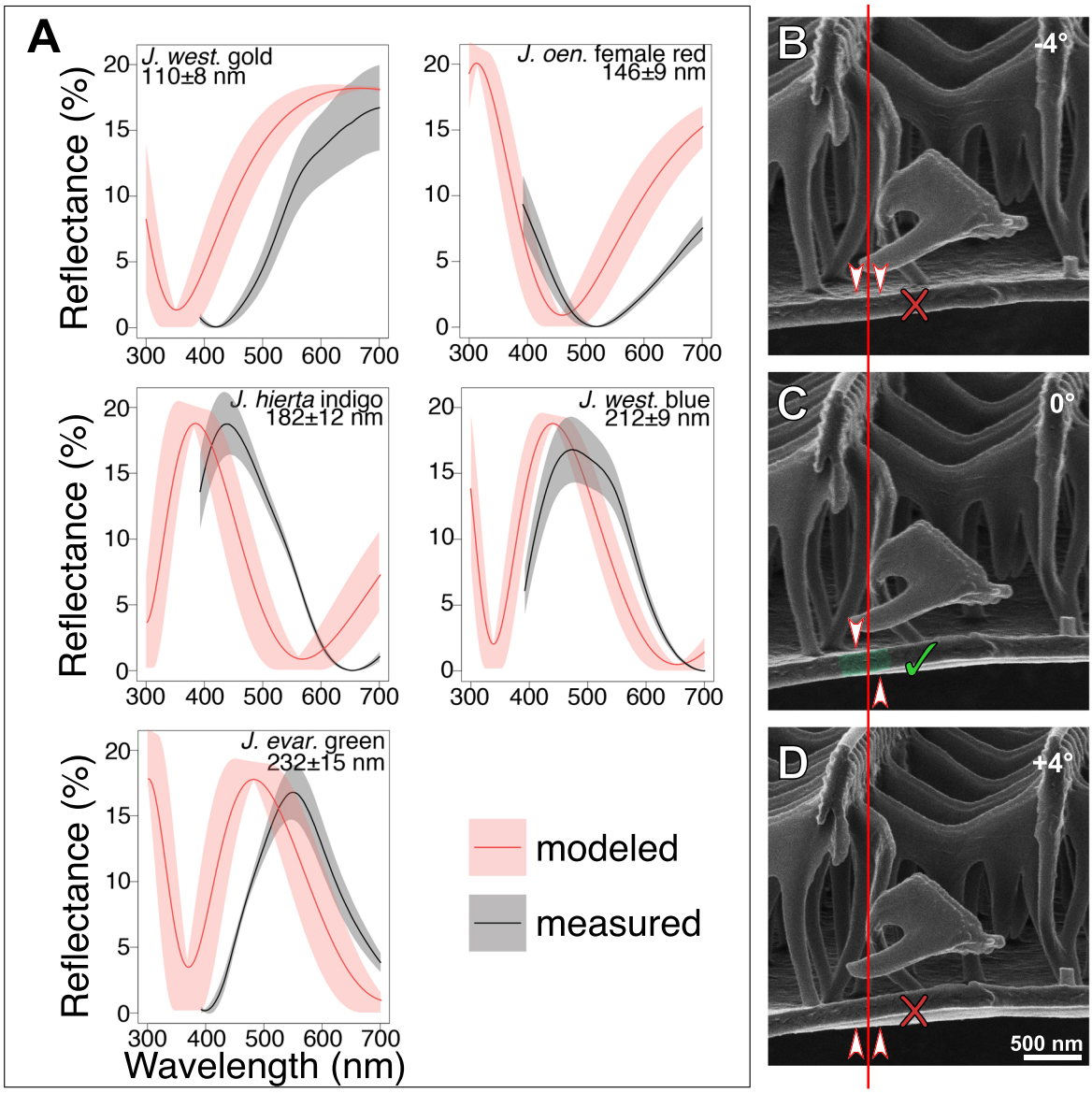

Figure 8—figure supplement 1: (A) Modeled reflectance for representative specimens, using the classical Fresnel thin film equations, recovers the general shape of observed reflectance spectra. Black lines show the mean measured reflectance spectra; the grey envelope is one standard deviation (N=3 scales per graph). In red, we show the modeled reflectance (solid red lines) and standard deviation (red envelopes), based on thickness measures from HIM images (See Methods). (B-D) Inflection point method for ensuring that lamina thicknesses are measured without sample tilt. At the position indicated by the vertical red line, an inflection point between the upper and lower surfaces of the lower lamina is visible only in (C). Arrowheads show whether the upper or lower surface of the lamina is visible in each panel, given the sample tilt and the lamina's curvature. If the lamina is tilted by 4-5° or more from the horizontal, no inflection point is observed at that position.

25 nm thicker than mean measurements). Possibly the lateral offset is due to a combination of the former. Alternatively, these results could indicate that scales have additional properties not fully described by the model. There are a number of differences between the idealized film and real scales, including curvature of the film and possible birefringence of the ridges. The lamina itself may not necessarily have a uniform material composition or refractive index. For example, contrasting sublayers within the lamina (as in Trzeciak, Wilts, Stavenga, & Vukusic, 2012) could create extra reflective interfaces. Thus, our data are compatible with the expected behaviors of thin films, but modeling the specific case of butterfly scale laminae with quantitative precision may require additional parameters or calibration to an empirical dataset.

Discussion

This study leverages the simplest photonic nanostructures, thin films, to interrogate the evolution and genetic regulation of structural color in *Junonia* butterfly scales. While there is a large body of literature attributing optical properties to various biological nanostructures, such claims commonly rest on correlation between mathematical models and spectral measurements. Here, we use two different experimental manipulations of the structure (artificial selection on wing color and knockout of the *optix* gene) in addition to broad interspecies comparisons to establish that lower lamina thickness quantitatively controls structural color wavelength in *Junonia* butterfly scales. The relationship between lamina thickness and wavelength holds over a wide range of thicknesses (90-260 nm) that generate Newton's color series for dielectric thin films. Moreover, lamina structural color is one important determinant of overall wing color, including in wing regions that also contain pigments. Lamina structural colors contribute to the color differences that distinguish sexes, species, seasonal variants, and selectively-bred lineages of *Junonia* butterflies, highlighting that quantitatively tuning lamina thickness is a vehicle for color evolution in both micro and macroevolutionary contexts.

Because the lower lamina is part of the typical architecture of butterfly scales, our findings have broad implications for future research on adult color in numerous butterfly taxa. Foundational literature drew a distinction between highly derived scales with vivid structural colors and "standard, undifferentiated scales," which conform to the butterfly scale Bauplan, have a simple monolayer lower lamina, and "are not truly iridescent, i.e., they do not produce brilliant structural colors" (Ghiradella, 1991). However, within the past ten years, individual examples of thin film interference from the lower lamina have emerged in diverse Lepidoptera, including in simple scales (Giraldo & Stavenga, 2016; Siddique et al., 2016; Stavenga et al., 2014a; Stavenga et al.,

2018; Trzeciak et al., 2012; Wasik et al., 2014; Wilts et al., 2017). These newer descriptions and our thorough examination of many scales indicate two points: first, although thin films are indeed less brilliant than some other classes of lepidopteran photonic structures (thin films only reflect around 20% of incident light), they are a consequential source of structural color. Second, thin films occur in many butterfly and moth lineages and likely arose early in lepidopteran evolution. The lower lamina has a thin film morphology in all scales that resemble the scale Bauplan, meaning that reflectance from the lamina is the shared condition except where it is masked by either heavy pigmentation or a derived structure with higher optical contrast. Because butterflies commonly produce multiple lamina colors across wing pattern elements and scale types, it is probable that the developmental genetic networks for quantitatively varying lamina thickness are deeply conserved as well. Hence, it will be useful to report which lamina colors are present, in addition to identifying pigments, when describing butterfly colors.

Physical constraints inherent to thin film colors may help explain the division of color space between pigments and photonic structures. It is not well understood why certain hues seem to be more often produced by pigments while others are more often produced by structural colors (e.g. the abundance of blue structural colors but lack of blue pigments in birds (Stoddard & Prum, 2011) and the rarity of one class of red structural color in birds and beetles (Magkiriadou, Park, Kim, & Manoharan, 2014)). In *Junonia,* we show that by tuning thickness, thin film laminae can produce nearly all the spectral colors (i.e. yellow, green, blue, indigo), and even light achromatic colors (e.g. light grey in *J. atlites*) via color mixing across a gradient. Yet thin films are fundamentally incapable of producing certain colors, notably dark brown, black, and pure red. The medium thickness films that most nearly approach red have inherently poor color properties due to the oscillating nature of the thin film reflectance function. Since the colors of mid-thickness films are a mix of two reflectance peaks (Fig. 8C), they are reddish but not pure or well-saturated, and are better described as copper, magenta, and purple. Further, mid-thickness films are not bright: they reflect less total visible light than other thicknesses we observed (compare Fig. 8D to 8C, E-G). By contrast, red, black, and brown are prevalent pigment colors in *Junonia*, making pigments and thin film structural colors complementary color palettes with little overlap. The optical limitations of thin films may have partially determined how pigment families and scale architecture evolved in early butterfly lineages, which in turn initialized whether pigments or structures provide the most accessible route to evolve specific hues during subsequent diversification.

Our findings uncover a link between artificially selectable responses in lamina thickness and natural butterfly color variation, and expand on a previous artificial selection study

on butterfly wing color (Wasik et al., 2014) which selected for violet structural color in *Bicyclus anynana*. In both *J. coenia* and *B. anynana*, color shift was accomplished by modifying the dimension of an existing structure, the lower lamina, with pigmentation being less important. Since the selected taxa diverged 78 million years ago (Wahlberg et al., 2009) this similarity may be informative about evolvability in nymphalid butterflies generally. However, artificial selection in *B. anynana* primarily increased thickness in the obscured layer of ground scales, which can only weakly influence color, whereas *Bicyclus* species with naturally evolved violet wing color have violet thin films in their cover scales. In our study, artificial selection continued longer (12 vs. 6 generations) and elicited a more extreme response (71% vs. 46% increase in lamina thickness). Moreover, in *J. coenia*, we show that lamina thickness increased in the cover scales and fully recapitulated the naturally evolved mechanism of structural color in the sister species *J. evarete*. The thickness increases caused a stark wing color change plainly visible by eye, with appropriate wing patterning that also resembled *J. evarete* (thickened blue scales filled the background dorsal wing, while eyespots, distal pattern elements, and the ventral wing were unaffected). Our results robustly connect a rapid microevolutionary process to macroevolutionary diversity.

By using butterflies with CRISPR/Cas9-generated knockout of the *optix* gene, we are able to provide insight into the genetic regulation of lamina thin films. It was previously known that the *optix* wing patterning gene can regulate a switch between wild-type brown and blue iridescent wing color in *J. coenia* (Zhang et al., 2017), but the mechanistic basis for the color switch remained unknown. Specifically, it was unclear whether *optix* regulated scale structure itself, or whether *optix* deletion merely caused the loss of brown pigment, thus unveiling a pre-existing iridescent structure. Here, we show explicitly that in certain wing regions and scale types, *optix* deletion substantially increases lamina thickness. Our findings also amend the earlier conclusion that *optix* represses structural coloration in *J. coenia* (Zhang et al., 2017). Rather, by regulating lamina thickness, *optix* regulates the wavelength of a photonic structure that exists in both wild types and mutants. This distinction has implications for the likely identities and behavior of downstream genetic factors, as well as the developmental basis of mutant blue coloration. For example, rather than preventing a cascade of downstream genes from acting to erect a photonic structure *de novo*, *optix* may subtly regulate the expression of a gene or genes that directly regulate lamina thickness, such as chitin synthase. Additionally, we uncover disparate effects of *optix* deletion on pigmentation, including promoting, suppressing, and switching the identity of pigments in different scale types. In aggregate, these results show that *optix*'s functions in *J. coenia* are highly context specific, depending on both wing region and scale type (i.e. ground or cover scale). Moreover, because *optix* can regulate both pigmentary and structural color, the

optix pathway is an especially interesting candidate for coordinated color evolution, and further work on the detailed regulation of *optix* and its downstream targets is called for.

In summary, thin film reflectors, a morphologically simple class of photonic structures, are experimentally manipulable and broadly employed in the lower lamina of *Junonia* butterfly wing scales. Lamina thickness explains variation in structural color wavelength, responds to selection on wing color, and is regulated by the *optix* wing patterning gene. Tuning lamina thickness facilitates both microevolutionary and macroevolutionary shifts in wing color patterning throughout the genus *Junonia,* making the buckeye butterflies a promising study system with which to decipher the genetic and developmental origins of structural color.

Materials and Methods

Butterfly specimens
Reared *J. coenia* were fed fresh *Plantago lanceolata* or artificial diet (Southland Products, Lake Village, AK) as larvae and kept at 27-30 °C on a 16/8 hour day/night cycle. Artificially selected blue *J. coenia* were purchased as larvae from Shady Oak Butterfly Farm in 2014 (Brooker, FL). Wild-type *J. coenia* were from an established laboratory colony, originally derived from females collected in Durham, North Carolina (Nijhout, H. Frederik, 1980b) (for the comparisons to both *optix* mutant and selected butterflies) or were collected in California (comparison to selected butterflies only). We acquired preserved specimens from various vendors and collaborators (Supplementary File 1). Species-level identification was generally unambiguous. However, relationships among Neotropical *Junonia* are not well-resolved and the limited molecular data available do not cleanly support current designations (Gemmell, Borchers, & Marcus, 2014; Neild & D'Abrera, 2008; Pfeiler, Johnson, & Markow, 2012). Two recognized species, *J. evarete* and *J. genoveva*, have large ranges with extensive overlap and many variable color forms, including both brown and blue. We therefore described three Neotropical specimens as belonging to the *J. evarete* species complex to avoid accidental misidentification. Available diagnostic details, including ventral antenna club color and full collection details, are in Supplementary File 1.

Optical Imaging
Scales were laid on glass slides. Optical images of scales were taken with a Keyence VHX-5000 digital microscope (500-5000x lens). For refractive index matching, we used immersion oil (nD=1.56) from Cargille Laboratories (Cedar Grove, New Jersey), and imaged with transmitted light. Scales were dissected by hand using a capillary

microinjection needle. Whole wings were also imaged on the Keyence VHX-5000, using the 20-200x lens.

Microspectrophotometry

For reflectance spectra, individual scales were laid flat on a glass slide, with the adwing surface facing up. We collected spectra of the adwing surface with an Ocean Optics Flame-S-UV-Vis-Es spectrophotometer mounted on a Zeiss AxioPhot reflected light microscope with a 20x/0.5 objective and a halogen light source. We took two technical replicates of each scale, with a minimum sample size of 3 scales per specimen. Measurements were normalized to the reflectance of a diffuse white reference ($BaSO_4$). Data were recorded with SpectraSuite 1.0 software with 3 scans to average and a boxcar width of 7 pixels. The software wizard determined optimal integration time from the reference sample; time was generally about .007 seconds. Spot size was roughly circular, 310 μm in diameter, and centered on the scale. We processed spectra in RStudio 1.0.153 with the package 'pavo,' version 0.5-4 (Maia et al., 2013). We first smoothed the data using the *procspec* function with *fixneg* set to zero and *span* set to 0.3. We then normalized the data using the "minimum" option of the *procspec* function, which subtracts the minimum from each sample. Because we use a diffuse standard and scales are specular, raw spectra overestimate reflectance. We therefore followed (Stavenga et al., 2014a) in dividing spectra by a correction factor. We used a smaller correction factor of only 2.5, because in our setup the scale does not fill the full field of view. Absorption spectra from scales submerged in index-matched oil were collected and processed similarly, but under transmitted light with an integration time of 0.01 seconds, and without the "minimum" option.

Helium Ion Microscopy

Surface imaging by HIM provides increased depth of field and enhanced topographic contrast compared to Scanning Electron Microscopy for a range of biological and other materials (Joens et al., 2013), including butterfly wing scales (Boden, Asadollahbaik, Rutt, & Bagnall, 2012). Samples were prepared for HIM by laying the wing on a glass slide with the region of interest facing down, wetting with ethanol, and freezing with liquid nitrogen. We then promptly cross-sectioned the wing through the region of interest with a new razor blade. After the sample warmed and dried, we used a capillary microinjection needle to transfer individual cut scales onto carbon tape. Scales were placed overhanging the edge of a strip of carbon tape, with one end pressed into the tape. We optically imaged the tape strip as a color reference and then transferred the tape to the vertical edge of a 90° stepped pin stub (Ted Pella #16177). While non-conductive samples can be imaged by HIM using low energy electrons for charge neutralization, we found that the unsupported overhanging edges of our scales tended to bend due to local charging (Allen et al., 2019). We thus sputter coated with 4.5 - 13

nm of Au-Pd using a Cressington 108auto or Pelco SC5. Images (secondary electron) of the sectioned scales were acquired with a Zeiss ORION NanoFab Helium Ion Microscope using a beam energy of 25 keV and beam current of 0.8 - 1.8 pA (10 μm aperture, spot size 4). We then used the line measurement tool in ImageJ software to measure lamina thickness from the micrographs. We corrected measurements for slight variations in working distance not accounted for by the software scale bar, using $T_{correct} = (T_{raw})/9058\ \mu m \times d\ \mu m$, where d is the measured working distance and 9058 μm is the reference working distance. Because these are point measures, and thickness and color vary extensively along the proximal-distal and lateral axes of individual laminae, we took measurements from multiple different positions along each cut scale. All thickness data were based on a minimum of 12 measures drawn from a minimum of 3 scales per specimen/treatment. Thickness of female *J. westermanni* scales was not measured because specimens were unavailable.

Even with vertical mounting, the sectioned surface of the scale was not always perfectly perpendicular to the direction of the imaging beam, largely due to the scales' tendency to curve. Viewing angle is critical, since measurements taken from a projected image viewed under erroneous tilt could cause systematic underestimation of thickness. We therefore tilted the microscope stage until the scale lamina was perpendicular at the measurement site, as diagnosed by observing an inflection point in lamina curvature (i.e. a switch between the upper and lower surfaces being visible). Thickness was only measured at visible inflection points (Figure 8—figure supplement 1 B-D). We performed a tilt calibration to test the precision of our inflection point criterion and determined that an inflection point was only visible if the sample was within 4-5° of perpendicular. Since erroneous tilt is limited to 5°, thickness underestimation is limited to 1 nm. Slight overestimations are likely, due to the sputter coating.

The sectioned scale shown in Fig. 1A was milled using the gallium ion beam of the Zeiss ORION NanoFab (beam energy 30 keV, beam current 300 pA).

Analyses

Statistical analyses were conducted in R 3.2.2. For Fig. 8 A-B, specimens were grouped following the largest natural breaks in the data for two metrics, mean thickness and weighted average reflected wavelength, which were in good agreement.

Modeling film thickness

We modeled the reflectance from chitin thin films as previously described (Stavenga, 2014), including integrating reflectance for values of θ from zero to the maximal angle of illumination (i.e. averaging reflectances to simulate the inverted cone of light collected by the objective lens used in microspectrophotometry, given its numerical

aperture). Specifically, since our objective had NA=0.5, we calculated reflectance over values of θ from 0 to 30°, multiplied by 2πθ, and then averaged over the cumulative circular surface area. For the model with Gaussian thickness distributions, we followed (Siddique et al., 2016) using n=400 observations from the simulated thickness distribution. The R code for these models is in Appendix 1.

Extended data for *Junonia* species

The preceding analyses summarized data drawn from many *Junonia* species. In this section, I display the supporting data for each species.

General layout

For most species, I first show a high-resolution photo of the dorsal wing, with a red arrow indicating the spot(s) from which scales were removed and analyzed. Next, when not already included in the preceding figures, I present optical images of both cover and ground scales in both adwing and abwing orientation, as well as immersed in refractive-index matched oil to show pigmentation. Additionally, I show a Helium Ion micrograph (HIM) of a cover scale in cross-section and reflectance measures taken from the adwing surfaces of cover scales. Formatting notes for these components are as follows: (C) in the top left panel corner denotes cover scales; (G) denotes ground scales. Black scale bars are 25 μm except where otherwise labeled; white scale bars on HIM micrographs are 500 nm. In the reflectance spectra graphs, each line is a single measurement, and measures taken from the same scale are the same color. There are generally six measures from three scales per characterized wing region. The optical images of scales were all taken with a Keyence VHX-5000 digital microscope, but may have had either of two different white balance settings, because images were taken at two different research facilities. Additionally, most of the following images of index-matched scales were taken under reflected light, rather than transmitted light as in the preceding figures. Consequently, such images are darker overall and less useful for quantifying pigment. They merely show qualitatively whether there is a lot, a little, or no pigment, and whether the pigment is brown/black versus orange/red. The methods used to collect these images and spectra are otherwise the same as described.

Extra data are available for certain species. These can include optical images of partially dissected scales in ab- and/or adwing orientation, or immersed in index-matched oil. In some cases (e.g. *J. oenone* and female *J. westermanni*) I include optical images of

individual scales from extra parts of the wing, or of alternately-colored cover scales that are scattered through the characterized region at low frequency (e.g. female *J. orithya,* female *J. oenone)*. For some species, I show images of overlapping scales to demonstrate how the overlap affects color saturation. The presented data may also include extra micrographs, including of the cross-sectioned ground scale (e.g. *J. coenia* specimen collected in California). Finally, I often included a magnified view of an attractive part of the wing surface, such as the area around an eyespot.

The last two pages have a different layout with miscellaneous data and are labeled in context. Briefly, images include: 1) micrographs of more cross-sectioned ground scales, including three images from the same scale taken at different points along its distal-proximal axis, showing how lamina thickness is variable within-scale. 2) A larger HIM micrograph of a dissected scale. 3) A series of images demonstrating how cross-sectional micrographs relate to whole scales, which also help explain my sample preparation protocol. 4) Assorted micrographs of a whole scale, the scale pedicel, and a cross-sectioned wing. 5) Spectra of dissected and doubled scales, discussed further below.

Discussion and analysis of extended *Junonia* data

Exceptional scales

Blue scales from *J. rhadama* were distinct from all other scales examined. Most importantly, the ridges were more elaborate and the ridges and/or microribs might constitute an optically relevant multilayer from certain angles of illumination. The ridges were much less elaborate or densely spaced than, for example, *Morpho* ridge multilayers, but comparable to some other published examples. Given the tilted angles of the ridge and microrib multilayers, they probably do not cause constructive interference under normal (90°) illumination, and almost certainly did not contribute to reflectance peaks that I measured from the adwing scale surface. The ridges were relatively distantly spaced, leaving much of the lamina exposed, so the lamina structural color is still expected to be quite important from an abwing view, especially at normal illumination. However, *rhadama* scales were also strongly curved, which probably makes the wing less iridescent. In other words, light that interacts with the intact wing at 90° would interact with the structures on the curved scale surfaces from a variety of angles, effectively averaging the structure's angle dependencies. More investigation into how the interaction of the lamina, ridges, microribs, and scale curvature produces the color of the intact wing over a range of angles would be worthwhile. In one male specimen (not shown) the gold-brown ground scales were also an unusual, long, tapered shape and also strongly curved.

Blue scales from *J. hierta* were sticky, by which I mean they would deform slightly to adhere with an airtight seal to smooth surfaces. They may have differences in their material composition or chemical coating compared to all the other scales I examined. These suctioning interactions allowed some interesting observations, shown and labeled in the figures. Part of one scale adhered to the glass slide and lost its structural color, presumably because the refractive index differential between chitin and glass is much smaller than between chitin and air. Other cover scales stuck together in pairs, or got folded and adhered to themselves (see *J. hierta* section of figure panels). This doubled the lamina thin film from 182 ± 12 nm to roughly 364 nm thick and shifted the structural color to green. On the last page of this section, I show measured and modeled reflectance spectra for these doubled films. As with all my comparisons, the modeled and measured spectra were offset laterally but had the same shape, with steeper slopes than did spectra for films under 270 nm thick. The reflectance and exact color of these very thick films differed from the ~250 nm green films because there was more UV and far red reflectance in addition to the main green peak.

Basal aura scales

J. hierta, J. *westermanni*, and *J. oenone* males all have a showy patch of blue at the anterior dorsal forewing, called the basal aura. In females, the blue patch is absent (*westermanni*) or reduced or variably present (*hierta, oenone*). This sexual dimorphism and the wing position suggest these basal auras may play a role in sexual signaling. The anterior dorsal hindwing may also have a patch of androconial (pheromone) scales, and the butterflies have extra behavioral control over whether or not to display this spot: in a relaxed stance with the wings open, the forewing will obscure the basal aura. By shrugging the forewing forward into a more alert stance, the butterflies can flash this blue patch. Basal aura scales had a suite of characteristics that distinguished them from other cover scales in the genus, and from scales on other parts of the same animals' hindwings. The basal aura cover scales were larger, rounder, completely unpigmented, and had especially uniform lamina color in optical images, suggesting minimal thickness variation and laminar wrinkling. Ground scales in basal auras were consistently melanic. Male *J. orithya* scales had most of these characteristics to a lesser degree.

Pigment location and interactions

Observations from several *Junonia* species suggest that pigment is typically restricted to the top surface of the scale (i.e. the ridges and crossribs). Absorbance measures of the intact versus lamina-only parts of dissected cover scales in both *J. coenia* and *J. orithya* showed that the lamina absorbed very little. These absorbance measures were taken through a 40x lens, so spot size is smaller than in my other spectra measurements (20x

lens). Still, I can't exclude the possibility that spectra taken with the illumination spot centered on the lamina also included a little bit of the intact region. For this reason, absorbance spectra are not conclusive as to whether there was a small amount of diffuse pigment in these laminae, or none. It is quite clear, however, that most pigment was deposited in the upper half of the scale. I also present partial dissections of the most heavily pigmented, melanic ground scales (*J. westermanni*, *J. hierta*) and a melanic cover scale (*J. oenone*). In each case, the exposed lamina was not melanic.

Several images demonstrate that the saturation of a lamina structural color is enhanced by a dark, absorbing background to reduce backscatter of wavelengths that were initially transmitted through the structure. For *J. oenone*, I show the wing surface with scales partly removed. The wing membrane is white/translucent, the exposed ground scales are dark, cover scales overlapping ground scales are saturated blue, and the few edges of cover scales that do not overlap a ground scale are only faintly blue. The same phenomenon can be seen at higher magnification with a *J. hierta* cover scale that only partly overlays a ground scale. Lastly, this phenomenon can also explain the appearance of dissected scales in optical images. One might wonder why, if the lamina is sufficient for structural color, dissected scales (e.g. Fig. 2 J", N") look only faintly colored compared to the adwing view of the same scale type (e.g. Fig J', N'). In the adwing view, the lamina overlays the pigmented ridges, reducing backscatter and improving saturation. To confirm, I include images of dissected and folded scales where the isolated lamina does have something more absorbing than a glass slide under it (*J. hierta, J. westermanni*) and consequently is as fully colorful as the corresponding intact, adwing-oriented scale.

Variation

Many comparisons beside cover scale lamina thickness and color might be drawn between species, and I will briefly comment on a few. First, HIM micrographs suggest which dimensions of the scale architecture are most variable or most conserved. There is a lot of variation in the proportional heights of trabeculae and microribs, the angle of the microribs and how defined they are, the angle of each ridge scute and how much scutes overlap, and how extensively fused the trabeculae are with the crossribs. By contrast, the distance between ridges seems fairly consistent. Some scales had a smooth texture; in others, texture resembled oriented strand board. In addition to variation among species, some of these characteristics were also variable between neighboring scales, along the distal-proximal axis of a single scale, or between the forewing and hindwing. Male *J. orithya* scales were particularly easy to dissect; I speculate this may be because they have especially short trabeculae with very solid trabeculae/crossrib junctions connecting the ridges. For cases where a particular scale dimension is consistent within species but contrasting between species, the mechanical and

hydrophobic properties of *Junonia* scales could be strategically tested and associated with their nanoscale dimensions.

As in *J. coenia*, lamina structural color, and presumably lamina thickness, were more variable in ground scales than in cover scales in most species. Individual ground scale laminae commonly had a gradient of colors, and there was also less uniformity between neighboring ground scales in a single specimen. Because ground scales usually contained more pigment than cover scales, and because less light would reach them on the wing, their lamina structural colors have little impact on wing color. It follows that there is probably less constraint on lamina thickness in ground scales. Perhaps ground scales harbor more standing thickness variation in *Bicyclus* too, explaining the finding that in *Bicyclus,* artificial selection for blue-shifted reflectance primarily affected ground scales (Wasik et al., 2014). By contrast, selection in *J. coenia* might have exploited elevated cover scale thickness variation from the outset. Selection began with individuals that already had a few blue cover scales. Allelic introgression is also a possible source of genetic variation. *J. coenia* is known to be interfertile with *J. evarete,* (Hafernik, 1982) which can have similar, naturally-evolved blue wing patterning, and the two species may encounter each other in Florida where selection occurred.

Extended details for *Junonia* species

Hindwing **Abwing** **Adwing** **Index match** **HIM cross section** **Reflectance**

J. rhadama, female, Madagascar

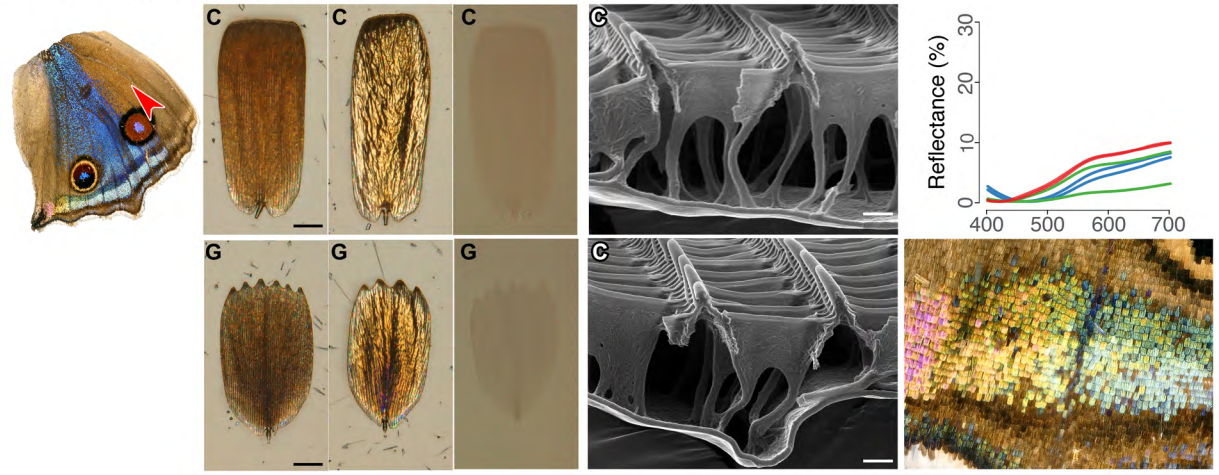

J. rhadama, male

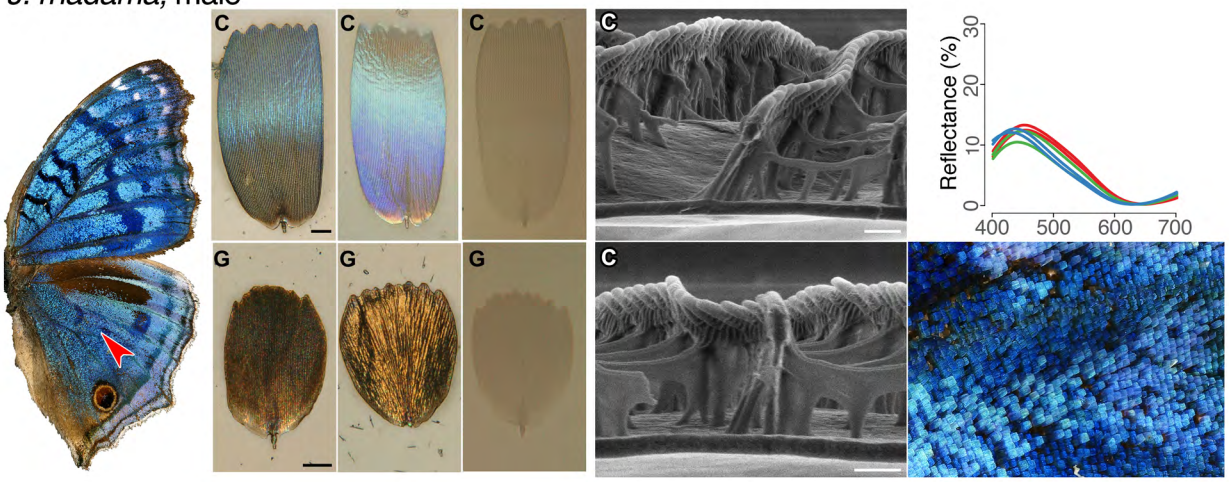

J. atlites, Sulawesi

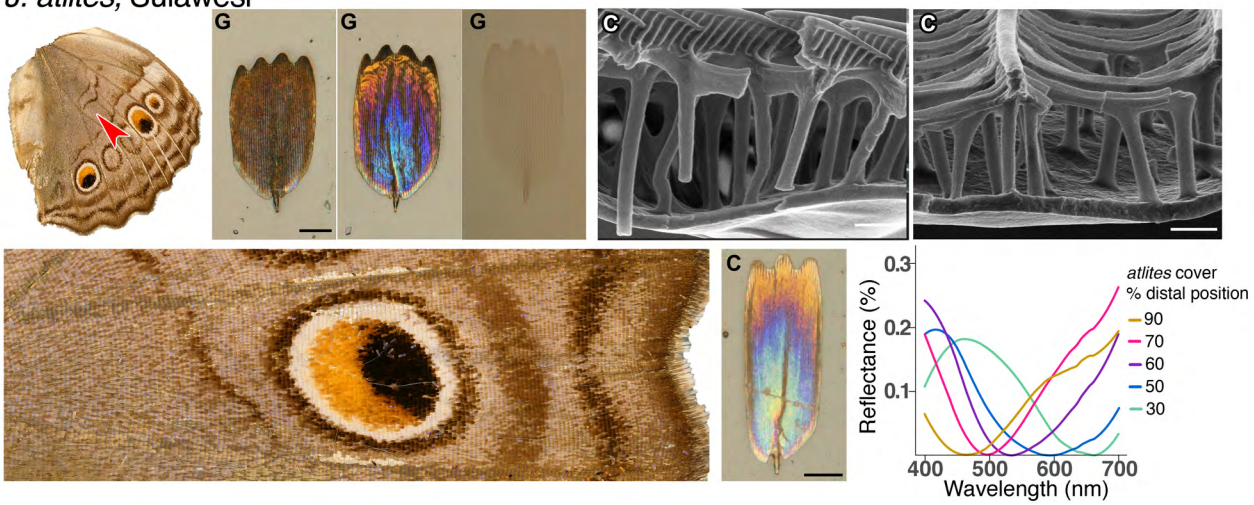

Extended details for *Junonia* species

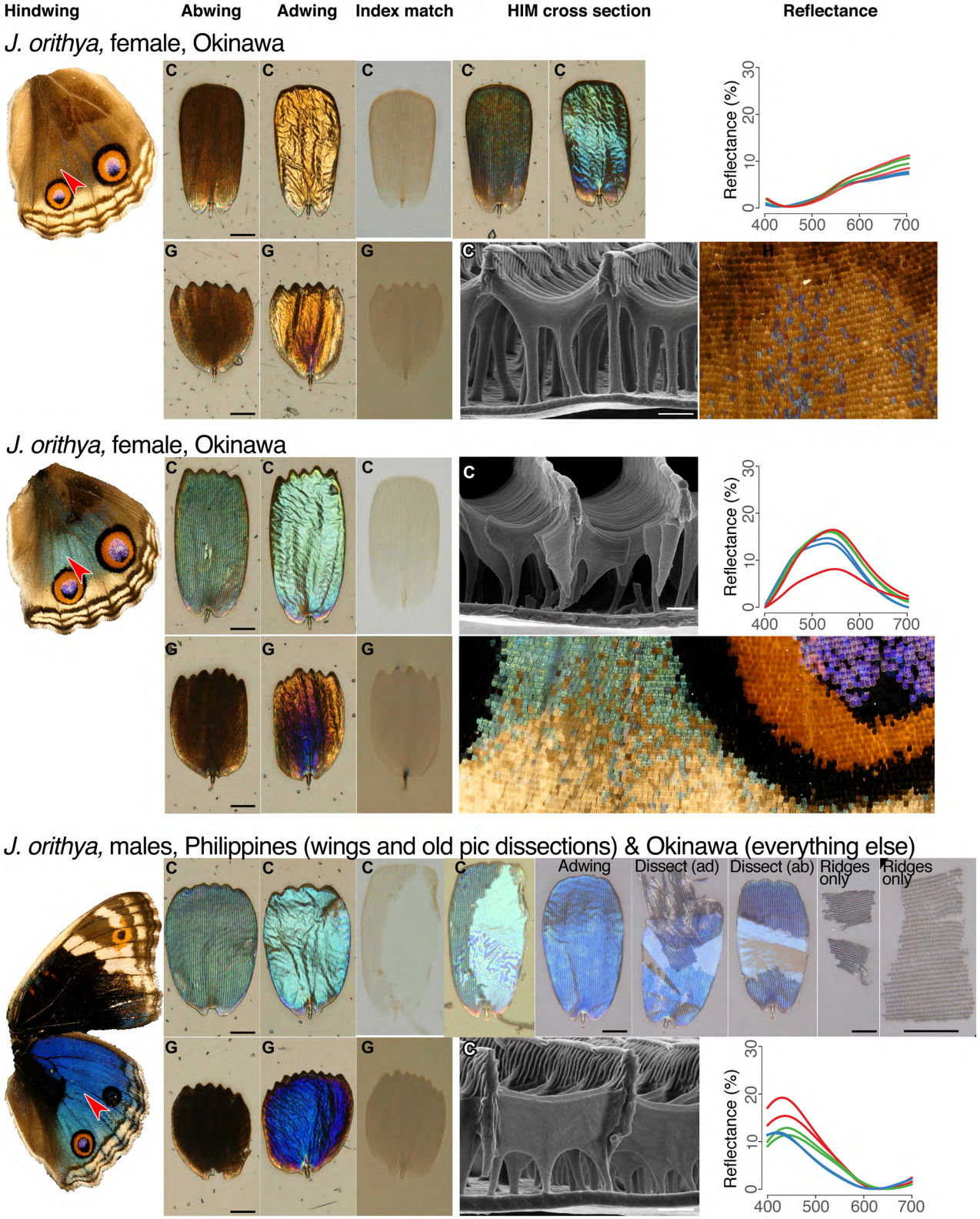

Extended details for *Junonia* species

Hindwing | Abwing | Adwing | Index match | HIM cross section | Reflectance

J. westermanni, female, Central African Republic

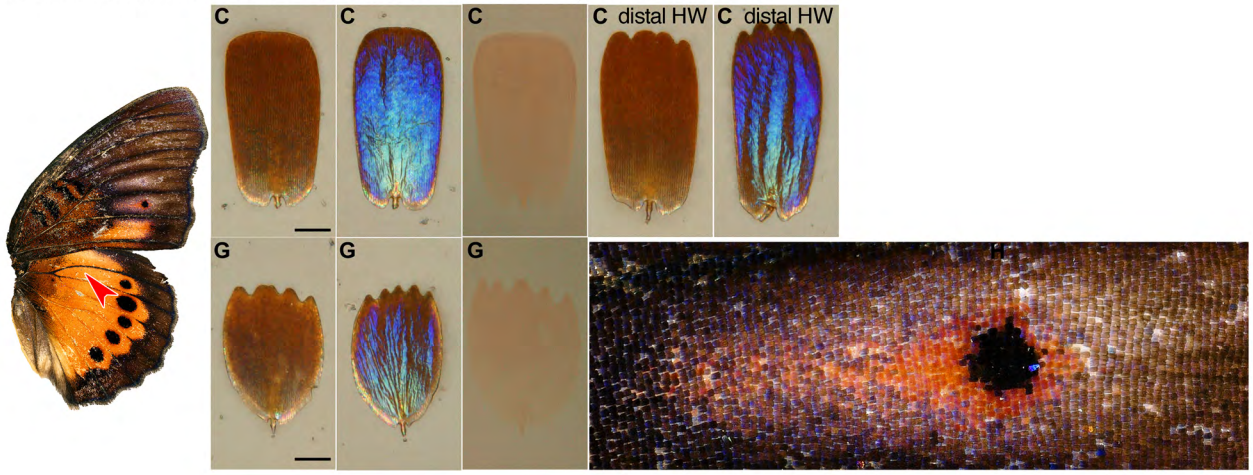

J. westermanni, male, basal aura, Central African Republic

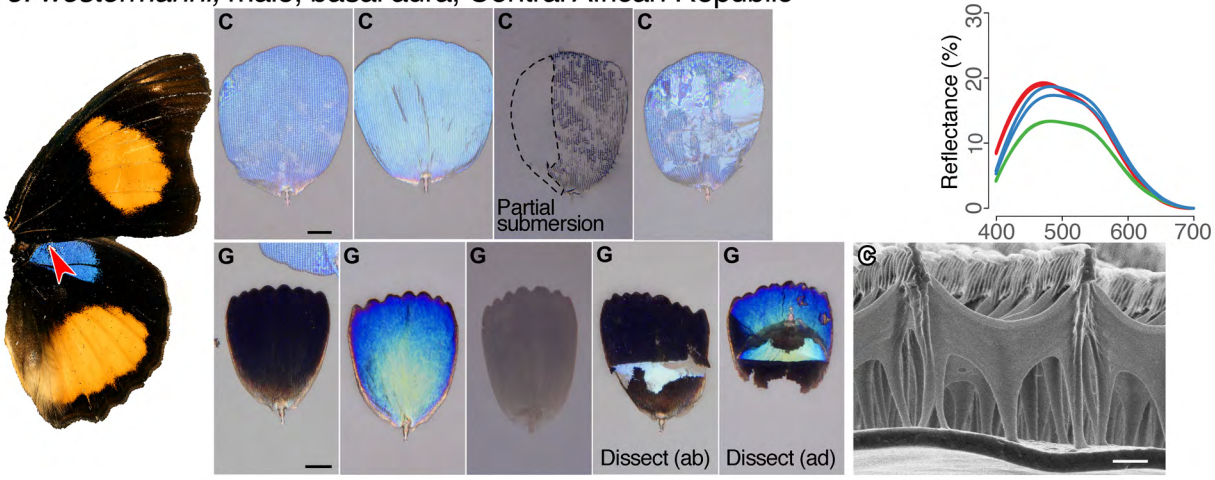

J. westermanni, male, distal hindwing, Congo

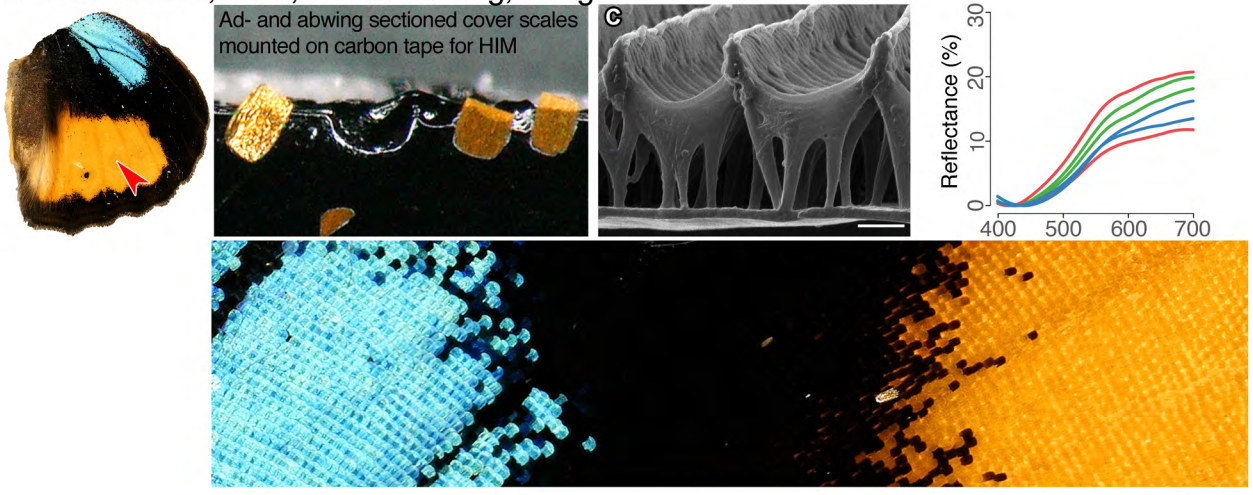

Extended details for *Junonia* species

Hindwing | Abwing | Adwing | Index match | HIM cross section | Reflectance

J. oenone, male, basal aura

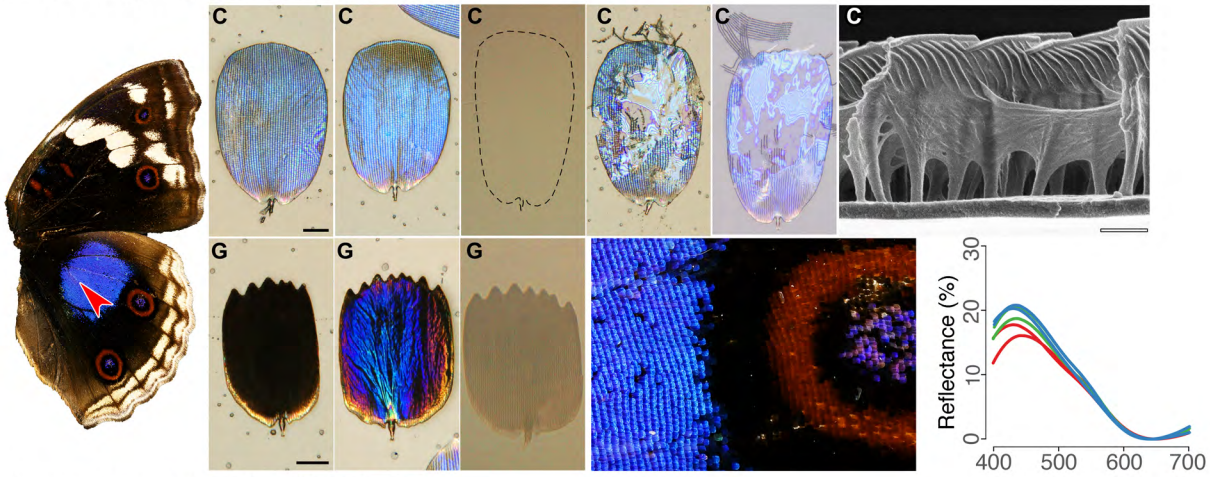

J. oenone, male, distal hindwing

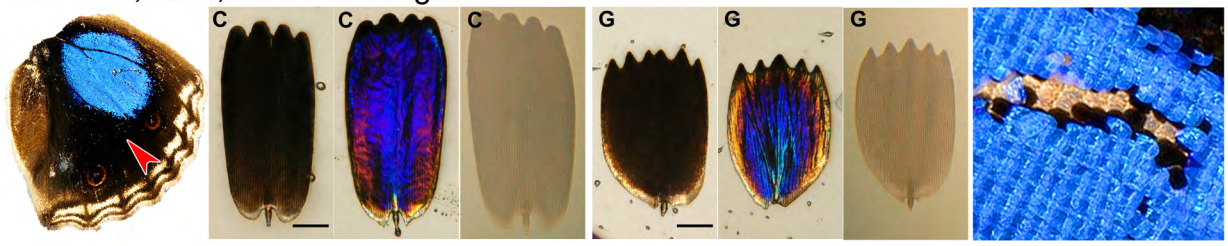

J. oenone, female, proximal hindwing

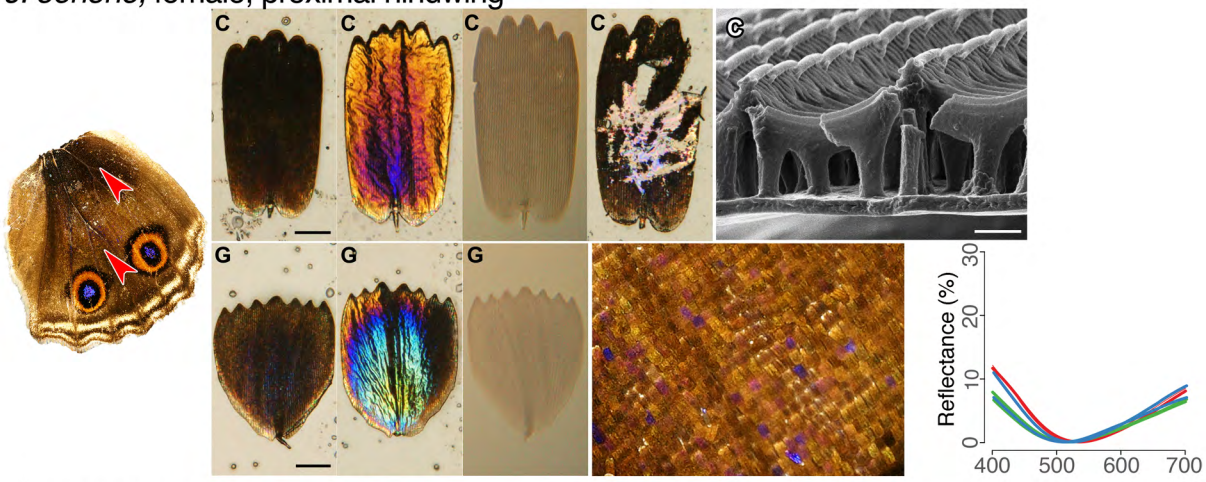

J. oenone, female, distal hindwing

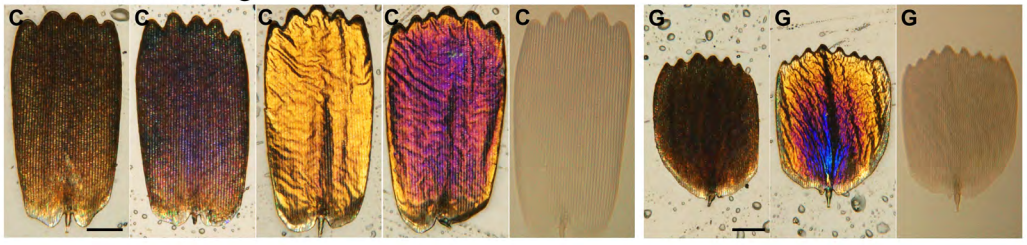

Extended details for *Junonia* species

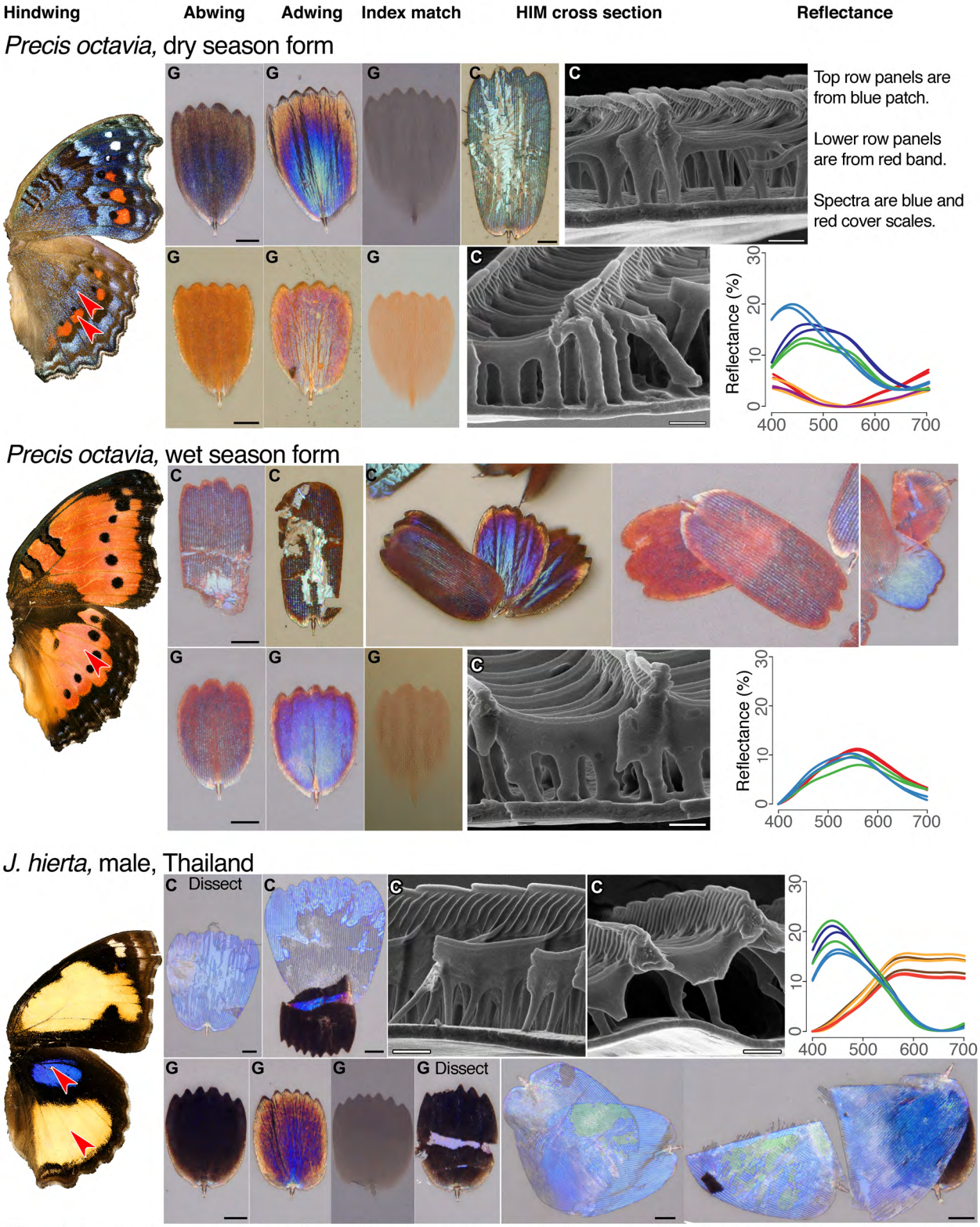

All panels from basal aura unless noted. Top row left to right: 1) Dissected. 2) Cover scale adhered airtight to slide loses structural color. Cracked ground scale exposes bare lamina. 3) Micrograph of blue aura cover scale. 4) Micrograph of yellow cover scale from distal hindwing. 5) Spectra from blue scales (blue, green, violet lines) and yellow scales (yellow, red, brown lines).

Bottom row left to right: 1-4) Series of ground scales from basal aura. 5) Two cover scales adhered together airtight, creating a film with doubled thickness that is structurally green. 6) Folded cover scale adhered to itself. 7) Blue color is most saturated where cover scale overlays the melanic ground scale.

Extended details for *Junonia* species

Hindwing | Abwing | Adwing | Index match | HIM cross section | Reflectance (% / nm)

J. evarete or *genoveva*

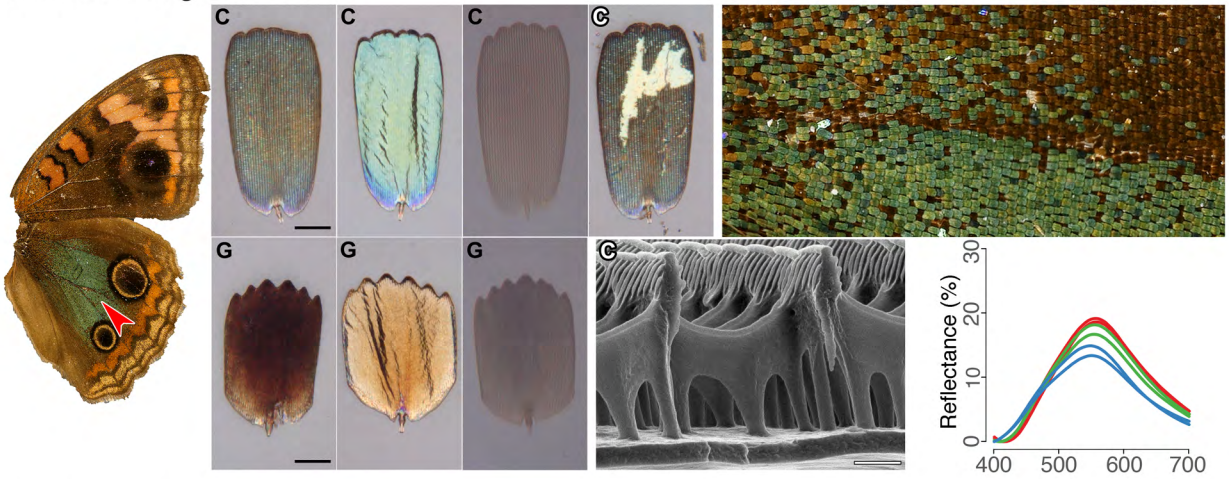

J. almana, Philippines

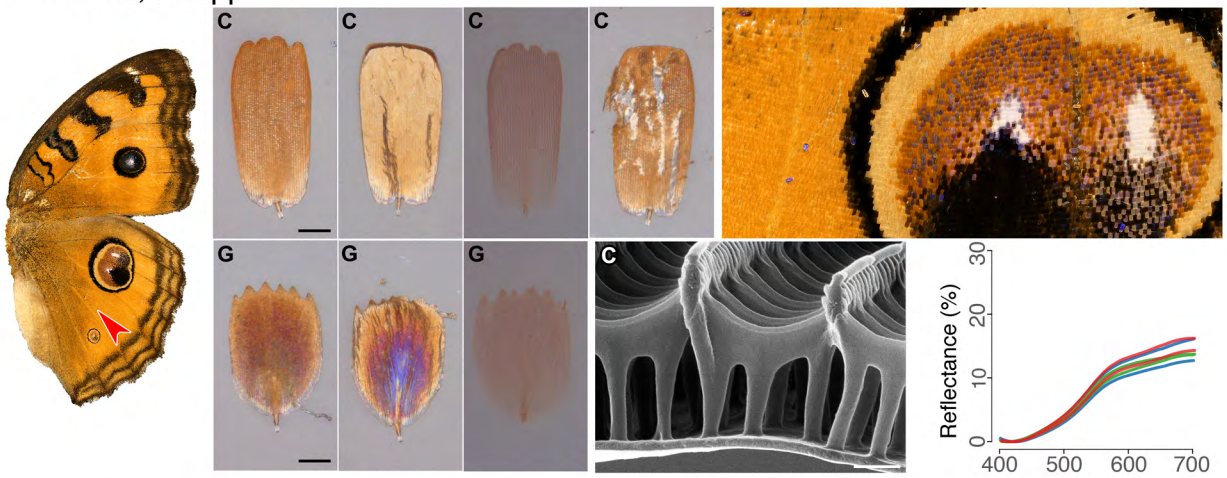

J. coenia, California

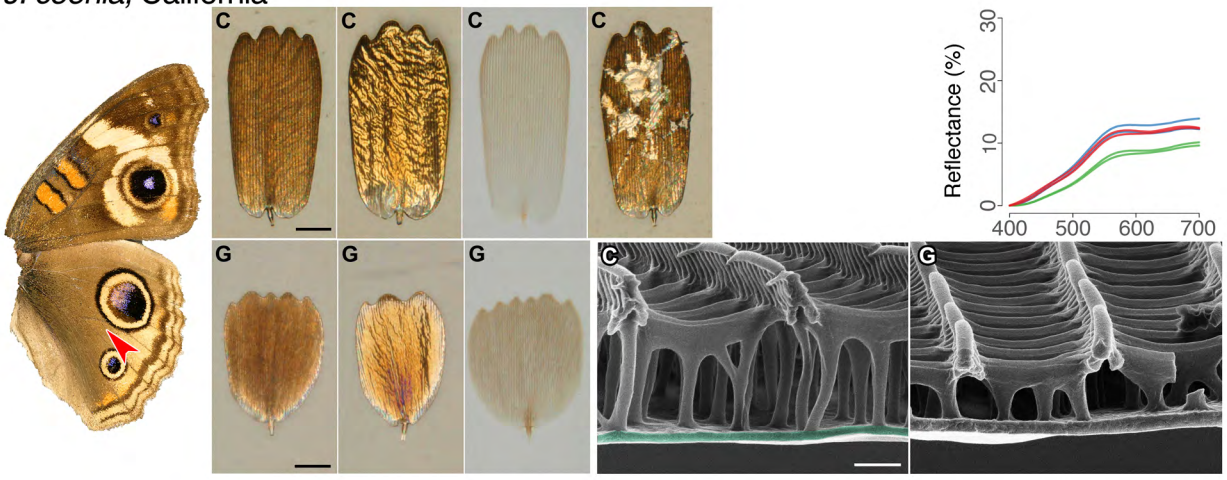

Extended details for *Junonia* species

Hindwing **Abwing** **Adwing** **Index match** **HIM cross section** **Reflectance**

J. evarete or *genoveva,* Bolivia (top) and Jamaica (bottom)

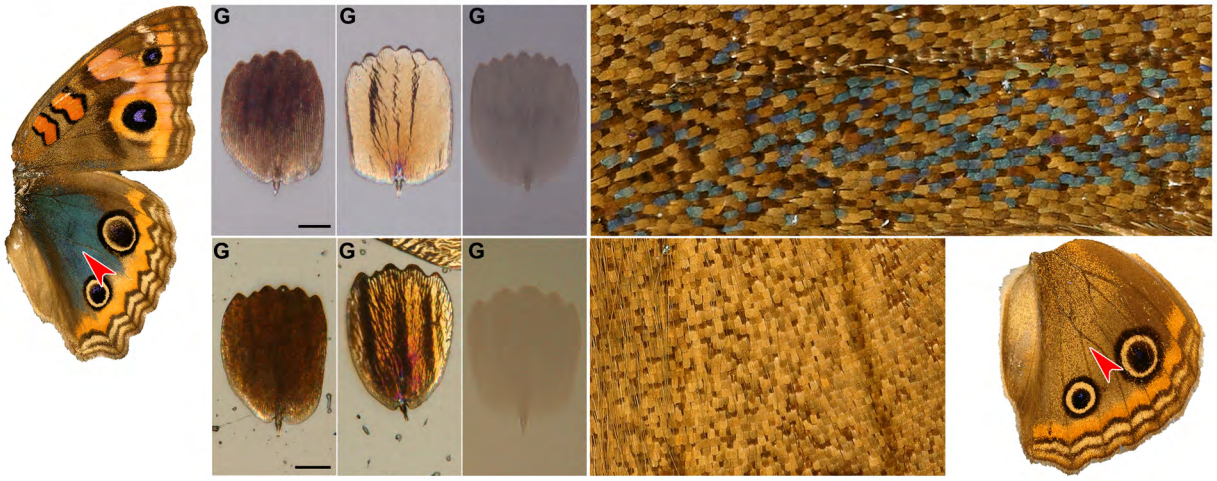

J. coenia, ground scale micrographs, all from hindwings

Top row left: Artificially selected from FL
Top row right: *Optix* mosaic knockout

Bottom: series of lab colony wild-type (NC derived)

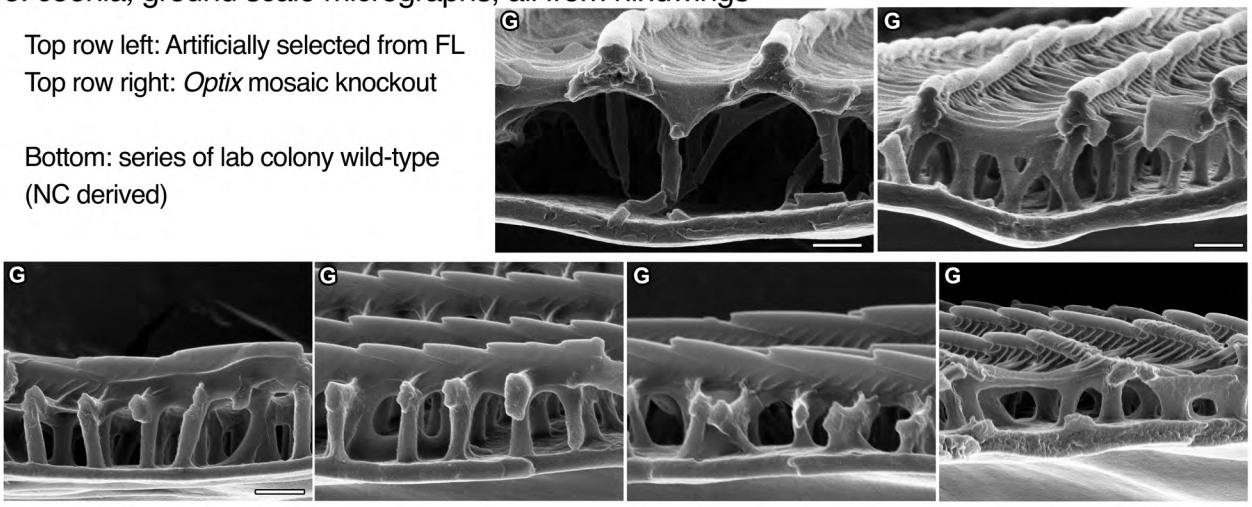

1) *J. coenia,* cover scale 2) *J. westermanni*, partially dissected orange cover scale

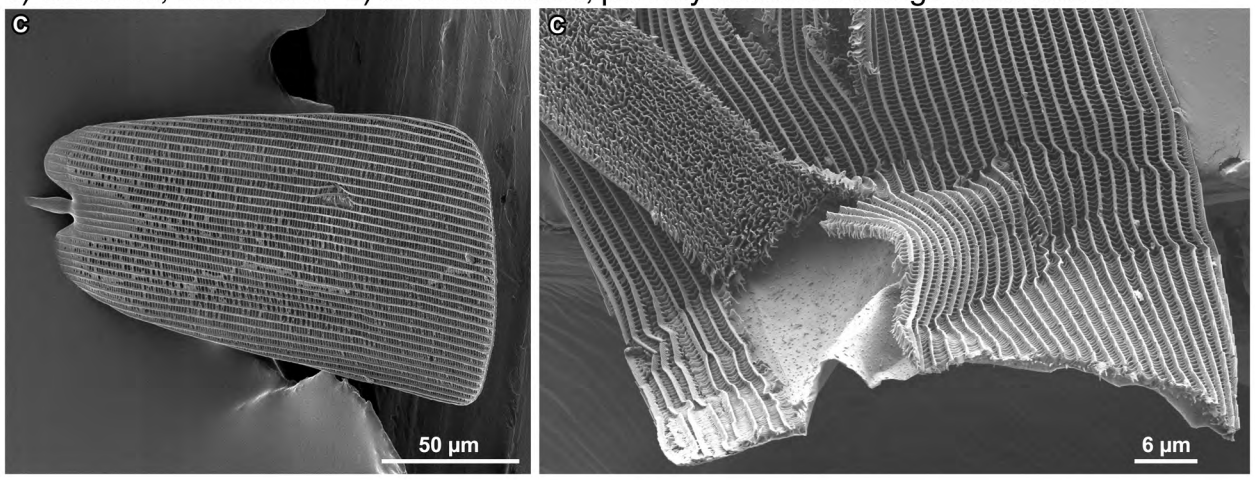

Extended details for *Junonia* species

Cross-sectioned scales mounted over edge of carbon tape for HIM

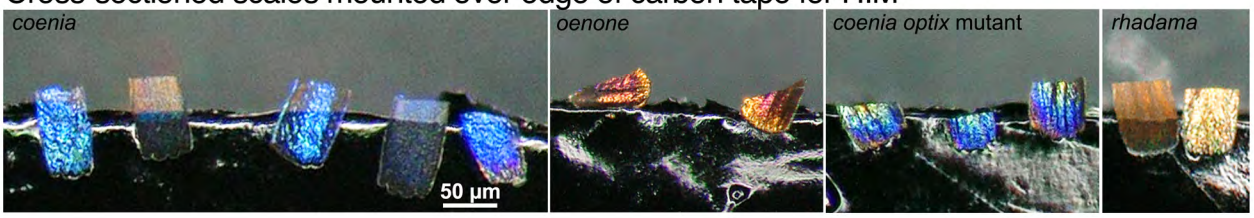

Micrograph of cross-sectioned scales mounted over edge of carbon tape

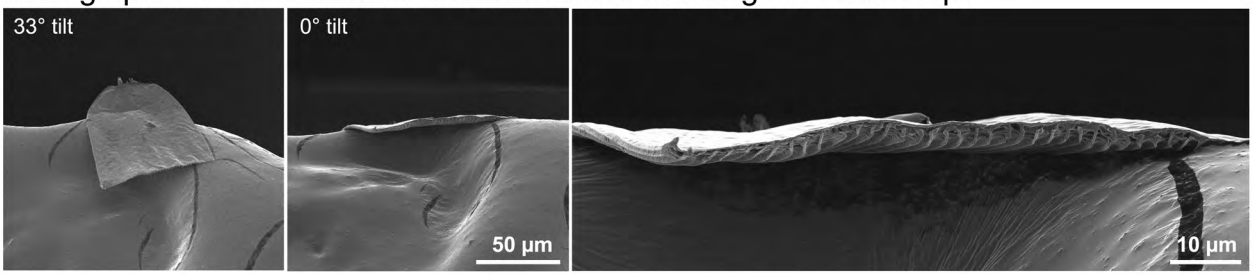

J. coenia, sectioned edge of ventral hindwing red cover scale

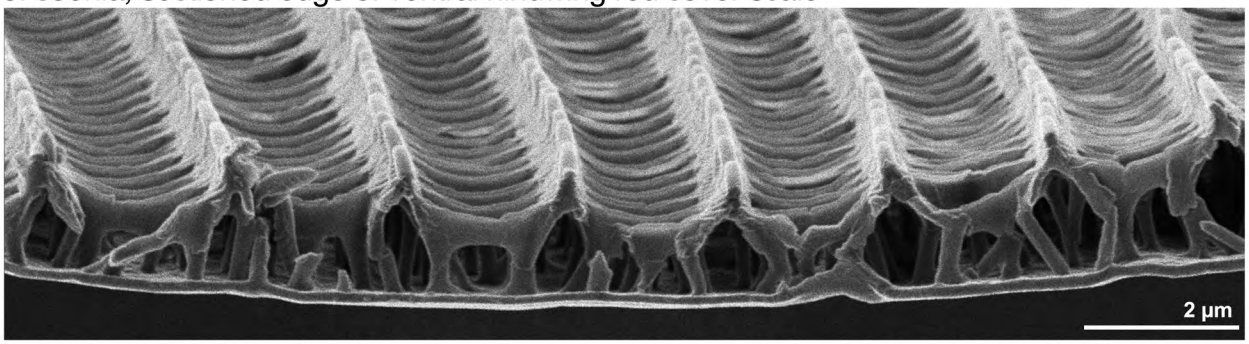

1) Cross-sectioned wing with vein, layered scales, and scale sockets. 2) Scale pedicel (stalk)

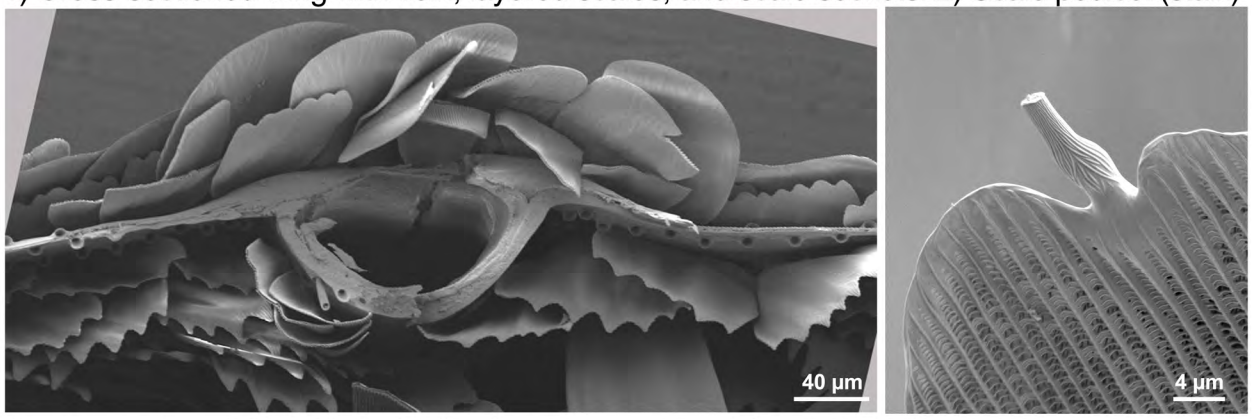

Spectra and model: *J. hierta* doubled part

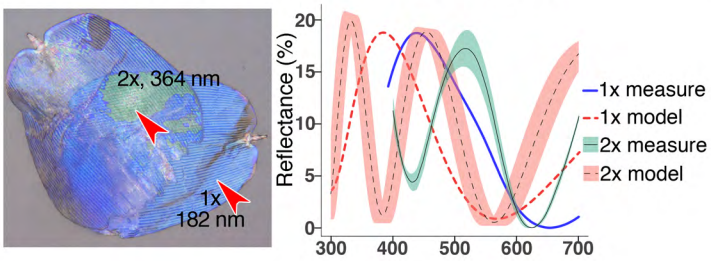

Pigmentation in dissected scales

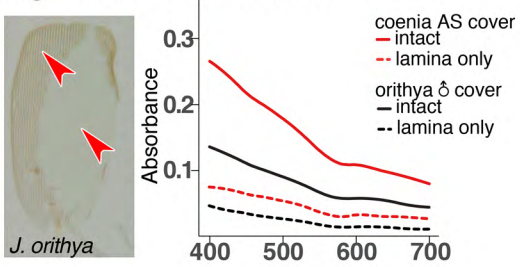

Supplementary File 1. Butterfly specimens used in this study.

Genus	Species	Sex	Sample_origin	Notes	SpecimenID_Fig8	Color_cluster_Fig8	Lamina color in cover scales	Pigment in cover scales
Junonia	almana	F	Mindoro; Philippines		J. almana	gold	gold	orange
Junonia	atlites	M	Greater Sunda Islands; Sulawesi; Decmber 2006; Bioquip catalog #20B2293		J. atlites	NA (rainbow)	gradient of gold, copper, magenta, indigo, blue within each scale	generally none. the occasional scale has very slight brown
Junonia	coenia	M	Middle Island, Cool, California; May 2008; collector Chris Garcia	thickness and pigmentation measured in Fig. 1,3,7,8. I2 in Fig 1 source data	J. coen. WT	gold	gold	dark brown, only in ridges + ribs
Junonia	coenia	M	reared; Rachel Thayer; UC Berkeley; egg laid by wild-collected female from Richmond, CA; December 2014; #102.1	pigmentation measured in Fig. 3	NA	NA	gold	dark brown, only in ridges + ribs
Junonia	coenia	M	reared; Rachel Thayer; UC Berkeley; ordered from Shady Oak butterfly farm (Brooker, FL, USA); October 2014; #00043	thickness, pigmentation, reflectance measured in Fig.s 1,2,3,4,7,8. I5 in Fig 1 source data	J. coen. AS	indigo	indigo	dark brown, only in ridges + ribs
Junonia	coenia	M	reared; Rachel Thayer; UC Berkeley; ordered from Shady Oak butterfly farm (Brooker, FL, USA); June 2015; #132	pigmentation measured in Fig. 3	NA	NA	blue	dark brown, only in ridges + ribs
Junonia	coenia	F	reared; Rachel Thayer; UC Berkeley; second generation in-lab from Shady Oak population (Brooker, FL, USA); July 2015; #140	thickness and pigmentation measured in Fig.s 1,3. I6 in Fig 1 source data	NA	NA	blue	dark brown, only in ridges + ribs
Junonia	coenia		reared; Ryan Null; Marine Biological Laboratory; ordered from Shady Oak butterfly farm (Brooker, FL, USA); June 2014; forewing	thickness measured in Fig. 1 (I7)	NA	NA	blue	dark brown, only in ridges + ribs
Junonia	coenia		reared; Ryan Null; Marine Biological Laboratory; ordered from Shady Oak butterfly farm (Brooker, FL, USA); June 2014	thickness measured in Fig. 1 (I3)	NA	NA	gold	dark brown, only in ridges + ribs
Junonia	coenia		reared; Rachel Thayer; UC Berkeley; shipped as eggs from Karin van der Burg CornellU; June 2015; forewing	thickness measured in Fig. 1 (I4)	NA	NA	gold	dark brown, only in ridges + ribs
Junonia	coenia	M	reared; Rachel Thayer; UC Berkeley; shipped as eggs from Karin van der Burg CornellU; July 2015; #126.41	WT thickness, reflectance, and pigmentation in Fig. 1,2,3,4,8. I1 in Fig. 1 source data.	J. coen. WT	gold	gold	dark brown, only in ridges + ribs
Junonia	coenia	M	reared; Linlin Zhang; CornellU; OptixKO-M30	Used for Fig. 1,2,4, and dorsal hindwing and discal bars in Fig. 5,6	J. coen. mKO	blue	teal	dark brown, only in ridges + ribs
Junonia	coenia	M	reared; Linlin Zhang; CornellU; OptixKO-M61	Used for ventral hindwing in Fig. 5,6	NA	NA	very light white-gold to gold (wild-type regions). gold to copper (mutant regions)	dark brown, only in ridges + ribs. less in wild-type regions than mutant regions
Junonia	evarete complex	M	Coroico; Bolivia; Caranavi 11-12/2000; 700m; collector W. Zöller.	Labeled as Precis lavinia. Dark ventral antenna club. Fig. 1,2,3,7,8.	J. evar. blue	indigo	indigo	dark brown, only in ridges + ribs
Junonia	evarete complex	M	Jamaica; Middlesex County; Manchester Parish; III-1980; Bioquip catalog #20B0320	labeled as J. genoveva neildi. Light ventral antenna club. Fig. 1,2,3,7,8.	J. evar. brown	gold	gold	dark brown, only in ridges + ribs
Junonia	evarete complex	M	unknown; collected prior to September 2014.	8/3/20	J. evar. green	green	green	dark brown, only in ridges + ribs
Junonia	hierta	M	Thailand (same specimen as yellow patch)		J. hier. M	indigo	indigo	none
Junonia	hierta	M	Thailand (same specimen as blue patch)		J. hier. yellow	gold	gold/yellow	yellow, more in distal part of scale
Precis	octavia	M	Tanzania; Tanga Region Amani Forest; October 2014	dry season	P. oct. DS	indigo	variable between adjacent scales, ranges from indigo to teal	slight amount of brown, ridges+ribs only
Precis	octavia	M	Tanzania; Tanga Region Amani Forest; October 2014	wet season	P. oct. WS	green	teal	red, only in ridges + ribs
Precis	octavia	M	reared ex ova; N. Bonkewitz	dry season	P. oct. red band	red	variable between scales and somewhat distal to proximal. Can be copper, magenta, or purple	lots of red
Junonia	oenone	F	Madagascar; Antananarivo province; Analamanga Region; V-2003; Bioquip catalog #20B0340	labeled as P. oenone epiclelia	J. oen. F	red	variable; copper, magenta, or purple	lots of very dark brown/black
Junonia	oenone	M	Madagascar; Antananarivo province; Analamanga Region; V-2003; Bioquip catalog #20B0340	labeled as P. oenone epiclelia	J. oen. M	indigo	indigo	none
Junonia	orithya	F	reared; Masaki Iwata; U of Ryukyus; No. 29; 08.12/1 ~ 12/9		J. orit. brown	gold	gold	dark brown, only in ridges + ribs
Junonia	orithya	F	Marinduque; Philippines		J. orit. F teal	blue	teal	dark brown, only in ridges + ribs
Junonia	orithya	M	Malaysia		J. orit. M	indigo	indigo	dark brown, only in ridges + ribs
Junonia	rhadama	F	Madagascar; February 2016		J. rhad. F	gold	gold	dark brown, only in ridges + ribs
Junonia	rhadama	M	Madagascar; January 2016		J. rhad. M	blue	blue	slight brown, only in ridges + ribs
Junonia	westermanni	M	Central Af Repub; Region de Bambiri; May 2016		J. west. blue	indigo	indigo	none
Junonia	westermanni	M	Central Republic Congo		J. west. orange	gold	gold	orange
Junonia	westermanni	F	Central African Republic		NA	NA	blue to indigo	red-orange

Chapter 3

The genetic architecture of evolved blue structural color in Buckeye butterflies includes *optix* and other loci

Introduction

The genes and pathways that sculpt photonic nanostructures and pattern their distribution over butterfly wing surfaces are largely unknown, but understanding the genetic basis for structural color variation is important to connect the evolutionary and developmental mechanisms that generate these structures. Despite two cross-breeding experiments showing sex-linkage for ridge multilayer structures (Brien et al., 2019; Silberglied & Taylor, 1973) and two artificial selection studies (Thayer et al., 2020; Wasik et al., 2014), only one specific gene, *optix,* has been shown to regulate structural coloration. Specifically, *optix* regulates the presence or absence of blue thin film structural coloration in *Junonia coenia* and *Heliconius doris* (Benson, 2020; Zhang, Mazo-Vargas, & Reed, 2017).

In Chapter 2, I showed that in *J. coenia*, the buckeye butterfly, twelve generations of artificial selection favoring blue wing color caused dorsal wing color to shift from brown to blue, owing to a 74% increase in scale lamina thickness (Thayer et al., 2020). The selected phenotype resembles the naturally evolved blue-winged sister species, *J. evarete*. Furthermore, CRISPR/Cas9-mediated mosaic knockout of *optix* results in a similar blue phenotype due to the same structural mechanism. These results raise an obvious next question: was *optix* itself, or were other genes in the *optix* pathway, responsible for the evolved difference in the artificially selected colony? If so, were the genetic changes in the regulatory sequence around *optix*, or in the protein coding region? More generally, how many genetic changes were required for the rapidly evolved color shift, and how strongly does each locus influence the phenotype? Were upstream patterning genes like transcription factors the loci of evolution, or might the genetic architecture of the selected blue color identify downstream classes of genes that directly sculpt the nanostructures at the subcellular level? To answer these questions, a genetic analysis of the artificially selected butterflies is needed.

Experimental crosses can be used to identify the genetic basis of variation in a trait (Lynch & Walsh, 1998). By intercrossing individuals with contrasting phenotypes for two generations, one can generate an experimental population that segregates variable phenotypes. Observing the relative frequencies of intermediate phenotypes in this

population allows estimates of the number of contributing loci with segregating alleles, and can provide initial evidence of dominance, epistasis, or sex-linkage. Subsequently, quantitative trait locus (QTL) mapping can be used to link genetic loci to the trait variation (Doebley & Stec, 1991; Doerge, 2002). Briefly, QTL mapping is a set of statistical tests for correlations between the trait values and genotypes at sites spread throughout the genome. As an example, QTL mapping could identify genetic regions at which the bluest butterflies always have the same allele as their artificially selected parent. QTL mapping is most successful when the butterflies to be interbred are genetically and phenotypically distinct, and when it is feasible to raise a large number of progeny. The wild-type and artificially selected butterflies have strongly contrasting, heritable structural color phenotypes but are interfertile, produce large broods, and can be bred and reared in a laboratory environment. Consequently, QTL mapping in an experimental cross is a promising approach to identify the full genetic architecture of the evolved blue structural color.

Here, I use a large experimental F2 cross and QTL mapping to discover how many and which loci underlie the evolved structural color change. I report multiple significant and suggestive linked loci for both the distribution of thin film structural colors across the wing surface and their precise hue, and am able to substantively address the questions raised by earlier studies about the role of *optix*. In the process, I construct the first genetic linkage map for *J. coenia* and uncover intriguing trends in structural color variation, including a new spatial patterning axis in the dorsal forewing.

Results

Experimental cross

To generate an F2 mapping population, I set up an experimental cross between an artificially-selected blue butterfly and a wild-type butterfly (Fig. 1). Artificially selected butterflies were purchased from a farm in Florida where the captive population's founders were originally collected (Thayer et al., 2020). Wild-type butterflies were chosen from a well-studied laboratory colony with a reference genome (Nijhout, 1980b; van der Burg et al., 2019). This lab line was originally derived from females collected in Durham, North Carolina, so the parental lines were long diverged. Both lines had presumably undergone population bottlenecks upon collection but were not inbred; consequently, both lines had phenotypic variation. I measured what percent of the dorsal forewing area was blue (Fig. 5) in the parental lines (Fig. 2). In butterflies from the selected line, on average 20.4 ± 6.5 % of the dorsal forewing surface was blue, while wild-type forewings were only 1.4 ± 1.1 % blue on average. Percent blue wing area was more variable within the selection line (Fig. 2). Moreover, in the selected line, the

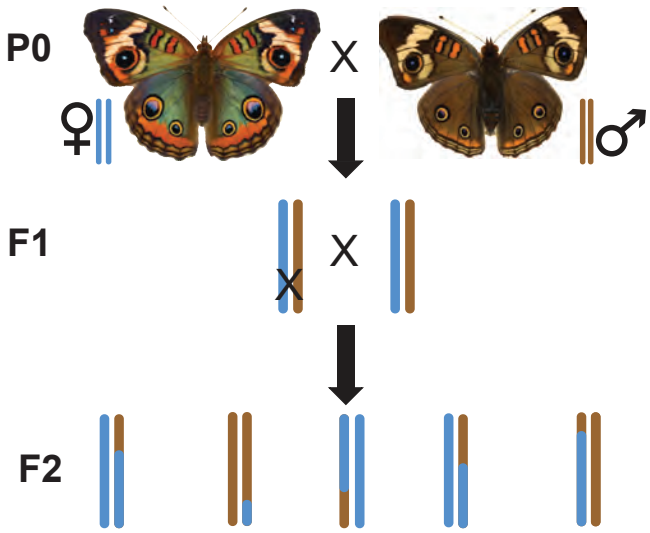

Figure 1: Breeding strategy used to generate the F2 mapping population. A single family of 501 F2 progeny was raised.

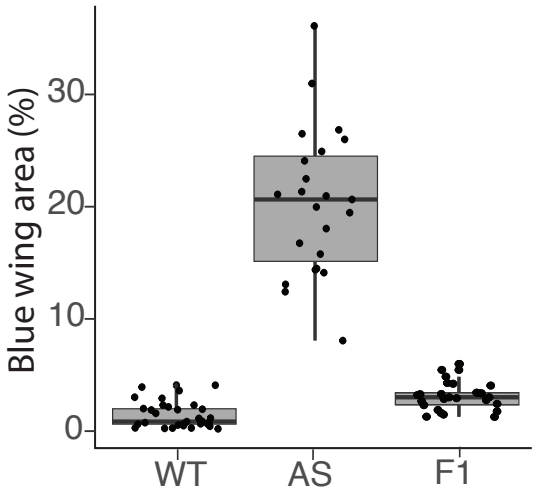

Figure 2: Dorsal forewing color variation in the wild-type (WT), artificially selected (AS), AND F1 lines.

Figure 3: Sample F2 wings showing color and pattern variation. Wings in the top right and bottom left corner have split-color wings (forewing with green/blue split and hindwing with violet/blue split). Subtle hue gradients from anterior forewing to posterior hindwing were common, but split wing colors were very rare.

modified "blue" wing color ranged from violet to green. This hue variation indicates subtler variation in lamina thickness, with greener scales having thicker laminae, up to about 240 nm, and more violet scales having thinner laminae, around 180 nm (Thayer et al., 2020). To select individuals with the most extreme phenotypes as the grandparents of the cross, I chose a green female with 20% green forewing area and a wild-type male with no blue scales outside his dorsal eyespots. Using reflectance spectra of the grandparental scales and the Fresnell thin film equation, adjusted based on empirical results (Stavenga, 2014; Thayer et al., 2020), I estimated that the grandmother had scale laminae around 230 nm thick, while laminae in the grandfather were around 110 nm. I next intercrossed two F1 progeny with intermediate phenotypes (Fig. 4) and raised 501 full-sibling F2 progeny.

Segregation of blue color

Mean percent blue wing area in F1s was 3.1 ± 1.2 (Fig. 2), suggesting partial dominance of wild-type alleles. As anticipated, blue wing area was highly variable among F2 butterflies (Fig. 3). They segregated percent blue wing area on both forewings and hindwings, with continuous variation and a strong positive skew in favor of browner wings (Fig. 4 A,B). Forewing and hindwing percent blue wing area measures were strongly correlated ($r = 0.878$, $p < 2x10^{-16}$), although only hindwings differed significantly by sex (ANOVA, hindwing $p = 0.0004$, forewing $p = 0.56$). Forewing segregation was slightly transgressive, with four progeny having more blue wing area than the grandmother (Fig. 4A). The Castle-Wright estimator (Castle & Wright, 1921; Lynch & Walsh, 1998) suggests that variation in blue wing area on the forewing could be explained by segregating alleles at a minimum of 1.8 genes.

The spatial patterns of blue wing area in F1s and F2s exposed a consistent trend (Fig. 6A). When a wing had little blue area, the blue scales always appeared first on the anterior wing between the discal bars. As blue area increased, it extended outward to fill the area surrounding the discal bars, then along the proximal side of the black wing band, and then inward through the center of the dorsal wing. Forewings with the largest blue wing area had blue scales cupping the outside of the posterior eyespot. There were not crisp transitions between blue and brown wing regions in intermediately blue wings. Rather, blue areas gave way gradually to brown, with transition zones that had intermingled blue and brown scales. The first 5 wings shown along the top row of Fig. 3 and the outlined wings along the x-axis in Fig. 4A are representative of these spatial patterning trends.

The precise hue of the nominally blue wing areas also varied among F2s, ranging from violet to green, as it did in the selected line (Fig. 3). Interestingly, no F2 individual had scale laminae between about 130-170 nm, as such scales would be magenta colored

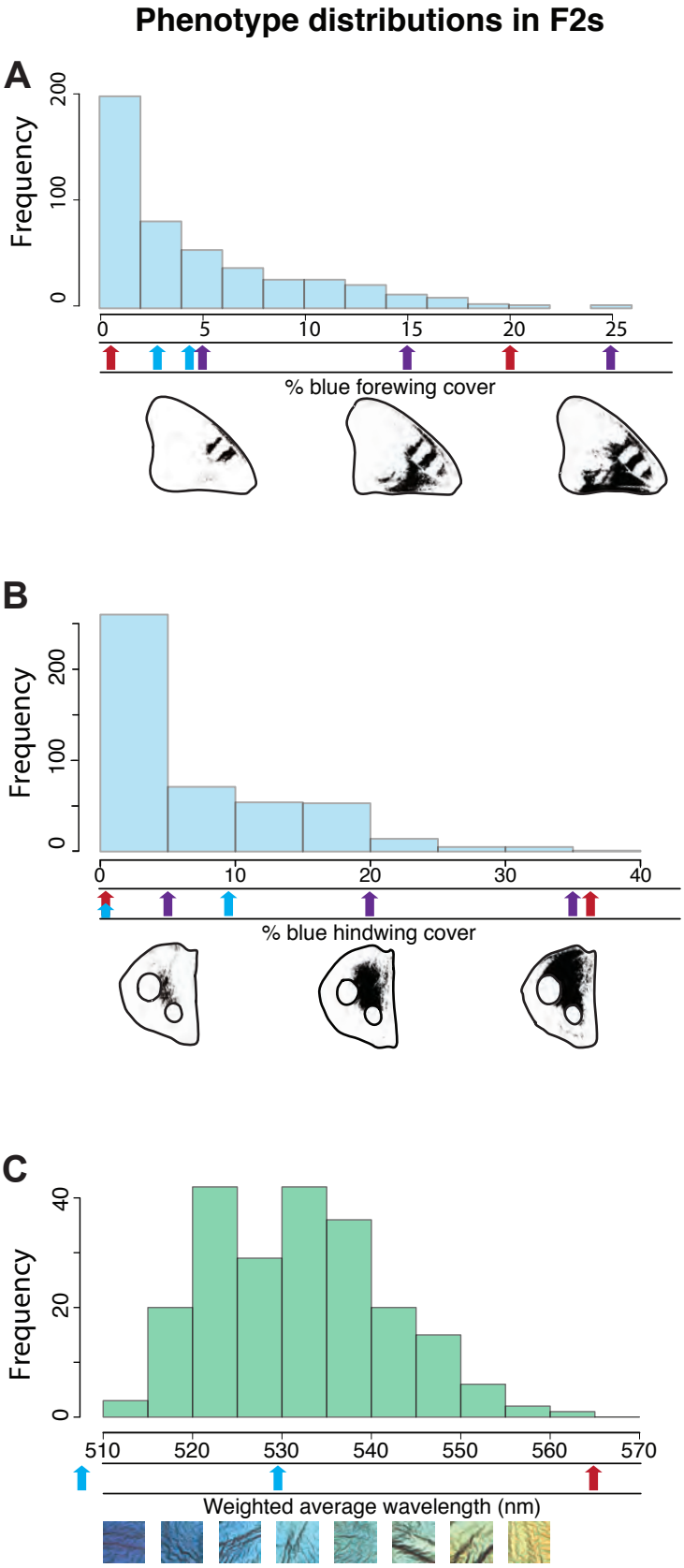

Figure 4: Structural color phenotype distributions in F2 progeny. A track below each histogram shows trait values for grandparents (red arrows) and F1 parents (blue arrows). Below, another track shows images of representative wings or scale colors. Purple arrows show trait values for the sample F2 wings. (A) Histogram of percent blue dorsal forewing coverage, N=484. (B) Histogram of percent blue dorsal hindwing coverage, N=463. (C) Histogram of structural color hues, measured as the mean weighted average reflected wavelength from three scales taken from between the discal bars on the dorsal forewing. Reflectivity at lower wavelengths here indicates a thinner lower lamina. N=217. The wild-type grandparent had exclusively brown scales, which were broadly reflective above 600 nm and much thinner than any colored scales measured from F2s.

(Thayer et al., 2020). Thus, lamina thickness did not vary continuously between the grandparental values. Rather, there was a discrete break such that scales were either very thin and gold or else much thicker and blue-green. Because virtually every F2 had at least 1-2 blue-green scales in the target area between the discal bars, and because the gold versus blue-green portion of color variation was already described by the measures of percent "blue" wing area, I decided to measure structural color a second way focused on only the hue variation between violet and green.

I wanted to measure hue in such a way that it was as non-composite a trait as possible, so as to numerically describe the phenotypic output of fewer genes and improve the likelihood of successfully mapping linked loci. Color on an intact wing is a highly composite trait, influenced by pigmentary and structural colors in both cover and ground scales, as well as their overlap, and by color mixing when disparately colored scales are intermingled, which was common in F2s. Because it was previously shown that cover scale lamina thickness is the most important cause of blue hue in selected buckeyes (Thayer et al., 2020), I prioritized isolating cover scale lamina structural color with my measurement strategy. For many photonic structures, reflectance from one structure is also a composite trait, influenced by multiple dimensions such as the number of layers in a multilayer, the thickness of each layer and inter-layer space, and density or filling fraction. One advantage of simple thin film colors is that the relationship between the sub-micron dimensions of the structure and reflectance is straightforward: peak reflected wavelength is driven by thickness (Fig. 6D), while spectral purity is determined by how uniform thickness is throughout the film (Stavenga, Leertouwer, & Wilts, 2014). As a result, the peak reflected wavelength in spectra of the adwing scale surface is nearly as good a measurement of lamina thickness as a cross sectional electron micrograph would be, but dramatically faster and less expensive to assay. Accordingly, I removed blue-green cover scales from each F2, took reflectance spectra from the adwing surface (i.e. lower lamina surface), and used the weighted average peak reflected wavelength as a proxy for lamina thickness (hereafter called "hue," Fig. 6B, C, Methods).

Hue (i.e. weighted average peak reflected wavelength) varied continuously between 510 - 560 nm, with nearly normal distribution with a small right skew (Fig. 4C). Hue did not differ by sex (ANOVA, $p = 0.184$) and was not correlated with percent blue wing area ($r = 0$, $p = 0.9$). Although I only took spectra from scales from between the forewing discal bars, I did qualitatively observe that hue at that site was largely predictive of hue wherever else blue-green scales occurred on the dorsal wings. If hue did differ, it exhibited a slight wavelength gradient from anterior forewing to posterior hindwing, with longer wavelength (i.e. thicker) scales at the anterior. This gradient was usually subtle, such that generally if a butterfly was qualitatively green by the discal bars, it

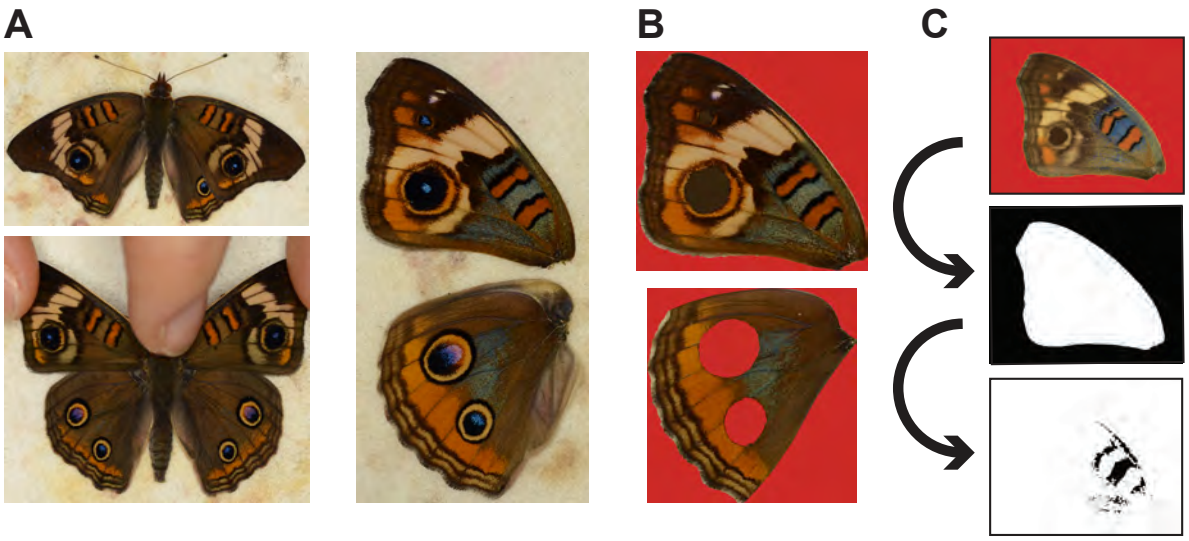

Figure 5: Measuring percent blue wing area in F2s. (A) Raw photos of a breeder and non-breeder F2. (B) Processed photos. (C) A custom script selected all pixels within a specified color range to measure the wing area and the area with violet-to-green scales. Blue scales in eyespots were excluded.

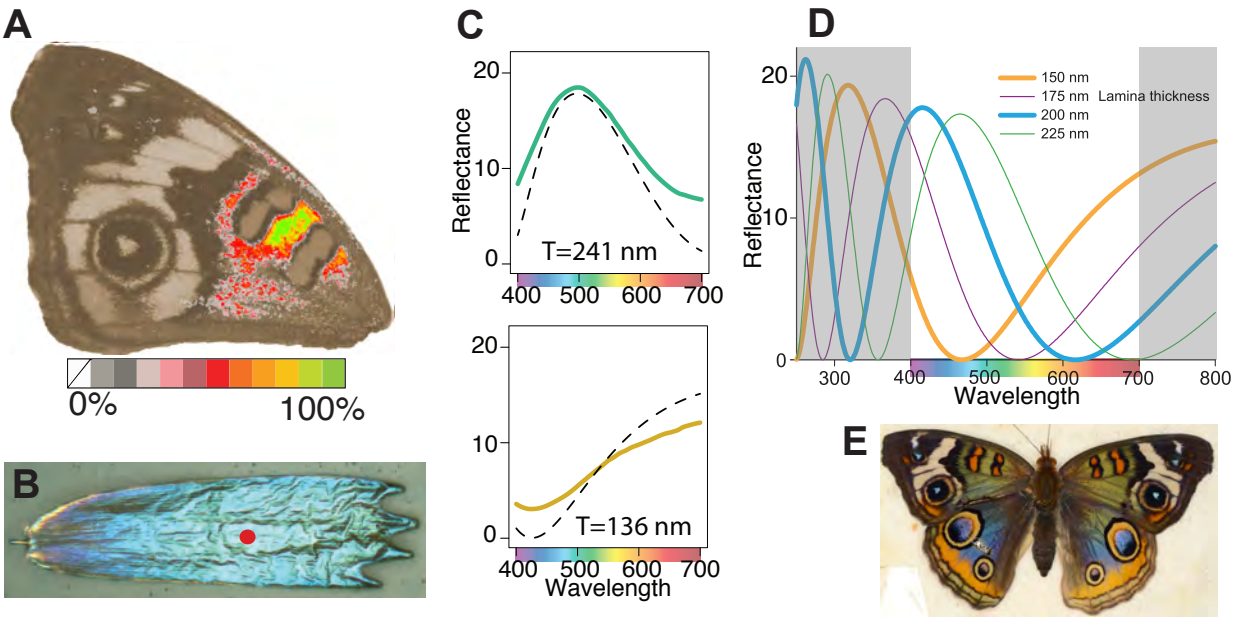

Figure 6: Measuring hue in F2s. (A) Heat map overlayed on a wing to show the proportion of F1 animals who had blue scales in each position, eyespots excluded. If blue scales never occurred in a wing region, e.g. the far distal tip, then the heat map overlay is transparent. All F1s had blue scales between the discal bars. (B) Spectral measurements were taken from the center of the adwing surface of cover scales removed from between the discal bars on the dorsal forewing. (C) Measured spectra (colored lines) compared to best-fit modeled spectra (dashed lines) with the indicated lamina thickness. (D) Theoretical reflectance spectra for laminae with varied thickness, based on Stavenga 2014. (E) Extreme example from the selection line of the hue gradient from greener and thicker anteriorly to more violet and thinner posteriorly.

would be qualitatively green on the hindwings too. A selected line butterfly that is an extreme outlier example of a gradient along the A-P axis is shown in (Fig. 6E). There were a few rare but striking F2s with split-colored wings (most extreme example shown in Fig. 3, top right).

Genetic analysis

To identify the genetic architecture of each structural color trait, I extracted genomic DNA from the thorax flight muscle of 245 F2s and the grandparents and genotyped them using ddRAD sequencing (Methods). After de-multiplexing and quality filtering reads, there were on average 1.8 million reads per animal, around 60% of which mapped to the *J. coenia* reference genome (van der Burg et al., 2019). Genotypes were called using Stacks (Catchen, Amores, Hohenlohe, Cresko, & Postlethwait, 2011), and a final set of 1354 polymorphic markers were retained after removing markers that were redundant or exhibited segregation distortion (Methods). After anchoring these markers to the reference genome, I found that the contigs they tagged had a combined length of about two-thirds of the genome assembly's total length. I removed one pair of duplicate individuals and one failed barcode, resulting in genotypes for 242 F2s. I also sequenced the wild-type and green grandparental genomes to 21x and 26x coverage, respectively, with Illumina Whole Genome sequencing.

To build a genetic linkage map, I estimated marker order using pairwise recombination fractions with R/qtl (Fig. 7, Methods, Broman, 2010). The algorithm recognized 23 linkage groups, but a visual inspection of linkage shows that there are actually 31 distinct clusters, in agreement with the *J. coenia* chromosome number.

I performed quantitative trait locus mapping separately for each structural color trait in R/qtl (Broman, Wu, Sen, & Churchill, 2003) using extended Haley-Knott regression. The genome scan for blue wing area yielded two significant QTL: one peak on linkage group 1 with a maximum LOD score of 13.8, and a second peak on linkage group 12 with a maximum LOD score of 7.1 (Fig. 8A). A scan for hue uncovered four suggestive QTL (Fig. 8B), more than the number of suggestive associations expected to be seen by chance. Of these, two had multiple sequential markers above the suggestive linkage threshold and higher maximum LOD scores: a peak on linkage group 6 with maximum LOD score of 3.5, and a peak on linkage group 20 with maximum LOD 3.1. The less compelling QTL for hue were on linkage groups 7 and 9, and had maximum LOD scores of 2.5 and 2.3.

I evaluated the genomic region inside a 1.5 LOD interval for each significant peak. The peaks on linkage group 1 and 12 spanned 33 cM and 47 cM, respectively. Both peaks included markers on more than two separate contigs in the genome assembly, making it

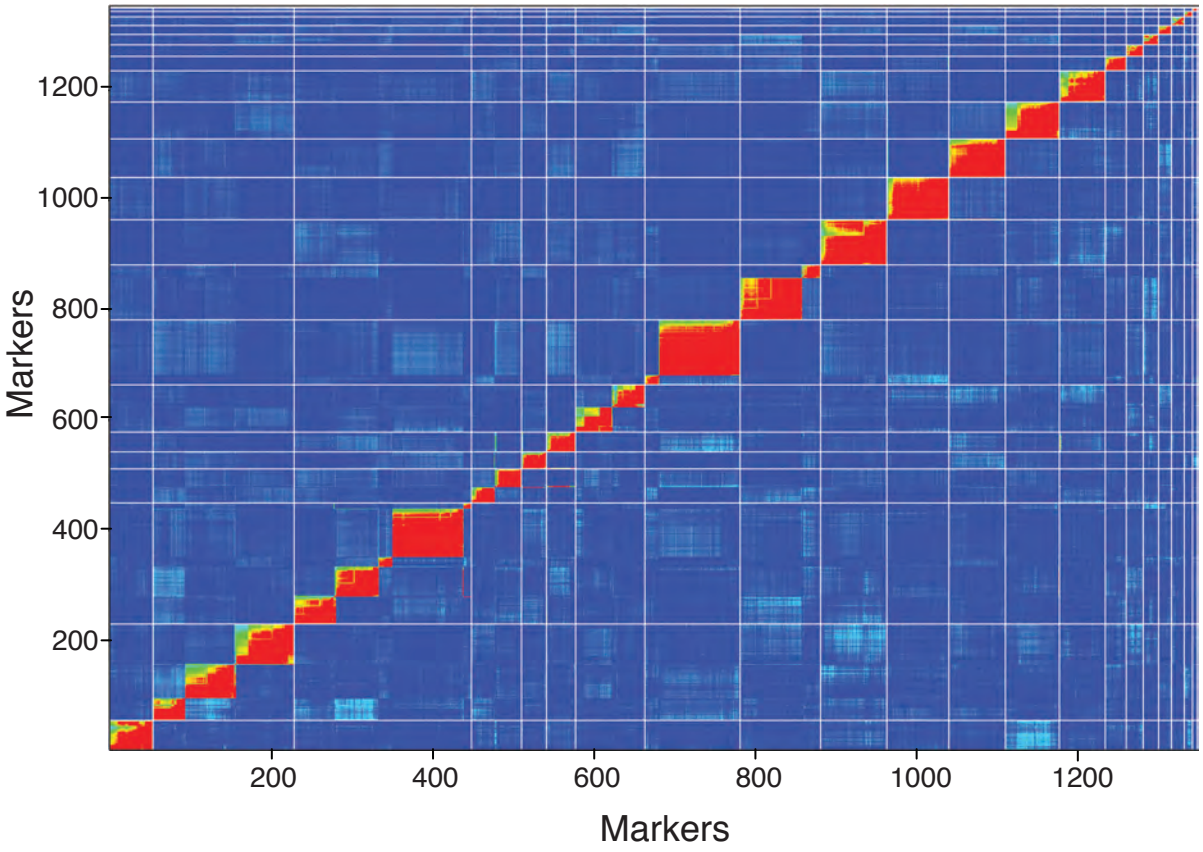

Figure 7: Genetic linkage map with estimated pairwise recombination fractions (upper left half) and LOD scores for a test of r = 1/2 (lower right) for all pairs of markers. Red corresponds to a large LOD or a small recombination fraction, while blue is the reverse. Clusters of linked markers form linkage groups.

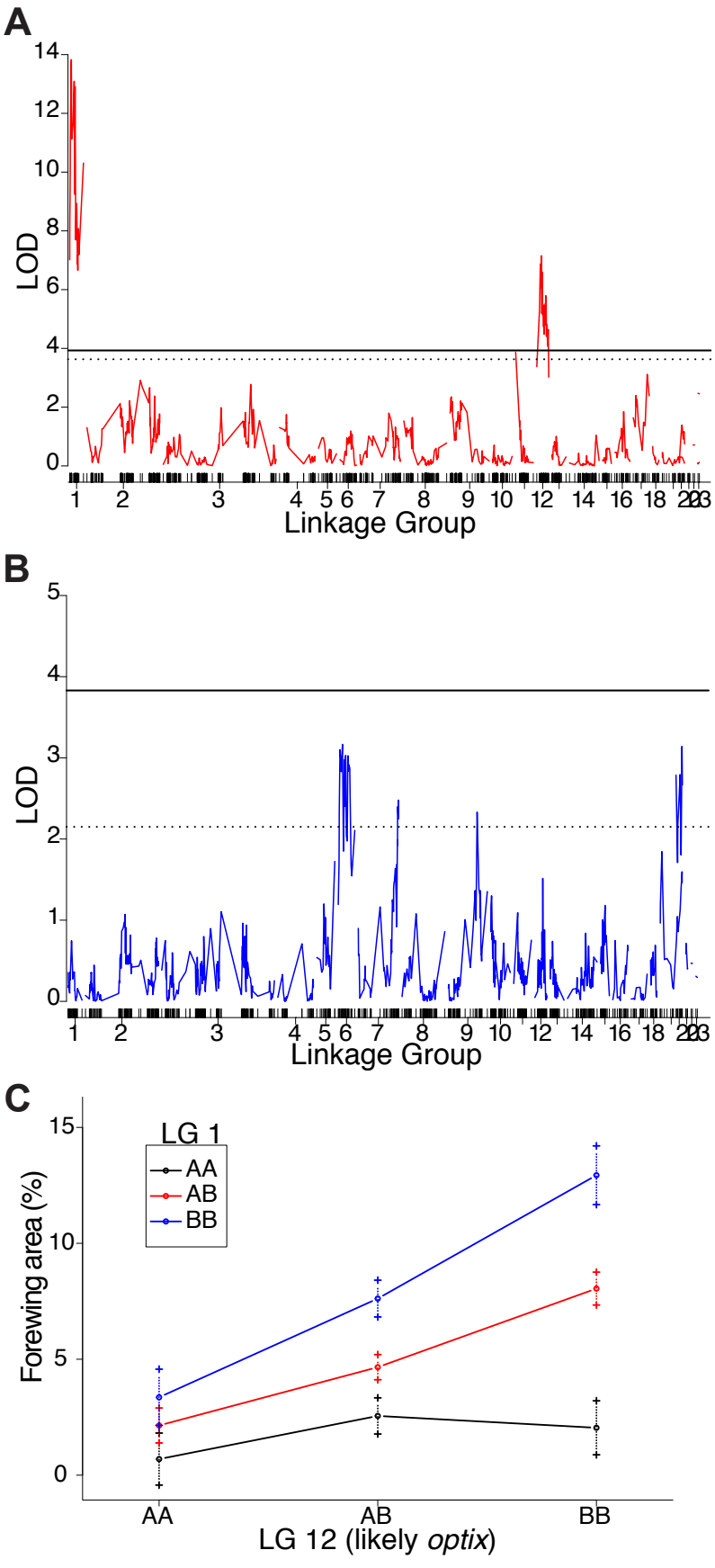

Figure 8: Quantitative trait loci associated with structural color. (A) LOD scores for marker association with forewing percent blue. (B) LOD scores for marker association with weighted average reflected wavelength, which is a proxy for lamina thickness. (A,B) The solid line shows the significance threshold determined with permutation testing (α=0.05 genome-wide). Dotted line shows the threshold for suggestive association (α =0.1 genome-wide). The rug along the x-axis shows individual marker positions. (C) Plot of the estimated phenotype averages ± 1 SE as a function of genotype at the marker nearest the peak LOD score on linkage groups 1 and 12. The phenotype is the percent of the forewing that is blue.

hard to say how broad they are or how many genes they contain, especially since small untagged contigs could potentially align inside the gaps. The intervals are likely to span on the order of three or four megabases and contain more than one hundred genes each. Insofar as I can determine, the QTL interval on LG 1 does not include any genes previously implicated in patterning wing colors, such as *WntA*, *cortex*, *domeless*, *aristaless, wingless, spalt,* or *engrailed*, though the interval does include several transcription factors. By contrast, the QTL interval on linkage group 12 includes the transcription factor *optix*, which was previously functionally tested by CRISPR/Cas9 knockout and confirmed to regulate the patterning of blue structural colors in *J. coenia* (Thayer et al., 2020; Zhang et al., 2017). There were no non-synonymous SNPs within the *optix* gene between the grandparental butterflies, so if *optix* underlies this QTL, the causative sequence difference or differences are likely in regulatory regions.

To investigate the phenotypic effects of each significant QTL peak, I plotted the mean blue wing area as a function of genotype at the markers nearest the peak LOD score for each QTL (Fig. 8C). The average phenotype of F2 butterflies that are homozygous for the wild-type allele at both loci was 0.7 ± 1.1%, while the average phenotype for a butterfly homozygous for both derived alleles was 12.9 ± 1.3%, so the combined effect of these two loci was large.

Discussion

Phenotypic and genetic analysis of an F2 experimental cross revealed a simple genetic basis for the patterning of structurally colored scales across the wing. The first of two significant QTL implicates the gene *optix,* and a second peak seems likely to identify a gene with no previously known role in butterfly wing development. Suggestive linkages with hue and, by proxy, lamina thickness, indicate a completely distinct set of loci on different chromosomes. To explain the relationship between these sets of loci and their associated structural color phenotypes, I propose a model wherein these loci operate at different levels of development (Fig. 9). Relatively early in wing development, it must be specified which cells will go on to build scales with a blue-shifted lamina structural color; this spatial regulation ultimately translates into the arrangement of blue scales across the wing. This cell fate determination may be carried out by *optix* and the locus on LG 1. As scale development proceeds, leading up to and during the stages when chitin is actively secreted, later-acting genes work at the sub-cellular level. The latter group of genes may include the mysterious “cellular rulers” that regulate subtle variation in lamina thickness and hue. Disparate categories of genes could conceivably play such a role, including genes involved with chitin secretion, cytoskeletal dynamics, cell and organelle membrane folding, or genes that regulate the

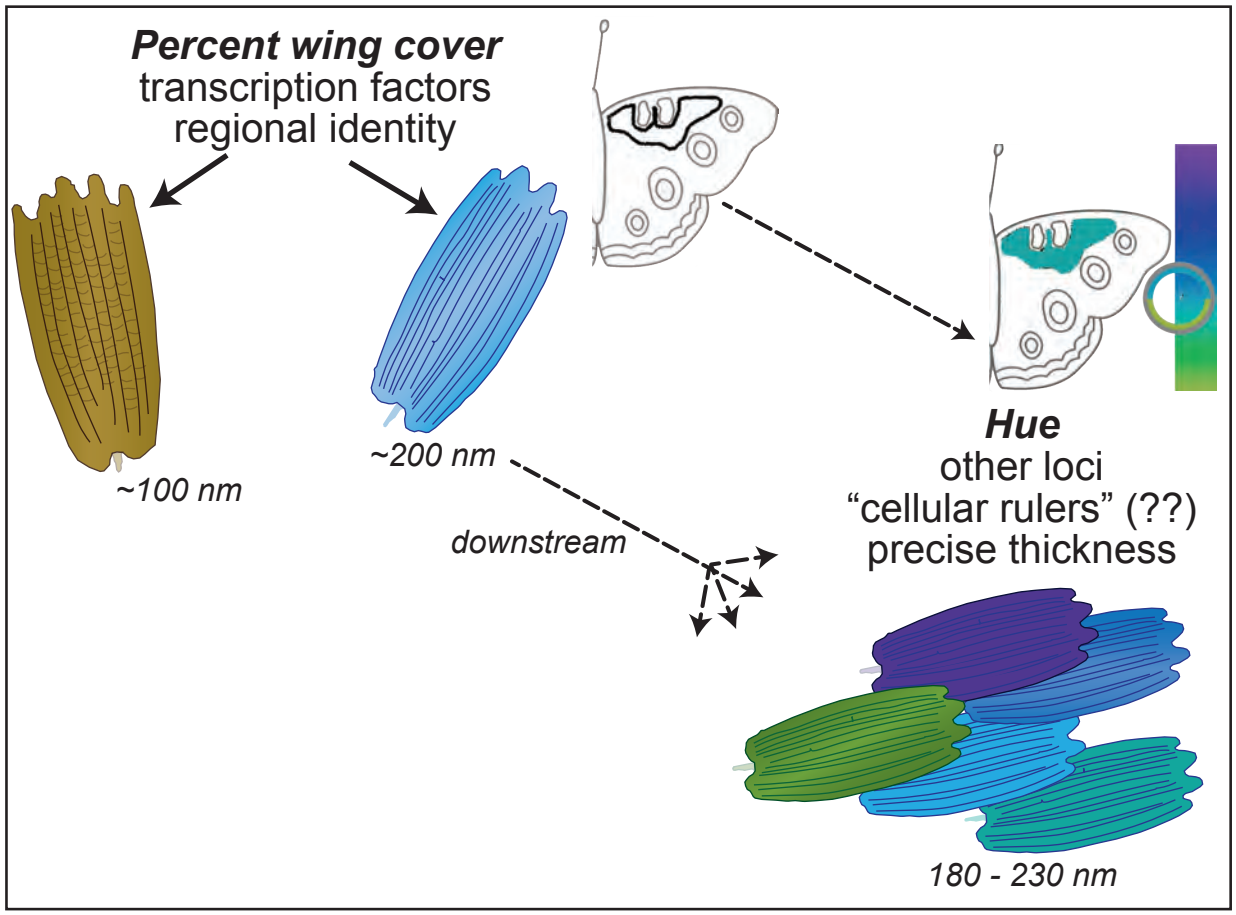

Figure 9: Proposed outline for how structural colors are sequentially patterned by two separate sets of genes. First, it is specified which wing cells will produce scales with thick laminae. Subsequently, downstream loci regulate the precise dimensions of the lamina, determining more subtle variation in hue. As a coloring book analogy, the first set of genes draw an outline and the second set of genes apply color within the lines.

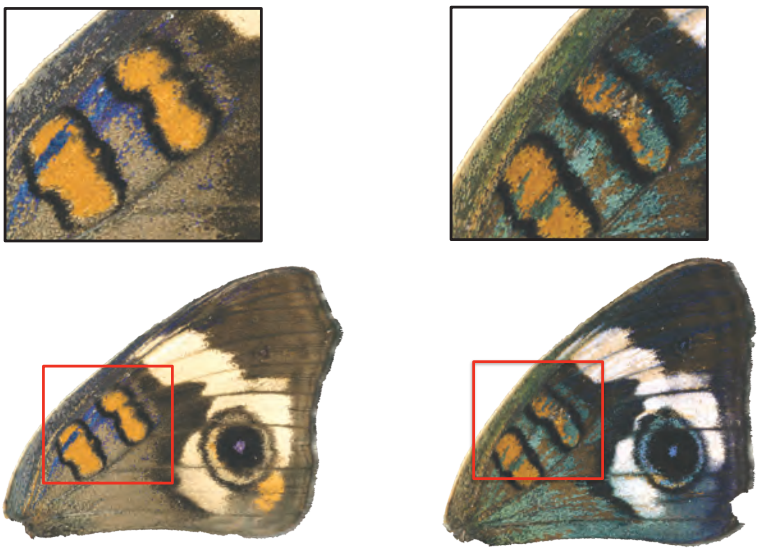

Figure 10: Butterflies with CRISPR/Cas9-induced mosaic knockout of *optix* gain ectopic blue scales, but the precise hue may range from violet to green. This observation is consistent with the QTL result that *optix* does not regulate lamina thickness directly (hue), but rather toggles a switch between specified scale types (percent wing cover).

timing and rate of developmental processes. Possibly the hue loci are directly downstream of the wing patterning loci.

The involvement of the transcription factor *optix* in regulating blue wing area is well compatible with this model (Fig. 9). *Optix* is already known to regulate pigment patterning although it is expressed much earlier than pigmentation stages and does not biosynthesize or transport ommochrome pigments directly (Martin et al., 2014). This behavior, together with *optix'*s role regulating structural color and investigations of the cis-regulatory elements around *optix,* (Lewis et al., 2019) imply that *optix* must have a variety of downstream targets and nuanced regulation, appropriate for a gene that specifies scale cell identity. Further support for this model is found in *optix* knockout butterflies (Zhang et al., 2017). While *optix* knockout in wild-type *J. coenia* results in ectopic blue scales, here again, the precise wavelength varies between violet and green (Fig. 10), consistent with my QTL result that *optix* exposes but does not regulate variation in blue hue. One implication of this model is that brown wild-type butterflies have a genetically encoded breeding value for a hue between violet and green, but the variation is cryptic because it pertains to an unexpressed cell type. Evolutionary or engineered modifications to upstream patterning pathways can expose this latent hue variation.

By combining this study with earlier results, we now have both genetic and functional evidence that the transcription factor *optix* not only regulates the patterning of structural colors in *J. coenia*, but is also a locus of both pigmentary and structural color evolution. The co-occurrence and interaction between pigments and structural colors is frequently important to achieve specific wing color effects (Giraldo, Yoshioka, & Stavenga, 2008; Wilts, Matsushita, Arikawa, & Stavenga, 2015), so it is interesting that *optix* can concurrently affect both, and may help explain why *optix* is recurrently implicated in butterfly evolution. In the selected blue buckeyes, increased melanization of ground scales also evolved, so a follow-up study mapping ground scale pigmentation or functionally dissecting the blue buckeyes' *optix* allele would be informative. Hybrid introgression may also help explain recurring roles for specific genes, and color pattern alleles including the *optix* locus are transferred among *Heliconius* (Dasmahapatra et al., 2012). In *Junonia*, artificially selected blue hindwings resemble naturally evolved blue patterns in the sister species, *J. evarete*. The two species are interfertile (Hafernik, 1982) and may encounter each other in Florida where selection was done, so introgression from *J. evarete* is another unexplored possibility.

Variation in the spatial distribution of blue scales among F2s exposes a previously undescribed patterning axis in the butterfly wing. The Nymphalid groundplan describes the set of underlying pattern elements that can be stretched, shifted, re-

colored, or dropped to produce the diversity of Nymphalid wing patterns; these elements are thought to be ancestral, core building blocks of wing pattern (Nijhout, 1991). The groundplan was independently described by multiple researchers (Schwanwitsch, 1924; Suffert, 1927) and more recently phylogenetically extended to moths (Gawne & Nijhout, 2019). Given the groundplan's broad explanatory power for homologizing patterns across disparate species, one might expect evolved changes to filter through the molecular underpinnings of the ground plan and, consequently, to affect one or more described pattern elements as units. Instead, the order of appearance of blue scales meanders through part of the medial cell, spreads over the MI boundary long before filling the medial cell, and can leak past the MII boundary without having filled either the basal or medial cell. Nor does blue wing area simply spread along the anterior-posterior nor distal-proximal axis, nor along wing veins, nor does blue spread outward from one point as though in response to a radially diffusing morphogen. This bemusing spatial pattern indicates that further genetic dissection of structural color regulation may facilitate important insights to the fundamental mechanisms of wing patterning across taxa.

All butterflies have scales with a lower lamina, so it is likely that the genetic pathway which regulates lamina development in *J. coenia* is also broadly conserved. Among *Junonia* butterflies, evolution has tuned lamina thickness to produce thin film structural colors across the spectrum from golden to blue, green, and even light grey (Thayer et al., 2020). Lamina thin films have been reported in many other Lepidoptera as well (Stavenga et al., 2014; Stavenga et al., 2018; Trzeciak, Wilts, Stavenga, & Vukusic, 2012; Wasik et al., 2014; Wilts, Vey, Briscoe, & Stavenga, 2017). The loci identified here are a promising first step toward understanding this broader evolutionary diversity in structural color.

Materials and Methods

Animal care

Artificially selected blue *J. coenia* were purchased as larvae from Shady Oak Butterfly Farm in 2015 (Brooker, FL). Wild-type *J. coenia* were generously provided from an established laboratory colony, originally derived from females collected in Durham, North Carolina (Nijhout, 1980b). Because larvae from Shady Oak arrived already habituated to leaves, they were fed fresh *Plantago lanceolata* to pupation. Wild-type, F1, and F2 larvae were fed artificial diet (Southland Products, Lake Village, AK) with added dried ground *P. lanceolata* leaves. All animals were kept at 27-30°C on a 16/8 hour day/night cycle. Adult pairs to be mated were put together in small cages under full spectrum light. Once the female began laying fertile eggs on the provided *P. lanceolata*

leaves, the male was removed. Eggs were regularly collected into separate dishes with artificial diet. Adults were fed dilute Gatorade from sponges.

Genotyping

Tissues were preserved for DNA extraction by separating the head, thorax, wings, legs, and abdomen, followed by cutting the thorax into quarters. Wings were stored in individual glassine envelopes. All other tissues were collected into a cryo tube, flash frozen in liquid Nitrogen, and stored at -80°C. Prior to dissection, butterflies were either chilled for a few minutes or frozen and stored at -20°C. DNA was extracted from the flight muscle in ¼ of the thorax per animal using QIAGEN Puregene extraction kit (#158689) and a high-throughput protocol (Andolfatto et al., 2011), with 2.5x the reagent volumes to accommodate the larger tissue fragments.

To prepare ddRAD DNA sequencing libraries, genomic DNA concentration was assessed by Quant-iT PicoGreen Assay (Invitrogen). DNA was digested with *Msp*I and *EcoR*I-HF restriction enzymes (New England Biolabs). Internal adapters with sequences from (Peterson, Weber, Kay, Fisher, & Hoekstra, 2012) were ligated. Multiplexing indexing oligo sequences followed (Meyer & Kircher, 2010). Inserts between 430-630 bp were size-selected with a Pippin prep, analyzed on an Agilent 2100 Bioanalyzer for quality control, and submitted for sequencing. Apart from the restriction enzyme identity and adapter and index sequences, the library protocol followed (Glazer, Killingbeck, Mitros, Rokhsar, & Miller, 2015). The library was sequenced with 100 base pair paired-end sequencing on an Illumina HiSeq 4000 sequencer.

Sequence data was de-multiplexed using the "process_radtags" module of Stacks 1.47 (Catchen et al., 2011). Reads were aligned to the *J. coenia* reference genome (van der Burg et al., 2019) with BWA 0.7.15 (Li & Durbin, 2010) and reads with a mapping quality Phred score below 10 were removed. SNPs were called in Stacks using the default settings of the "ref_map.pl" module and exported in Joinmap format using the "genotypes" module. Only markers with genotype calls for at least 80% of the individuals were exported. The exported genotype file was converted to R/qtl format with the script "filter_jp_file.py" (Kostyun, Gibson, King, & Moyle, 2019).

Grandparental genomic DNA was submitted to a commercial library preparation service, sequenced with 150 base pair paired-end sequencing on an Illumina HiSeq 4000 sequencer, and aligned to the reference genome.

Genetic map

Genotype data was cleaned and a genetic map was estimated using R/qtl 1.38-4 (Broman et al., 2003) following the tutorial (Broman, 2010). I used "comparegeno" to

exclude one pair of duplicate individuals, "findDupMarkers" to thin redundant markers, and "geno.table" to exclude markers with severe segregation distortion ($p < 0.05$ on a test for departure from 1:2:1 genotype frequencies after a Bonferroni correction for multiple tests). These filters retained a final set of 1354 markers and 242 individuals. Marker order was estimated following (Broman, 2010). The function "formLinkageGroups" was used with options max.rf=0.5 and min.lod=18. The "ripple" function was used first with a window size of 7 markers and again with a window size of 4 markers and "method" set to "likelihood".

Photography

Wings were photographed with a Nikon D7000 camera with an AF Micro Nikkor 60mm lens and an LED ring light, mounted on a focusing rail. The camera was controlled with Sofortbild v 1.3 software using 1/160th second shutter time, an F9 aperture, ISO = 500, large image size, and centered metering. White balance was set on a grey card. Focus was adjusted manually. Of the 501 F2s, about half were promptly processed two days after eclosure. The other half were first released in a flight cage to found an intercross line. Consequently, there were also small differences in how breeder and non-breeder F2s were phenotyped (Fig. 5A). Breeders were photographed 1-2 days after eclosing into individual cups, prior to being in the flight cage, so that their wing cuticle had fully hardened but did not yet have wing wear. Breeders were anaesthetized with CO_2 and arranged with spread wings on a white CO_2 fly pad using feather forceps. Two images were taken of each breeder, one each with fore or hindwings in focus. They were then labeled with a sharpie pen on the ventral hindwing, so that tissues and photos could later be matched. Disarticulated wings from dissected non-breeders were laid on the same white CO_2 pad surface and photographed in a single image.

To convert photos into measurements of percent blue wing area (Fig. 5), I first manually selected the forewing from an image and pasted it onto a uniform red background (#cc2a27). Next I covered the forewing eyespots with a brown hue also found in wings (#35230d), so that eyespots would be included in the wing area but not conflated with the target blue area. For hindwings, for consistency between breeders and non-breeders, I used only the portion of the wing that is visible when the wing is still articulated (i.e. not the proximal flap that hugs the abdomen nor the anterior-most edge, Fig. 5 A,B). Because hindwing eyespot size was highly variable, and because hindwings with huge eyespots had little remaining area with the potential to be blue, eyespots were removed (i.e. replaced with red). Individual wing photos were saved as JPG files and input to a high-throughput custom python/Fiji pipeline (Appendix 2). I used a Fiji script to select and measure pixels within a specified HSB color range. I used a python wrapper script to sequentially measure total wing area (i.e. red area, Hue 0-10, Saturation 128-255, Brightness 130-255, subtracted from total image size), followed by "blue" area (violet

through green inclusive, H 34-239, S 0-217, B 28-207), and finally calculate the percent of wing area that was blue (Fig. 5C). I used percent blue wing area rather than raw blue area to remove the effect of wing size, which is variable generally and differs by sex.

Microspectrophotometry

Three blue cover scales were removed with forceps from between the discal bars on the dorsal forewing, corresponding to the position in (Fig. 6A). When possible (i.e. in non-breeders), scales were taken from the left forewing, exactly next to the notch along the inner edge of the distal discal bar. Post-breeding, wings were worn with many missing scales, so up to 3 suitable cover scales were taken from anywhere between the discal bars on either the right or left forewing. Scales were arranged flat on a glass slide with the adwing surface facing up (Fig. 6B), using a capillary glass microinjection needle.

I took reflectance spectra using an Ocean Optics Flame-S-UV-Vis-Es spectrophotometer mounted on a Zeiss AxioPhot reflected light microscope with a 20x/0.5 objective and a halogen light source. Measurements were normalized to the reflectance of a diffuse white reference ($BaSO_4$). Data were recorded with either SpectraSuite 1.0 or OceanView software, with 3 scans to average and a boxcar width of 7 pixels. The software wizard determined optimal integration time from the reference sample; time was generally about .007 seconds. Spot size was roughly circular, 310 μm in diameter, and centered on the center of the scale. I processed spectra in RStudio 1.0.153 with the package 'pavo,' version 0.5-4 (Maia et al., 2013). First, I smoothed the data using the *procspec* function with *fixneg* set to zero and *span* set to 0.3. I then normalized the data using the "minimum" option of the *procspec* function, which subtracts the minimum from each sample.

To simplify reflectance vectors to a single value for genetic mapping, I used a variation of the peak reflected wavelength, which is a common measure of hue. I used the weighted average maximally reflected wavelength of ten 30 nm bins from 400-700nm. This essentially describes maximally reflected wavelength without being sensitive to noise or plateaus in the spectral curve (plateaus can occur in scales with internally heterogeneous thickness). For the range of thicknesses that occured in F2 samples, higher weighted average wavelengths correspond to thicker (greener) scales, while lower wavelengths correspond to thinner (more violet) scales. Finally, I took the mean of the three scales' weighted average peak wavelengths per butterfly.

Quantitative trait locus mapping

Extended Haley-Knott regression was implemented with the "scanone" function in R/qtl (Broman et al., 2003). Percent wing coverage phenotype values were log-transformed prior to regression. Significance thresholds were determined separately for

each phenotype by permutation testing (Churchill & Doerge, 1994). I used 1000 permutations, a significance threshold of α=0.05 genome-wide, and a suggestive linkage threshold of α=0.1 genome-wide (Lander & Kruglyak, 1995). QTL intervals were estimated as 1.5-LOD support intervals using "lodint."

References

Akey, J.M., Ruhe, A.L., Akey, D.T., Wong, A.K., Connelly, C.F., Madeoy, J., Nicholas, T.J., and Neff, M.W. (2010). Tracking footprints of artificial selection in the dog genome. *Proceedings of the National Academy of Sciences 3,* 1160-1165.

Allen, F.I., Velez, N.R., Thayer, R.C., Patel, N.H., Jones, M.A., Meyers, G.F., and Minor, A.M. (2019). Gallium, neon and helium focused ion beam milling of thin films demonstrated for polymeric materials: study of implantation artifacts. *Nanoscale 3,* 1403-1409.

Anderson, T. F., & Richards Jr, A. G. (1942). An electron microscope study of some structural colors of insects. *Journal of Applied Physics, 13*(12), 748-758.

Andolfatto, P., Davison, D., Erezyilmaz, D., Hu, T. T., Mast, J., Sunayama-Morita, T., & Stern, D. L. (2011). Multiplexed shotgun genotyping for rapid and efficient genetic mapping. *Genome Research, 21*(4), 610-617.

Bálint, Z., Katona, G. P., Horváth, Z. E., Kertész, K., Piszter, G., & Biró, L. P. (2019). High accuracy of color-generating nanoarchitectures is kept in lowland and mountainous populations of *Polyommatus dorylas* (Lepidoptera: Lycaenidae: Polyommatinae). *Arthropod Structure & Development, 53*, 100887.

Bálint, Z., Kertész, K., Piszter, G., Vértesy, Z., & Biró, L. P. (2012). The well-tuned blues: The role of structural colours as optical signals in the species recognition of a local butterfly fauna (Lepidoptera: Lycaenidae: Polyommatinae). *Journal of the Royal Society Interface, 9*(73), 1745-1756.

Bálint, Z., Moser, A., Kertesz, K., Biró, L. P., & Parker, A. R. (2009). A supposition: Structural colours resulting from both natural and sexual selection on an individual wing in the butterfly genus *Cyanophrys* (Lepidoptera: Lycaenidae). *Ann.Hist.Nat.Mus.Natl.Hung, 101*, 63-79.

Benson, C. (2020). Genetics of a color polymorphism in *Heliconius doris*.

Biró, L. P., & Vigneron, J. (2011). Photonic nanoarchitectures in butterflies and beetles: Valuable sources for bioinspiration. *Laser & Photonics Reviews, 5*(1), 27-51.

Biró, L. P., Bálint, Z., Kertész, K., Vértesy, Z., Márk, G. I., Horváth, Z. E., . . . Lousse, V. (2003). Role of photonic-crystal-type structures in the thermal regulation of a lycaenid butterfly sister species pair. *Physical Review E, 67*(2), 021907.

Biró, L. P., Kertész, K., Vértesy, Z., Márk, G. I., Bálint, Z., Lousse, V., & Vigneron, J. (2007). Living photonic crystals: Butterfly scales—nanostructure and optical properties. *Materials Science and Engineering: C, 27*(5-8), 941-946.

Boden, S.A., Asadollahbaik, A., Rutt, H.N., and Bagnall, D.M. (2012). Helium ion microscopy of Lepidoptera scales. *Scanning 2,* 107-120.

Boyle, J. H., Kaliszewska, Z. A., Espeland, M., Suderman, T. R., Fleming, J., Heath, A., & Pierce, N. E. (2015). Phylogeny of the Aphnaeinae: Myrmecophilous African butterflies with carnivorous and herbivorous life histories. *Systematic Entomology, 40*(1), 169-182.

Brien, M. N., Enciso-Romero, J., Parnell, A. J., Salazar, P. A., Morochz, C., Chalá, D., . . . Nadeau, N. J. (2019). Phenotypic variation in *Heliconius erato* crosses shows that iridescent structural colour is sex-linked and controlled by multiple genes. *Journal of the Royal Society Interface Focus, 9*(1), 20180047.

Broman, K. W. (2010). Genetic map construction with R/qtl. *University of Wisconsin-Madison, Department of Biostatistics & Medical,*

Broman, K. W., Wu, H., Sen, Ś, & Churchill, G. A. (2003). R/qtl: QTL mapping in experimental crosses. *Bioinformatics, 19*(7), 889-890.

Carroll, S.B., Gates, J., Keys, D.N., Paddock, S.W., Panganiban, G.E., Selegue, J.E., and Williams, J.A. (1994). Pattern formation and eyespot determination in butterfly wings. *Science 5168,* 109-114.

Castle, W. E., & Wright, S. (1921). A method of estimating the number of genetic factors in cases of blending inheritances. *Science N S, 54.*

Catchen, J. M., Amores, A., Hohenlohe, P., Cresko, W., & Postlethwait, J. H. (2011). Stacks: Building and genotyping loci de novo from short-read sequences. *G3: Genes, Genomes, Genetics, 1*(3), 171-182.

Churchill, G. A., & Doerge, R. W. (1994). Empirical threshold values for quantitative trait mapping. *Genetics, 138*(3), 963-971.

Cuthill, I.C., Allen, W.L., Arbuckle, K., Caspers, B., Chaplin, G., Hauber, M.E., Hill, G.E., Jablonski, N.G., Jiggins, C.D., and Kelber, A. (2017). The biology of color. *Science 6350,* eaan0221.

Dasmahapatra, K. K., Walters, J. R., Briscoe, A. D., Davey, J. W., Whibley, A., Nadeau, N. J., . . . Martin, S. H. (2012). Butterfly genome reveals promiscuous exchange of mimicry adaptations among species. *Nature, 487*(7405), 94.

Davis, A. L., Nijhout, H. F., & Johnsen, S. (2020). Diverse nanostructures underlie thin ultra-black scales in butterflies. *Nature Communications, 11*(1), 1-7.

Dechkrong, P., Jiwajinda, S., Dokchan, P., Kongtungmon, M., Chomsaeng, N., Chairuangsri, T., . . . Shiojiri, M. (2011). Fine structure of wing scales of butterflies, *Euploea mulciber* and *Troides aeacus*. *Journal of Structural Biology, 176*(1), 75-82.

Dinwiddie, A., Null, R., Pizzano, M., Chuong, L., Krup, A. L., Tan, H. E., & Patel, N. H. (2014). Dynamics of F-actin prefigure the structure of butterfly wing scales. *Developmental Biology, 392*(2), 404-418.

Doebley, J., & Stec, A. (1991). Genetic analysis of the morphological differences between maize and teosinte. *Genetics, 129*(1), 285-295.

Doerge, R. W. (2002). Mapping and analysis of quantitative trait loci in experimental populations. *Nature Reviews Genetics, 3*(1), 43-52.

Espeland, M., Breinholt, J., Willmott, K. R., Warren, A. D., Vila, R., Toussaint, E. F., . . . Eastwood, R. (2018). A comprehensive and dated phylogenomic analysis of butterflies. *Current Biology, 28*(5), 770-778. e5.

Fresnel, A.J. (1834). Mémoire sur la loi des modifications que la réflexion imprime a la lumière polarisée (Paris: De l'Imprimerie de Firmin Didot Fréres ...).

Galant, R., Skeath, J. B., Paddock, S., Lewis, D. L., & Carroll, S. B. (1998). Expression pattern of a butterfly achaete-scute homolog reveals the homology of butterfly wing scales and insect sensory bristles. *Current Biology, 8*(14), 807-813.

Gawne, R., & Nijhout, H.F. (2019). Expanding the nymphalid groundplan's domain of applicability: Pattern homologies in an arctiid moth (*Utetheisa ornatrix*). *Biological Journal of the Linnean Society, 126*(4), 912-924

Ge, D., Wu, G., Yang, L., Kim, H., Hallwachs, W., Burns, J. M., . . . Yang, S. (2017). Varying and unchanging whiteness on the wings of dusk-active and shade-inhabiting *Carystoides escalantei* butterflies. *Proceedings of the National Academy of Sciences, 114*(28), 7379-7384.

Gemmell, A.P., Borchers, T.E., and Marcus, J.M. (2014). Molecular population structure of *Junonia* butterflies from French Guiana, Guadeloupe, and Martinique. *Psyche: A Journal of Entomology.*

Gerould, J. H. (1943). Genetic and seasonal variations of orange wing-color in *Colias* butterflies. *Proceedings of the American Philosophical Society,* 405-438.

Ghiradella, H. (1974). Development of ultraviolet-reflecting butterfly scales: How to make an interference filter. *Journal of Morphology, 142*(4), 395-409.

Ghiradella, H. (1984). Structure of iridescent lepidopteran scales: Variations on several themes. *Annals of the Entomological Society of America, 77*(6), 637-645.

Ghiradella, H. (1985). Structure and development of iridescent lepidopteran scales: The Papilionidae as a showcase family. *Annals of the Entomological Society of America, 78*(2), 252-264.

Ghiradella, H. (1989). Structure and development of iridescent butterfly scales: Lattices and laminae. *Journal of Morphology, 202*(1), 69-88.

Ghiradella, H. (1991). Light and color on the wing: Structural colors in butterflies and moths. *Applied Optics, 30*(24), 3492.

Ghiradella, H. (1994). Structure of butterfly scales: Patterning in an insect cuticle. *Microscopy Research and Technique, 27*(5), 429-438.

Ghiradella, H. (1998). Hairs, bristles and scales. *Microscopic Anatomy of Invertebrates, 11*, 257-287.

Ghiradella, H. (2010). Insect cuticular surface modifications: Scales and other structural formations. *Advances in Insect Physiology* (pp. 135-180) Elsevier.

Giraldo, M. A., Yoshioka, S., & Stavenga, D. G. (2008). Far field scattering pattern of differently structured butterfly scales. *Journal of Comparative Physiology A, 194*(3), 201-207.

Giraldo, M. A., Yoshioka, S., Liu, C., & Stavenga, D. G. (2016). Coloration mechanisms and phylogeny of *Morpho* butterflies. *Journal of Experimental Biology, 219*(24), 3936-3944.

Giraldo, M.A., and Stavenga, D.G. (2016). Brilliant iridescence of *Morpho* butterfly wing scales is due to both a thin film lower lamina and a multilayered upper lamina. *Journal of Comparative Physiology A 5,* 381-388.

Glazer, A. M., Killingbeck, E. E., Mitros, T., Rokhsar, D. S., & Miller, C. T. (2015). Genome assembly improvement and mapping convergently evolved skeletal traits in sticklebacks with genotyping-by-sequencing. *G3: Genes, Genomes, Genetics, 5*(7), 1463-1472.

Hafernik, J. E. (1982). *Phenetics and ecology of hybridization in buckeye butterflies: Lepidoptera: Nymphalidae* Univ of California Press.

Heikkilä, M., Kaila, L., Mutanen, M., Pena, C., & Wahlberg, N. (2012). Cretaceous origin and repeated tertiary diversification of the redefined butterflies. *Proceedings of the Royal Society B: Biological Sciences, 279*(1731), 1093-1099.

Huxley, J. (1975). The basis of structural colour variation in two species of *Papilio*. *Journal of Entomology Series A, General Entomology, 50*(1), 9-22.

Huxley, J. (1976). The coloration of *Papilio zalmoxis* and *P. antimachus*, and the discovery of tyndall blue in butterflies. *Proceedings of the Royal Society of London.Series B.Biological Sciences, 193*(1113), 441-453.

Imafuku, M., Hirose, Y., & Takeuchi, T. (2002). Wing colors of *Chrysozephyrus* butterflies (Lepidoptera; Lycaenidae): Ultraviolet reflection by males. *Zoological Science, 19*(2), 175-183.

Ingram, A. L., & Parker, A. R. (2008). A review of the diversity and evolution of photonic structures in butterflies, incorporating the work of John Huxley (the Natural History Museum, London from 1961 to 1990). *Philosophical Transactions of the Royal Society B: Biological Sciences, 363*(1502), 2465-2480.

Ingram, A. L., Lousse, V., Parker, A. R., & Vigneron, J. P. (2008). Dual gratings interspersed on a single butterfly scale. *Journal of the Royal Society Interface, 5*(28), 1387-1390.

Iwata, M., Ohno, Y., & Otaki, J. M. (2014). Real-time in vivo imaging of butterfly wing development: Revealing the cellular dynamics of the pupal wing tissue. *PLoS One, 9*(2), e89500.

Joens, M.S., Huynh, C., Kasuboski, J.M., Ferranti, D., Sigal, Y.J., Zeitvogel, F., Obst, M., Burkhardt, C.J., Curran, K.P., and Chalasani, S.H. (2013). Helium Ion Microscopy (HIM) for the imaging of biological samples at sub-nanometer resolution. Scientific reports 3514.

Kazama, M., Ichinei, M., Endo, S., Iwata, M., Hino, A., & Otaki, J. M. (2017). Species-dependent microarchitectural traits of iridescent scales in the triad taxa of ornithoptera birdwing butterflies. *Entomological Science, 20*(1), 255-269.

Kertész, K., Piszter, G., Bálint, Z., & Biró, L. P. (2019). Biogeographical patterns in the structural blue of male *Polyommatus icarus* butterflies. *Scientific Reports, 9*(1), 1-9.

Kertész, K., Piszter, G., Horváth, Z. E., Bálint, Z., & Biró, L. P. (2017). Changes in structural and pigmentary colours in response to cold stress in *Polyommatus icarus* butterflies. *Scientific Reports, 7*(1), 1-12.

Kingsolver, J. G., & Wiernasz, D. C. (1991). Seasonal polyphenism in wing-melanin pattern and thermoregulatory adaptation in *Pieris* butterflies. *The American Naturalist, 137*(6), 816-830.

Kinoshita, S., Yoshioka, S., & Miyazaki, J. (2008). Physics of structural colors. *Reports on Progress in Physics, 71*(7), 076401.

Koch, P. B., Keys, D. N., Rocheleau, T., Aronstein, K., Blackburn, M., & Carroll, S. B. (1998). Regulation of dopa decarboxylase expression during colour pattern formation in wild-type and melanic tiger swallowtail butterflies. *Development, 125*(12), 2303-2313.

Kodandaramaiah, U. (2009). Eyespot evolution: phylogenetic insights from *Junonia* and related butterfly genera (Nymphalidae: Junoniini). Evol. Dev. *5*, 489-497.

Kostyun, J. L., Gibson, M. J., King, C. M., & Moyle, L. C. (2019). A simple genetic architecture and low constraint allow rapid floral evolution in a diverse and recently radiating plant genus. *New Phytologist, 223*(2), 1009-1022.

Kronforst, M. R., Young, L. G., Kapan, D. D., McNeely, C., O'Neill, R. J., & Gilbert, L. E. (2006). Linkage of butterfly mate preference and wing color preference cue at the genomic location of wingless. *Proceedings of the National Academy of Sciences, 103*(17), 6575-6580.

Lander, E., & Kruglyak, L. (1995). Genetic dissection of complex traits: Guidelines for interpreting and reporting linkage results. *Nature Genetics, 11*(3), 241-247.

Lawrence, C., Vukusic, P., & Sambles, R. (2002). Grazing-incidence iridescence from a butterfly wing. *Applied Optics, 41*(3), 437-441.

Leertouwer, H. L., Wilts, B. D., & Stavenga, D. G. (2011). Refractive index and dispersion of butterfly chitin and bird keratin measured by polarizing interference microscopy. *Optics Express, 19*(24), 24061.

Lewis, J. J., Geltman, R. C., Pollak, P. C., Rondem, K. E., Van Belleghem, S. M., Hubisz, M. J., . . . Mazo-Vargas, A. (2019). Parallel evolution of ancient, pleiotropic enhancers underlies butterfly wing pattern mimicry. *Proceedings of the National Academy of Sciences, 116*(48), 24174-24183.

Li, H., & Durbin, R. (2010). Fast and accurate long-read alignment with Burrows-Wheeler transform. *Bioinformatics, 26*(5), 589-595.

Li, W., Cong, Q., Shen, J., Zhang, J., Hallwachs, W., Janzen, D. H., & Grishin, N. V. (2019). Genomes of skipper butterflies reveal extensive convergence of wing patterns. *Proceedings of the National Academy of Sciences, 116*(13), 6232-6237.

Lippert, W., & Gentil, K. (1959). Über lamellare Feinstrukturen bei den Schillerschuppen der Schmetterlinge vom Urania-und Morpho-typ. *Zeitschrift für Morphologie Und Ökologie der Tiere, 48*(2), 115-122.

Lynch, M., & Walsh, B. (1998). Genetics and analysis of quantitative traits. *Sinauer Assocs. Inc.*, Sunderland, MA, 980.

Magkiriadou, S., Park, J., Kim, Y., and Manoharan, V.N. (2014). Absence of red structural color in photonic glasses, bird feathers, and certain beetles. *Physical Review E 6,* 062302.

Maia, R., Eliason, C.M., Bitton, P., Doucet, S.M., Shawkey, M.D., and Tatem, A. (2013). pavo: an R package for the analysis, visualization and organization of spectral data. *Methods in Ecology and Evolution 10,* 906-913.

Martin, A., McCulloch, K. J., Patel, N. H., Briscoe, A. D., Gilbert, L. E., & Reed, R. D. (2014). Multiple recent co-options of *optix* associated with novel traits in adaptive butterfly wing radiations. *EvoDevo, 5*(1), 7.

Mason, C. W. (1926-1927). Structural colors in insects. I-III. *J.Physical Chem, 30*, 383-395.

Matsuoka, Y., and Monteiro, A. (2018). Melanin Pathway Genes Regulate Color and Morphology of Butterfly Wing Scales. *Cell Reports 1,* 56-65.

Meadows, M. G., Morehouse, N. I., Rutowski, R. L., Douglas, J. M., & McGraw, K. J. (2011). Quantifying iridescent coloration in animals: A method for improving repeatability. *Behavioral Ecology and Sociobiology, 65*(6), 1317-1327.

Medina, I., Vega-Trejo, R., Wallenius, T., Symonds, M. R., & Stuart-Fox, D. (2020). From cryptic to colorful: Evolutionary decoupling of larval and adult color in butterflies. *Evolution Letters, 4*(1), 34-43.

Meyer, M., & Kircher, M. (2010). Illumina sequencing library preparation for highly multiplexed target capture and sequencing. *Cold Spring Harbor Protocols, 2010*(6), pdb. prot5448.

Michelson, A. A. (1911). LXI. on metallic colouring in birds and insects. *The London, Edinburgh, and Dublin Philosophical Magazine and Journal of Science, 21*(124), 554-567.

Mielke, O. H. H. (2005). *Catalogue of the american Hesperioidea: Hesperiidae (lepidoptera).: Pyrginae 2: Pyrgini* Sociedade brasileira de Zoologia.

Morehouse, N. I., Vukusic, P., & Rutowski, R. (2007). Pterin pigment granules are responsible for both broadband light scattering and wavelength selective absorption in the wing scales of pierid butterflies. *Proceedings of the Royal Society B: Biological Sciences, 274*(1608), 359-366.

Morris, R. B. (1975). Iridescence from diffraction structures in the wing scales of *Callophrys rubi*, the green hairstreak. *Journal of Entomology Series A, General Entomology, 49*(2), 149-154.

Mouchet, S. R., & Vukusic, P. (2018). Structural colours in lepidopteran scales. *Advances in Insect Physiology* (pp. 1-53) Elsevier.

Müller, F. (1879). *Ituna* and *Thyridia*: A remarkable case of mimicry in butterflies. *Trans.Entomol.Soc.Lond, 1879*, 20-29.

Neild, A.F., and D'Abrera, B. (2008). *The butterflies of Venezuela* Meridian.

Neville, A. C. (1977). Metallic gold and silver colours in some insect cuticles. *Journal of Insect Physiology, 23*(10), 1267-1274.

Nijhout, H.F. (1980a). Ontogeny of the color pattern on the wings of *Precis coenia* (Lepidoptera: Nymphalidae). *Developmental Biology, 2,* 275-288.

Nijhout, H.F. (1980b). Pattern formation on lepidopteran wings: Determination of an eyespot. *Developmental Biology, 80*(2), 267-274.

Nijhout, H.F. (1991). The development and evolution of butterfly wing patterns. *Smithsonian series in comparative evolutionary biology* (USA).

Nijhout, H.F., and Koch, P.B. (1991). The distribution of radiolabeled pigment precursors in the wing patterns of nymphalid butterflies. *Journal of Research on the Lepidoptera 1-2,* 1-13.

Noyes, J. A., Vukusic, P., & Hooper, I. R. (2007). Experimental method for reliably establishing the refractive index of buprestid beetle exocuticle. *Optics Express, 15*(7), 4351-4358.

Onslow, H. (1923). I.—On a periodic structure in many insect scales, and the cause of their iridescent colours. *Philosophical Transactions of the Royal Society of London.Series B, Containing Papers of a Biological Character, 211*(382-390), 1-74.

Overton, J. (1966). Microtubules and microfibrils in morphogenesis of the scale cells of *Ephestia kuhniella*. *The Journal of Cell Biology, 29*(2), 293-305.

Parnell, A. J., Bradford, J. E., Curran, E. V., Washington, A. L., Adams, G., Brien, M. N., . . . Vukusic, P. (2018). Wing scale ultrastructure underlying convergent and divergent iridescent colours in mimetic heliconius butterflies. *Journal of the Royal Society Interface, 15*(141), 20170948.

Peña, C., Wahlberg, N., Weingartner, E., Kodandaramaiah, U., Nylin, S., Freitas, A. V., & Brower, A. V. (2006). Higher level phylogeny of Satyrinae butterflies (Lepidoptera: Nymphalidae) based on DNA sequence data. *Molecular Phylogenetics and Evolution, 40*(1), 29-49.

Peterson, B. K., Weber, J. N., Kay, E. H., Fisher, H. S., & Hoekstra, H. E. (2012). Double digest RADseq: An inexpensive method for de novo SNP discovery and genotyping in model and non-model species. *PloS One, 7*(5), e37135.

Pfeiler, E., Johnson, S., and Markow, T.A. (2012). DNA barcodes and insights into the relationships and systematics of buckeye butterflies (Nymphalidae: Nymphalinae: Junonia) from the Americas. *The Journal of the Lepidopterists' Society 4*, 185-198.

Pinna, C. S., Vilbert, M., Borenztajn, S., de Marcillac, W. D., Piron-Prunier, F., Pomerantz, A. F., . . . Gomez, D. (2020). Convergence in light transmission properties of transparent wing areas in clearwing mimetic butterflies. *bioRxiv,*

Prum, R. O., Quinn, T., & Torres, R. H. (2006). Anatomically diverse butterfly scales all produce structural colours by coherent scattering. *Journal of Experimental Biology, 209*(4), 748-765.

Rayleigh, L. (1919). VII. on the optical character of some brilliant animal colours. *The London, Edinburgh, and Dublin Philosophical Magazine and Journal of Science, 37*(217), 98-111.

Reed, R. D. (2004). Evidence for notch-mediated lateral inhibition in organizing butterfly wing scales. *Development Genes and Evolution, 214*(1), 43-46.

Reed, R. D., Papa, R., Martin, A., Hines, H. M., Counterman, B. A., Pardo-Diaz, C., . . . Chen, R. (2011). *Optix* drives the repeated convergent evolution of butterfly wing pattern mimicry. *Science, 333*(6046), 1137-1141.

Saba, M., Wilts, B. D., Hielscher, J., & Schröder-Turk, G. E. (2014). Absence of circular polarisation in reflections of butterfly wing scales with chiral gyroid structure. *Materials Today: Proceedings, 1*, 193-208.

Sackey, J., Berthier, S., Maaza, M., Beuvier, T., & Gibaud, A. (2018). Comparative study on nanostructured order–disorder in the wing eyespots of the giant owl butterfly, caligo memnon. *IET Nanobiotechnology, 12*(7), 951-955.

Schmidt, K., & Paulus, H. (1970). Die Feinstruktur der Flüigelschuppen einiger Lycaeniden (Insecta, Lepidoptera). *Zeitschrift für Morphologie der Tiere, 66*(3), 224-241.

Schwanwitsch, B. N. (1924). On the ground-plan of wing-pattern in nymphalids and certain other families of the Rhopalocerous Lepidoptera. Paper presented at the *Proceedings of the Zoological Society of London, , 94*(2) 509-528.

Shevtsova, E., Hansson, C., Janzen, D.H., and Kjærandsen, J. (2011). Stable structural color patterns displayed on transparent insect wings. *Proceedings of the National Academy of Sciences 2*, 668-673.

Shields, O. (1989). World numbers of butterflies. *Journal of the Lepidopterists' Society, 43*(3), 178-183.

Siddique, R. H., Vignolini, S., Bartels, C., Wacker, I., & Hölscher, H. (2016). Colour formation on the wings of the butterfly *Hypolimnas salmacis* by scale stacking. *Scientific Reports, 6*, 36204.

Silberglied, R. E., & Taylor, O. R. (1973). Ultraviolet differences between the sulphur butterflies, *Colias eurytheme* and *C. philodice*, and a possible isolating mechanism. *Nature, 241*(5389), 406.

Simonsen, T. J. (2007). Comparative morphology and evolutionary aspects of the reflective under wing scale-pattern in fritillary butterflies (Nymphalidae: Argynnini). *Zoologischer Anzeiger-A Journal of Comparative Zoology, 246*(1), 1-10.

Srinivasarao, M. (1999). Nano-optics in the biological world: Beetles, butterflies, birds, and moths. *Chemical Reviews, 99*(7), 1935-1962.

Stavenga, D. G. (2014). Thin film and multilayer optics cause structural colors of many insects and birds. *Materials Today: Proceedings, 1*, 109-121.

Stavenga, D. G., Giraldo, M. A., & Leertouwer, H. L. (2010). Butterfly wing colors: Glass scales of *Graphium sarpedon* cause polarized iridescence and enhance blue/green pigment coloration of the wing membrane. *Journal of Experimental Biology, 213*(10), 1731-1739.

Stavenga, D. G., Leertouwer, H. L., & Wilts, B. D. (2014a). Coloration principles of nymphaline butterflies: Thin films, melanin, ommochromes and wing scale stacking. *Journal of Experimental Biology, 217*(12), 2171-2180.

Stavenga, D. G., Leertouwer, H. L., & Wilts, B. D. (2014b). The colouration toolkit of the pipevine swallowtail butterfly, *Battus philenor*: Thin films, papiliochromes, and melanin. *Journal of Comparative Physiology A, 200*(6), 547-561.

Stavenga, D. G., Leertouwer, H. L., Hariyama, T., De Raedt, H. A., & Wilts, B. D. (2012). Sexual dichromatism of the damselfly *Calopteryx japonica* caused by a melanin-chitin multilayer in the male wing veins. *PloS One, 7*(11), e49743.

Stavenga, D. G., Leertouwer, H. L., Meglič, A., Drašlar, K., Wehling, M. F., Pirih, P., & Belušič, G. (2018). Classical lepidopteran wing scale colouration in the giant butterfly-moth *Paysandisia archon*. *PeerJ, 6*, e4590.

Stavenga, D. G., Stowe, S., Siebke, K., Zeil, J., & Arikawa, K. (2004). Butterfly wing colours: Scale beads make white pierid wings brighter. *Proceedings of the Royal Society of London.Series B: Biological Sciences, 271*(1548), 1577-1584.

Stavenga, D.G. (2014). Thin Film and Multilayer Optics Cause Structural Colors of Many Insects and Birds. *Materials Today: Proceedings* 109-121.

Stavenga, D.G., Leertouwer, H.L., and Wilts, B.D. (2014). Coloration principles of nymphaline butterflies: Thin films, melanin, ommochromes and wing scale stacking. *Journal of Experimental Biology 12,* 2171-2180.

Stavenga, D.G., Leertouwer, H.L., Meglič, A., Drašlar, K., Wehling, M.F., Pirih, P., and Belušič, G. (2018). Classical lepidopteran wing scale colouration in the giant butterfly-moth. *PeerJ* e4590.

Steinbrecht, R. A., Mohren, W., Pulker, H. K., & Schneider, D. (1985). Cuticular interference reflectors in the golden pupae of Danaine butterflies. *Proceedings of the Royal Society of London.Series B.Biological Sciences, 226*(1244), 367-390.

Stoddard, M.C., and Prum, R.O. (2011). How colorful are birds? Evolution of the avian plumage color gamut. *Behav. Ecol. 5,* 1042-1052.

Stossberg, M. (1938). Die zellvorgänge bei der entwicklung der flügelschuppen von ephestia kühniella Z. *Zeitschrift Für Morphologie Und Ökologie Der Tiere, 34*(2), 173-206.

Suffert, F. (1927). Zur vergleichende analyse der schmetterlingszeichnung. *Biol.Zbl., 47*, 385-413.

Suzuki, T. K., Tomita, S., & Sezutsu, H. (2014). Gradual and contingent evolutionary emergence of leaf mimicry in butterfly wing patterns. *BMC Evolutionary Biology, 14*(1), 1-13.

Thayer, R. C., Allen, F. I., & Patel, N. H. (2020). Structural color in *Junonia* butterflies evolves by tuning scale lamina thickness. *Elife, 9*, e52187.

Tilley, R., Eliot, J. N., & Yoshimoto, H. (2002). Scale microstructure and its phylogenetic implications in Lycaenid butterflies (Lepidoptera, Lycaenidae). *Lepidoptera Science, 53*(3), 153-180.

Trzeciak, T. M., Wilts, B. D., Stavenga, D. G., & Vukusic, P. (2012). Variable multilayer reflection together with long-pass filtering pigment determines the wing coloration of papilionid butterflies of the *Nireus* group. *Optics Express, 20*(8), 8877-8890.

van der Burg, K.R.L, Lewis, J. J., Martin, A., Nijhout, H. F., Danko, C. G., & Reed, R. D. (2019). Contrasting roles of transcription factors *spineless* and *EcR* in the highly dynamic chromatin landscape of butterfly wing metamorphosis. *Cell Reports, 27*(4), 1027-1038.

van Zandt Brower, J. (1958). Experimental studies of mimicry in some North American butterflies: Part I. the monarch, *Danaus plexippus*, and viceroy, *Limenitis archippus archippus*. *Evolution,* 32-47.

Vigneron, J. P., Simonis, P., Aiello, A., Bay, A., Windsor, D. M., Colomer, J., & Rassart, M. (2010). Reverse color sequence in the diffraction of white light by the wing of the male butterfly *Pierella luna* (Nymphalidae: Satyrinae). *Physical Review E, 82*(2), 021903.

Vukusic, P., Kelly, R., and Hooper, I. (2009). A biological sub-micron thickness optical broadband reflector characterized using both light and microwaves. *Journal of the Royal Society Interface Suppl 2,* S19-S201.

Vukusic, P., Sambles, J. R., & Lawrence, C. R. (2000). Colour mixing in wing scales of a butterfly. *Nature, 404*(6777), 457.

Vukusic, P., Sambles, J.R., Lawrence, C.R., and Wootton, R.J. (1999). Quantified interference and diffraction in single *Morpho* butterfly scales. *Proceedings of the Royal Society of London B: Biological Sciences 1427,* 1403-1411.

Wahlberg, N., Leneveu, J., Kodandaramaiah, U., Peña, C., Nylin, S., Freitas, A.V.L., and Brower, A.V.Z. (2009). Nymphalid butterflies diversify following near demise at the Cretaceous/Tertiary boundary. *Proceedings of the Royal Society B: Biological Sciences 1677,* 4295-4302.

Wasik, B. R., Liew, S. F., Lilien, D. A., Dinwiddie, A. J., Noh, H., Cao, H., & Monteiro, A. (2014). Artificial selection for structural color on butterfly wings and comparison with natural evolution. *Proceedings of the National Academy of Sciences of the United States, 111*(33), 12109.

Watt, W. B. (1968). Adaptive significance of pigment polymorphisms in *Colias* butterflies. I. variation of melanin pigment in relation to thermoregulation. *Evolution,* 437-458.

White, T. E., Zeil, J., & Kemp, D. J. (2015). Signal design and courtship presentation coincide for highly biased delivery of an iridescent butterfly mating signal. *Evolution, 69*(1), 14-25.

Wickham, S., Large, M. C., Poladian, L., & Jermiin, L. S. (2006). Exaggeration and suppression of iridescence: The evolution of two-dimensional butterfly structural colours. *Journal of the Royal Society Interface, 3*(6), 99-109.

Wijnen, B., Leertouwer, H. L., & Stavenga, D. G. (2007). Colors and pterin pigmentation of pierid butterfly wings. *Journal of Insect Physiology, 53*(12), 1206-1217.

Wilts, B. D., Giraldo, M. A., & Stavenga, D. G. (2016). Unique wing scale photonics of male rajah brooke's birdwing butterflies. *Frontiers in Zoology, 13*(1), 1-12.

Wilts, B. D., IJbema, N., & Stavenga, D. G. (2014). Pigmentary and photonic coloration mechanisms reveal taxonomic relationships of the cattlehearts (Lepidoptera: Papilionidae: Parides). *BMC Evolutionary Biology, 14*(1), 1-11.

Wilts, B. D., Leertouwer, H. L., & Stavenga, D. G. (2009). Imaging scatterometry and microspectrophotometry of lycaenid butterfly wing scales with perforated multilayers. *Journal of the Royal Society Interface, 6*(suppl_2), S185-S192.

Wilts, B. D., Matsushita, A., Arikawa, K., & Stavenga, D. G. (2015). Spectrally tuned structural and pigmentary coloration of birdwing butterfly wing scales. *Journal of the Royal Society Interface, 12*(111), 20150717.

Wilts, B. D., Mothander, K., & Kelber, A. (2019). Humidity-dependent colour change in the green forester moth, *Adscita statices*. *Biology Letters, 15*(9), 20190516.

Wilts, B. D., Pirih, P., Arikawa, K., & Stavenga, D. G. (2013). Shiny wing scales cause spec (tac) ular camouflage of the angled sunbeam butterfly, *Curetis acuta*. *Biological Journal of the Linnean Society, 109*(2), 279-289.

Wilts, B. D., Vey, A. J., Briscoe, A. D., & Stavenga, D. G. (2017). Longwing (*Heliconius*) butterflies combine a restricted set of pigmentary and structural coloration mechanisms. *BMC Evolutionary Biology, 17*(1), 226.

Wilts, B. D., Zubiri, B. A., Klatt, M. A., Butz, B., Fischer, M. G., Kelly, S. T., . . . Schröder-Turk, G. E. (2017). Butterfly gyroid nanostructures as a time-frozen glimpse of intracellular membrane development. *Science Advances, 3*(4), e1603119.

Wilts, B.D., Pirih, P., and Stavenga, D.G. (2011). Spectral reflectance properties of iridescent pierid butterfly wings. *Journal of Comparative Physiology A 6,* 693-702.

Wright, S.I., Bi, I.V., Schroeder, S.G., Yamasaki, M., Doebley, J.F., McMullen, M.D., and Gaut, B.S. (2005). The effects of artificial selection on the maize genome. *Science 5726,* 1310-1314.

Yeh, P., Yariv, A., and Cho, A.Y. (1978). Optical surface waves in periodic layered media. *Appl. Phys. Lett. 2,* 104-105.

Yoshioka, S., & Kinoshita, S. (2006). Single-scale spectroscopy of structurally colored butterflies: Measurements of quantified reflectance and transmittance. *Josa A, 23*(1), 134-141.

Yoshioka, S., & Kinoshita, S. (2007). Polarization-sensitive color mixing in the wing of the Madagascan sunset moth. *Optics Express, 15*(5), 2691-2701.

Zhang, D., Zhang, W., Gu, J., Fan, T., Liu, Q., Su, H., & Zhu, S. (2015). Inspiration from butterfly and moth wing scales: Characterization, modeling, and fabrication. *Progress in Materials Science, 68*, 67-96.

Zhang, K., Zhou, S., Tang, Y., Wang, G., Zhou, H., Fan, T., & Zhang, D. (2014). Polarization-sensitive color in iridescent scales of butterfly *Ornithoptera*. *RSC Advances, 4*(94), 51865-51871.

Zhang, L., Mazo-Vargas, A., & Reed, R. D. (2017). Single master regulatory gene coordinates the evolution and development of butterfly color and iridescence. *Proceedings of the National Academy of Sciences, 114*(40), 10707-10712.

Appendix 1:

Mathematical model relating reflectance and lamina thickness

```
# R code for modeling thin film reflectance measured through microscope objective
    lens

# following Stavenga 2014 "Thin film and multilayer optics cause structural color
    in many insects and birds," Mat. Today:Proc
# by Rachel Thayer, in collaboration with Sam Thayer, 2019
# used in Thayer 2020, "Structural color in Junonia butterflies evoves by tuning
    scale lamina thickness," eLife



#########################################################################
## DEFINE BASELINE VARIABLES

# wavelengths
lambda = seq(300, 700, by=1)

# angles of light that are collected by your microscope objective. 0-30º
    inclusive is for Num. Aperture = 0.5
# granularity adjustable but MUST match indexing inside 'averaging' function
    later!
angles = seq(0, 30, by=0.03)

# thickness
d_mu = 183 #lamina thickness in nm
d_sigma = 12 #thickness standard deviation in nm
d_list <- seq(d_mu-d_sigma, d_mu+d_sigma, by=0.5) #Use inclusive list of
    thickness values to allow for measurement error in modeled reflectance

# refractive indices
n_chitin = 1.56 + (8.80 * 10^3)/ (lambda^2) #from Leertouwer 2011
n_air = 1

k = 2*pi/lambda



#########################################################################
## COMPONENT FUNCTIONS

# this one gets unpolarized reflectance for a single specific angle
# theta must be given in degrees, not radians
unpolarized_reflectance <- function(theta, d){
  theta0 = theta *pi/180 #convert to radians. Input value in degrees!
  theta1 = asin((n_air*sin(theta0))/n_chitin)
  theta2 = theta0  #Proof: thetatwo = asin((n_air*sin(thetazero))/n_air)
  phi = k * n_chitin * d * cos(theta1)

  TE_R01_num = n_air * cos(theta0) - n_chitin * cos(theta1)
  TE_R01_den = n_air * cos(theta0) + n_chitin * cos(theta1)
  TE_R01 = TE_R01_num / TE_R01_den

  TE_R12_num = n_chitin * cos(theta1) - n_air * cos(theta2)
  TE_R12_den = n_chitin * cos(theta1) + n_air * cos(theta2)
  TE_R12 = TE_R12_num / TE_R12_den
```

Mathematical model relating reflectance and lamina thickness (continued)

```
  R_num_TE = TE_R01^2 + TE_R12^2 + 2 * TE_R01 * TE_R12 * cos(2 * phi)
  R_den_TE = 1 + TE_R01^2 * TE_R12^2 + 2 * TE_R01 * TE_R12 * cos(2*phi)
  R_TE = R_num_TE / R_den_TE

  TM_R01_num = n_air * cos(theta1) - n_chitin * cos(theta0)
  TM_R01_den = n_air * cos(theta1) + n_chitin * cos(theta0)
  TM_R01 = TM_R01_num / TM_R01_den

  TM_R12_num = n_chitin * cos(theta2) - n_air * cos(theta1)
  TM_R12_den = n_chitin * cos(theta2) + n_air * cos(theta1)
  TM_R12 = TM_R12_num / TM_R12_den

  R_num_TM = TM_R01^2 + TM_R12^2 + 2 * TM_R01 * TM_R12 * cos(2 * phi)
  R_den_TM = 1 + TM_R01^2 * TM_R12^2 + 2 * TM_R01 * TM_R12 * cos(2*phi)
  R_TM = R_num_TM / R_den_TM

  R_unpolarized = (R_TE + R_TM) /2
  return(R_unpolarized)
}

# this gets reflectance averaged from 0 to the maximal angle, mimicking
    spectrophotometer readings through an objective lens
# assumes constant light flux, meaning that not more total light reaching probe
    from 0º than any other point
averaging <- function(d, maximal_angle){
  raw_r <- t(sapply(angles, unpolarized_reflectance, d=d))
  radiuses <- angles*pi/180  #in radians
  circumferences <- raw_r * 2*pi*radiuses
  inclusive <- circumferences[1:(maximal_angle/.03+1),] #divide by granularity I
      set at top
  if(is.array(inclusive)){
    sumz <- colSums(inclusive)
    reflectance <- sumz /(2*pi*sum(radiuses[1:(maximal_angle/.03+1)]))
    return(reflectance)
  } else { return(raw_r[1,]) } #theta0 = 0 is a special case. Don't average
      anything.
}



#########################################################################
#call to apply the component functions
#average_me has one column of modeled reflectance per thickness value in d_list
average_me <- as.data.frame(sapply(d_list, averaging, maximal_angle=30))

#useful for graphing results
model_reflectance <- as.data.frame(lambda)
model_reflectance$type <- "sample_name"
model_reflectance$mean <- apply(average_me, 1, mean)
model_reflectance$min <- apply(average_me, 1, min)
model_reflectance$max <- apply(average_me, 1, max)
```

Mathematical model relating reflectance and lamina thickness (continued)

```
#########################################################################
### this makes the Gaussian-sampled reflectance for a single uneven film. Runs
    slow.
# similar to Siddique 2016
d_Gaus <- rnorm(400, d_mu, d_sigma) #n, d_mu, d_sigma

average_me_Gaus <- sapply(d_Gaus_gold, averaging, maximal_angle=30)

plot(lambda, apply(average_me_Gaus_gold, 1, mean), ylim = c(0,0.25), type = "l",
    col="red", main="Gaussian model")
```

Appendix 2:
Custom script to measure blue wing area: python wrapper


```python
#!/usr/bin/env python

# Analyze Images
# Usage: python image_analysis_pipeline.py directory_of_jpgs (WingAreaResults)
(ColorAreaResults)
# Rachel C. Thayer, 2015
# written with reference to http://www.fzu.cz/~dominecf/misc/imagej_particles.html
# Used for phenotyping J. coenia F2 wings


################################################################################
# REQUIREMENTS

import os, sys, glob, subprocess

# requires 2 .imj macros in their precise paths
# the two imageJ macros that will be used:
path_to_imagej_macro_wingarea="/Users/Documents/imageJ_macro_wingarea.imj"
path_to_imagej_macro_colorscalearea="/Users/Documents/imageJ_macro_colorscalearea.imj"

# requires ij.jar, specific path in line 49 and 79

# make sure your image files are lowercase .jpgs


################################################################################
# COMPONENT FUNCTIONS

# subfunction 1a:
# takes a directory of cropped .jpgs, submits them individually to subfunction 1b
# collects the results into a tab-delimited file
def wingarea_cropped(directory, path_to_imagej_macro_wingarea):
    data_list = []
    for filename in glob.glob(os.path.join(directory, '*.jpg')):
        out = run_command_wingarea_cropped(filename, path_to_imagej_macro_wingarea)
        #print out[1].split('\t') gives us e.g. ['1', 'hind_left_21i2015_106__0024',
'3861585', '79.654', '\n']
        data_list.append(out[1])
    out_file =  directory + '/Results_wingarea.txt'
    fh = open(out_file, 'w')
    fh.write(' \tLabel\tArea\tPercentArea\n')
    fh.writelines(data_list)
    fh.close()



#subfunction 1b: called by 1a. Actually issues the system command to Fiji/ImageJ
# calls the macro that measures % of picture that is background red color.
# 100 - [red area] is the % of image that is wing area
def run_command_wingarea_cropped(filename, path_to_imagej_macro_wingarea):
    command = "java -jar ~/Documents/ij.jar -Xmx2g -batch " + path_to_imagej_macro_wingarea +
" " + filename
    out=[]
    p = subprocess.Popen(command, shell=True, stderr=subprocess.PIPE, stdout=subprocess.PIPE)
    for lineA in p.stdout:
        line=str(lineA, 'utf-8')
        out.append(line)
    return out

```

Custom script to measure blue wing area: python wrapper


```
57
58
59  #subfunction 2a:
60  # takes a directory of cropped .jpgs, submits them individually to subfunction 2b
61  # collects the results into a tab-delimited file
62  #BLANK LINE IN OUTPUT FILE = AN IMAGE THAT DIDN'T GET THROUGH!!!
63  def colorscalearea_cropped(directory, path_to_imagej_macro_colorscalearea):
64      data_list = []
65      for filename in glob.glob(os.path.join(directory, '*.jpg')):
66          out = run_command_colorscalearea_cropped(filename,
    path_to_imagej_macro_colorscalearea)
67          #print out[1].split('\t')   #['1', 'hind_left_21i2015_106__0024', '3861585', '79.654',
    '\n']
68          data_list.append(out[1])
69      out_file =  directory + '/Results_colorscalearea.txt'
70      fh = open(out_file, 'w')
71      fh.write(' \tLabel\tArea\tPercentArea\n')
72      fh.writelines(data_list)
73      fh.close()
74
75
76
77  #subfunction 2b: called by 2a.  Actually issues the system command to Fiji/ImageJ
78  # calls the macro that measures % of image that's colored scales, violet-green inclusive.
79  def run_command_colorscalearea_cropped(filename, path_to_imagej_macro_colorscalearea):
80      command = "java -jar ~/Documents/scripts/ij.jar -Xmx2g -batch " +
    path_to_imagej_macro_colorscalearea + " " + filename
81      out=[]
82      p = subprocess.Popen(command, shell=True, stderr=subprocess.PIPE, stdout=subprocess.PIPE)
83      for lineA in p.stdout:
84          line=str(lineA, 'utf-8')
85          out.append(line)
86      return out
87
88
89
90  #subfunction 4: divides the .txts from 1 and 2 to get the % blue wing area
91  # writes results to a tab delimited file.
92  def do_division(directory, filename_wingarea, filename_colorscalearea):
93      wingarea_dict = {}
94      colorscalearea_dict = {}
95
96      fh1 = open(filename_wingarea, 'r')
97      lines = fh1.readlines()
98      for line in lines:
99          if line[0]==' ':
100             pass
101         elif line[0]=='1':
102             wingarea_dict[line.split('\t')[1]] = float(line.split('\t')[3])
103         else:
104             print 'something weird on ', line
105     fh1.close()
106
107     fh2 = open(filename_colorscalearea, 'r')
108     lines = fh2.readlines()
109     for line in lines:
110         if line[0]==' ':
111             pass
112         elif line[0]=='1':
```

```
            colorscalearea_dict[line.split('\t')[1]] = float(line.split('\t')[3])
        else:
            print 'something weird on ', line
    fh2.close()

    data_list = []
    keys_colorscalearea = colorscalearea_dict.keys()
    values_colorscalearea = colorscalearea_dict.values()
    keys_wingarea = wingarea_dict.keys()
    if len(keys_wingarea) != len(keys_colorscalearea):
        print 'wingarea & colorscalearea have nonequivalent data sets. L 121 in subfunc 3'
    for x in keys_colorscalearea:
        if x in wingarea_dict:
            inverse = 100 - wingarea_dict[x]
            percent = colorscalearea_dict[x] / inverse * 100
            parsed_label= x.split('_')
            newstring = '%s\t%s\t%s\t%s\t%s\t%s\t%s\t%s\t%s\t%s\n'%(parsed_label[0],
parsed_label[1], parsed_label[2], parsed_label[3], parsed_label[4], parsed_label[5], percent,
colorscalearea_dict[x], wingarea_dict[x], inverse)
            data_list.append(newstring)
        else:
            print x, ' in colorscalearea but not wingarea'

    data_list.sort()
    out_file =  directory + '/Results_percent_cover.txt'
    fh3 = open(out_file, 'w')

fh3.write('F_H\tL_R\tdate_imaged\tfamily_num\tindv_num\tsex\tpercent_cover_color\
tcolor_scale_area\tbackground_area\twing_area\n')
    fh3.writelines(data_list)
    fh3.close()



################################################################################
# CALL TO APPLY FUNCTIONS

# Use only one set at a time, either this set:

in_directory = sys.argv[1]
wingarea_cropped(in_directory, path_to_imagej_macro_wingarea)
colorscalearea_cropped(in_directory, path_to_imagej_macro_colorscalearea)

# Or else this set:

in_directory = sys.argv[1]
filename_wingarea = sys.argv[2]
filename_colorscalearea = sys.argv[3]
do_division(in_directory, filename_wingarea, filename_colorscalearea)

```

Custom script for measuring blue wing area

imageJ_macro_wingarea.imj


```
// called by the wrapper image_analysis_pipeline.py
// measures what percent of an image is red screen:
// Hue: 0-10. Saturation: 128-255. Brightness: 130-255. Hexadecimal color #cc2a27
//referred to in wrapper as path_to_imagej_macro_wingarea L 17
//and in the subfunctions 1a, 1b
//created by recording actions in ImageJ's macro recorder, and then by modifying to interact correctly with python wrapper


open(getArgument());

//run("Color Threshold...");  //THIS LINE OPENS A GUI WINDOW
// Color Thresholder 2.0.0-rc-15/1.49m
// Autogenerated macro, single image only!

min=newArray(3);
max=newArray(3);
filter=newArray(3);
a=getTitle();
run("HSB Stack");
run("Convert Stack to Images");
selectWindow("Hue");
rename("0");
selectWindow("Saturation");
rename("1");
selectWindow("Brightness");
rename("2");
min[0]=0;
max[0]=10;
filter[0]="pass";
min[1]=128;
max[1]=255;
filter[1]="pass";
min[2]=130;
max[2]=255;
filter[2]="pass";
for (i=0;i<3;i++){
  selectWindow(""+i);
  setThreshold(min[i], max[i]);
  run("Convert to Mask");
  if (filter[i]=="stop")  run("Invert");
}
imageCalculator("AND create", "0","1");
imageCalculator("AND create", "Result of 0","2");
for (i=0;i<3;i++){
  selectWindow(""+i);
  close();
}
selectWindow("Result of 0");
close();
selectWindow("Result of Result");
rename(a);
// Colour Thresholding-------------

run("Set Measurements...", "area area_fraction limit display redirect=None decimal=3");
run("Measure");
```

Custom script for measuring blue wing area

imageJ_macro_colorscalearea.imj


```
// called by the wrapper image_analysis_pipeline.py
// measures what percent of image is "blue" scales i.e. violet to green inclusive
// Hue: 34-239. Saturation: 0-217. Brightness: 28-207.
// referred to in wrapper as path_to_imagej_macro_colorscalearea L 18
// and by the functions 2a, 2b
// written primarily by using the ImageJ macro recorder function


open(getArgument());

// Color Thresholder 2.0.0-rc-15/1.49m
// Autogenerated macro, single image only!

min=newArray(3);
max=newArray(3);
filter=newArray(3);
a=getTitle();
run("HSB Stack");
run("Convert Stack to Images");
selectWindow("Hue");
rename("0");
selectWindow("Saturation");
rename("1");
selectWindow("Brightness");
rename("2");
min[0]=34;
max[0]=239;
filter[0]="pass";
min[1]=0;
max[1]=217;
filter[1]="pass";
min[2]=28;
max[2]=207;
filter[2]="pass";
for (i=0;i<3;i++){
  selectWindow(""+i);
  setThreshold(min[i], max[i]);
  run("Convert to Mask");
  if (filter[i]=="stop")  run("Invert");
}
imageCalculator("AND create", "0","1");
imageCalculator("AND create", "Result of 0","2");
for (i=0;i<3;i++){
  selectWindow(""+i);
  close();
}
selectWindow("Result of 0");
close();
selectWindow("Result of Result");
rename(a);
// Colour Thresholding-------------

run("Set Measurements...", "area area_fraction limit display redirect=None decimal=3");
run("Measure");

close();
```